



MDOT RC-1618A



Research on Evaluation and Standardization of Accelerated Bridge Construction Techniques

FINAL REPORT—SEPTEMBER 2015

Rct v/KK



Department of Civil & Construction Engineering
College of Engineering and Applied Sciences
Western Michigan University

RESEARCH

1. Report No. RC-1618A	2. Government Accession No. N/A	3. MDOT Project Manager Corey Rogers, P.E.	
4. Title and Subtitle Research on Evaluation and Standardization of Accelerated Bridge Construction Techniques		5. Report Date 09/30/2015	
		6. Performing Organization Code N/A	
7. Author(s) Haluk Aktan, Ph.D., P.E. Upul Attanayake, Ph.D., P.E.		8. Performing Org. Report No. N/A	
		9. Performing Organization Name and Address Western Michigan University 1903 West Michigan Avenue Kalamazoo, Michigan 49008	
12. Sponsoring Agency Name and Address Michigan Department of Transportation Research Administration 8885 Ricks Road. P.O. Box 30049 Lansing, MI 48909		10. Work Unit No. (TRAIS) N/A	
		11. Contract No. 2013-0069	
		11(a). Authorization No. Z4	
13. Type of Report & Period Covered Final Report 09/30/2015		14. Sponsoring Agency Code N/A	
		15. Supplementary Notes	
16. Abstract The Michigan Department of Transportation (MDOT) uses Accelerated bridge construction (ABC) to reduce delays and minimize construction impacts. MDOT contracted and completed several bridges using prefabricated bridge elements and systems (PBES). In 2014, two slide-in bridge construction (SIBC) projects were contracted and completed. These two projects included three bridge replacements. Currently, self-propelled modular transporter (SPMT) moves are being planned for three bridge replacement projects. This study goals are to advance the implementations by expanding scoping guidelines to include all ABC alternatives, standardize the bridge slides operations, and develop guidelines for foundation construction while an existing bridge is in service. The tasks completed during this project include (a) reviewing the ABC activities nationally and monitor ongoing ABC projects in Michigan, (b) defining scoping parameters for the implementation of SIBC and SPMT moves, (c) reviewing and evaluating substructure construction and upgrades, along with constructability of deep foundations while an existing bridge is in service, (d) developing specific cost methodologies for SIBC, SPMT moves, and foundation construction, and (e) developing recommendations for updating the multi-criteria decision-making process and the associated software platform by incorporating the updated framework and the cost-benefit analysis models, foundation construction while an existing bridge is in service, and improving SIBC implementations.			
17. Key Words Accelerated Bridge Construction, ABC, Cost-Benefit Analysis, Foundation Construction, Foundation Reuse, Scoping Framework, Standardizing SIBC		18. Distribution Statement No restrictions. This document is available to the public through the Michigan Department of Transportation.	
19. Security Classification - report Unclassified	20. Security Classification - page Unclassified	21. No. of Pages 295 (excluding appendices)	22. Price N/A

Research on Evaluation and Standardization of Accelerated Bridge Construction Techniques

**Final Report
(2013-2015)**

Project Manager: Mr. Corey Rogers, P.E.

Submitted to:



Submitted by:

Haluk Aktan, Ph.D., P.E.
Professor
(269) – 276 – 3206
haluk.aktan@wmich.edu

Upul Attanayake, Ph.D., P.E.
Associate Professor
(269) – 276 – 3217
upul.attanayake@wmich.edu



Western Michigan University
Department of Civil & Construction Engineering
College of Engineering and Applied Sciences
Kalamazoo, MI 49008
Fax: (269) 276 – 3211

DISCLAIMER

“This publication is disseminated in the interest of information exchange. The Michigan Department of Transportation (hereinafter referred to as MDOT) expressly disclaims any liability, of any kind, or for any reason, that might otherwise arise out of any use of this publication or the information or data provided in the publication. MDOT further disclaims any responsibility for typographical errors or accuracy of the information provided or contained within this information. MDOT makes no warranties or representations whatsoever regarding the quality, content, completeness, suitability, adequacy, sequence, accuracy or timeliness of the information and data provided, or that the contents represent standards, specifications, or regulations.”

ACKNOWLEDGEMENTS

This project is funded by the Michigan Department of Transportation. The authors would like to acknowledge the support and effort of Mr. David Juntunen and Mr. Corey Rogers for initiating this research. The authors also wish to acknowledge the continuing assistance of the Research Advisory Panel (RAP) members in contributing to the advancement of this study. Contribution of doctoral student: Mr. Abdul Wahed Mohammed, M.S.E., EIT., for the success of the project is greatly appreciated. Contribution of graduate students: Bryce Wegner, Camila Guerrero Ramirez, and Ozan Utku Ridvanoglu is highly appreciated.

6 STANDARDIZING BRIDGE SLIDES

6.1 OVERVIEW

SIBC is different from the conventional bridge construction because of the activity required to move the bridge to its final position following construction. Moving activity requires the bridge to be on a temporary support structure, resting on a sliding system such as bearings suitable for sliding and a system of force actuation pushing or pulling the bridge. Also, as the bridge moves to the permanent location, a transition support structure is also required between the temporary and permanent substructures.

The critical components of SIBC are the temporary substructure, sliding system, transition substructure and actuation system. In the two recent SIBC projects, different sliding and actuation systems were designed. Also, there were some differences in temporary substructures and transition structures. In both cases, however, observations indicated that primary complications during the move appear from the sliding and actuation system.

The purpose of this chapter is to bring in clarity to the parameters to be considered for specifying the sliding and actuation system. The parameters will be defined and analyzed on the numerical simulation of the US-131 SB Bridge over 3 Mile Road in Mecosta County, Michigan. The goal is to produce some standards in specifying sliding and actuation systems.

In this chapter, the force actuation system will be briefly described as ‘hydraulics and actuators.’ During the simulation modeling, sliding systems and associated parameters will be discussed and defined.

6.2 HYDRAULICS AND ACTUATORS

The weight of the superstructure to be moved is generally in excess of one million pounds. The force that is required to start the motion will be around half a million pounds. The magnitude of required forces immediately implies the need to specify a hydraulic actuator system.

The components of a hydraulic actuator system are a cylinder, power supply, and manifolds fitted with pressure control valves. The power supply generates hydraulic oil under pressure. The oil under pressure is regulated to a constant range at the manifold. The oil under constant pressure flows into the cylinder and generates a force proportional to the cylinder area and oil pressure. The level of oil pressure is often between 3000 to 5000 psi. In principle, the cylinder is designed to generate a constant force that can be manipulated by the pressure control valves at the manifold. The control of forces using the pressure control valves at the manifold is often quite slow. To allow accurate and rapid force control during the move operation, a servo controller is required.

The inclusion of the servo controller requires the use of electronics and most likely a field computer. The advantage of using a servo controller is the ability to establish force, displacement, or combined targets for the movement of the piston. For example, displacement targets can be defined for both pulling jacks in order to keep the bridge superstructure in alignment during the move. However, workers need to be cautious of moving the structure with displacement targets alone. In the case something gets jammed, the actuator will continue developing forces until full capacity is reached and may cause damage in the meantime. To prevent uncontrolled force buildup, the servo system can be programmed with force limits so that in unforeseen situations, such as the move being restrained, the movement will stop when force limits are reached.

The bridge slide simulations presented below will demonstrate moves with only the ability to regulate forces in comparison with sliding using displacement targets.

6.3 MONITORING BRIDGE SLIDES

6.3.1 US-131 over 3 Mile Road Bridge Slide - Learning from Experience

The US-131 over 3 Mile Road project consisted of two bridge replacements. The project site is located at about 40 miles north of Grand Rapids in Mecosta County, Michigan. The old side-by-side box beam superstructures of North Bound (NB) and South Bound (SB) bridges on US-131 were severely deteriorated, especially the beams underneath the truck lane. According to 2014 data, the average daily traffic (ADT) on US-131 is 20,400 with average daily truck traffic (ADTT) of 9%. US-131 is the primary access to the resort areas on the

west side of the state. Therefore, a large volume of ADT is observed between Friday and Sunday afternoons. The 3 Mile Road is a low ADT local route. Thus, this site was selected for Slide-In Bridge Construction (SIBC) ABC technology implementation as the first project in Michigan. A feature of this project location is the surrounding Amish community. MDOT needed to put forth an extra effort toward public awareness with the community before the start of the project.

The project scope included superstructure replacement and widening of NB and SB US-131 bridges (Figure 6-1), and 3 Mile Road improvements. The old NB and SB structures were single spans with 86 ft in length and 42 ft in clear width. (The out-to-out dimension was 45 ft and 10.5 in.) The new NB and SB structures are also single spans with 86 ft in length and 53 ft 8 in. in clear width. (The out-to-out dimension is 56 ft 11 in.) The new NB and SB superstructures weigh about 1.6 million pounds each. The existing abutments were used for the new superstructures with substructure widening to accommodate the widening.

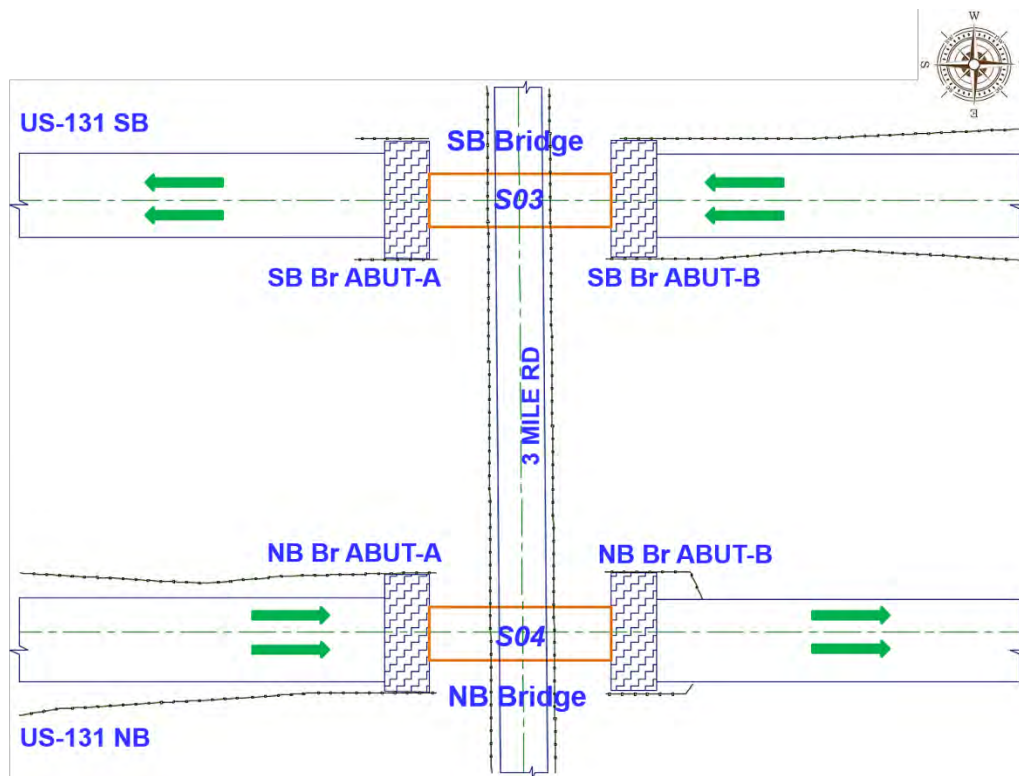


Figure 6-1. NB and SB US-131 bridges and abutment labels

The Construction Manager/General Contractor (CMGC) procurement method was utilized on this project. The prime contractor was C.A. Hull, Inc., and the designers were MDOT Bridge

Design Division and Parsons, Inc. MDOT designed the replacement structure while Parsons, Inc. designed the temporary structures. The new NB and SB bridges were designed without dowel bars for connecting the girders to the abutments. This was because the designer reasoned that dowel bars were required for the regions/states that encounter lateral forces such as earthquakes and or when a bridge is not on a grade.

The ABC window included a 5-day detour for each bridge replacement. The contract allowed for a 5-day closure and detour of US-131 traffic. The traffic restrictions for the NB included no closures from Friday 12 PM to 11:59 PM, and for the SB, no closures from Sunday 12 PM to 11:59 PM. The detour route for US-131 the NB and SB extended for approximately 10 miles via Jefferson Road to Northland Drive to 8 Mile Road. The 3 Mile Road, a low ADT local route, was closed to traffic for the entire project duration; consequently, it was used as the staging area.

6.3.1.1 Substructure Monitoring

The designer was concerned about the abutment movement when the old superstructure was demolished. An automated robot similar to *Total Station* was used for monitoring the abutments movement to maintain allowable limits and ensuring stability. The robot station powered with a solar panel is shown in Figure 6-2.



Figure 6-2. Robot to continuously measure abutment movement

Six (6) targets were installed on the each abutment wall (Figure 6-3). The robot was programmed to measure the displacements of the abutment walls continuously and report any readings that exceed the tolerances. The robot reported any suspicious readings (alarms) via text messages to the project engineer. During the construction, there were several false alarms due to construction equipment obstructing the line of sight between the robot and the targets.

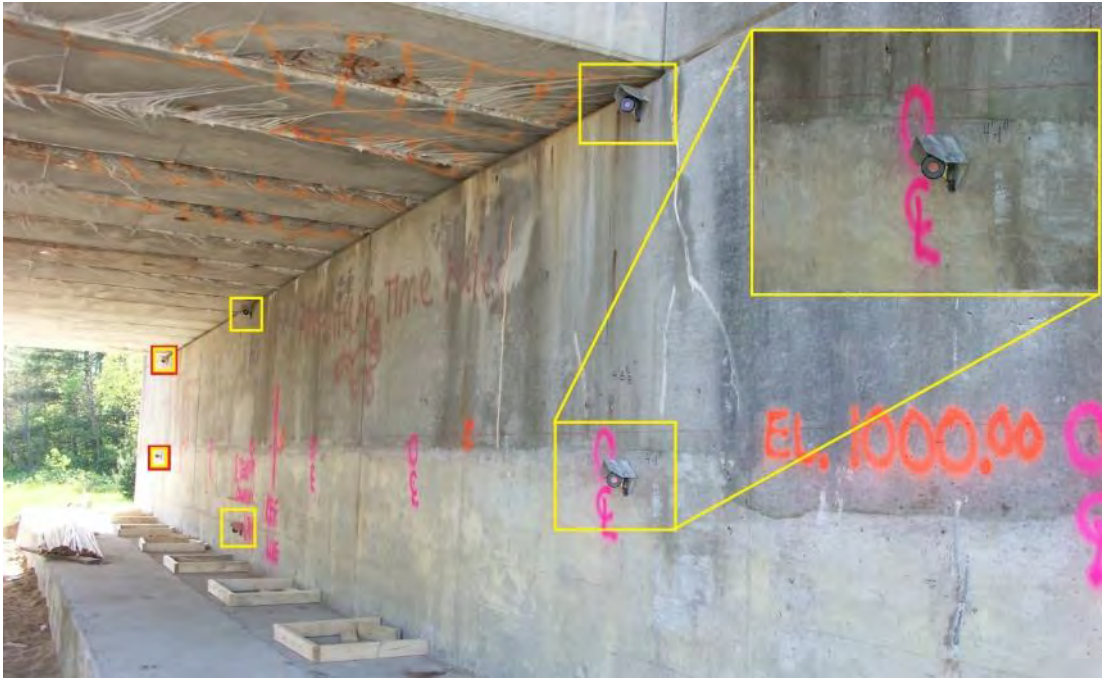


Figure 6-3. Targets on abutment wall to measure the displacements using the robot

6.3.1.2 Temporary Substructure Details

The project consisted of replacing the NB and SB superstructures on existing abutments. The existing abutments are supported on spread footings (Figure 6-4). The existing abutments and spread footings were widened for the replacement project (Figure 6-5).



Figure 6-4. Existing abutment and spread footing



Figure 6-5. Widened existing abutment and spread footing

The new superstructures for both bridges were built adjacent to old structures on temporary substructures outside of the existing alignment of the bridges as shown in Figure 6-6. Each temporary substructure consisted of HP14×73 driven piles, HP14×73 columns, a railing girder, a transition girder, and a sliding girder. Each temporary substructure for the NB and SB US-131 bridges consisted of 8 vertically driven H-piles and 4 battered H-piles (Figure 6-7).

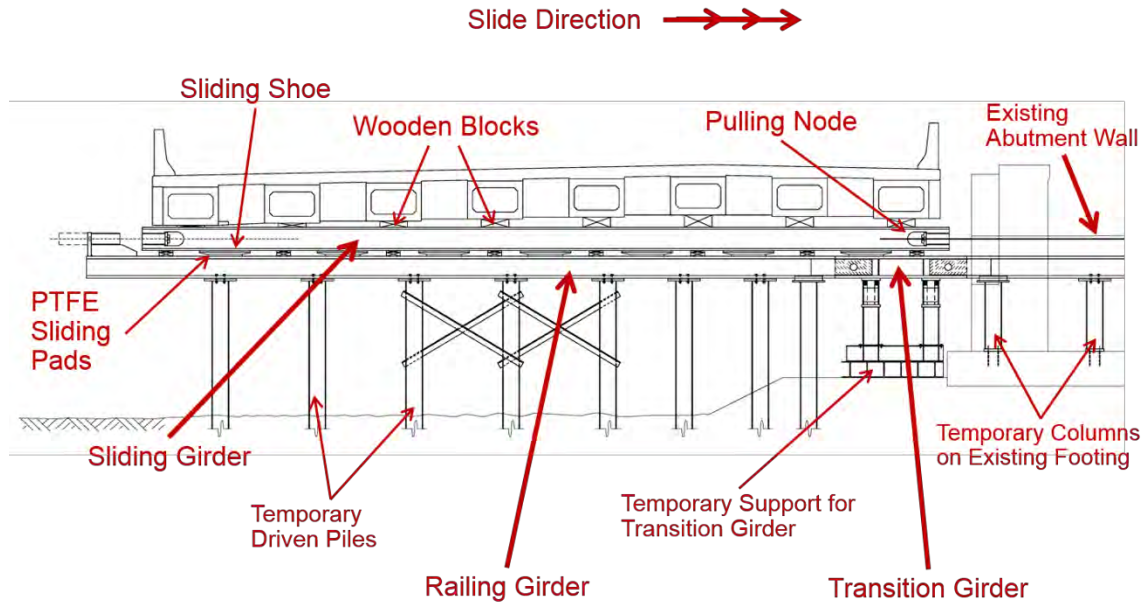


Figure 6-6. Section through the deck of the new superstructure on temporary substructure



Figure 6-7. Temporary substructure extending onto the spread footing

Test boreholes were driven up to 66 ft depth near the existing abutments. The test borings showed medium dense to very dense - fine to coarse sand fill with a trace of fine gravel. Considering this soil profile, vertical piles were driven 70 ft. Each H-pile was 40 ft long, and splicing was required to reach the 70 ft penetration. The battered H-piles were driven 30 ft into the ground. The temporary driven piles were specified to be 10 ft (minimum) away from the existing foundation to comply with the analysis reported in Zekkos et al. (2013). The temporary piles for NB and SB US-131 bridges were driven at 25 ft distance from the existing foundation.

At alternate pile locations, battered piles were added to provide lateral stiffness to the substructure. At those locations, a short HP14×73 section was welded on top as an extension (Figure 6-8). Two sets of holes were drilled in the pile extensions to connect the railing girder (Figure 6-9) and the sliding girder.



Figure 6-8. Pile extension



Figure 6-9. The railing girder connected to pile extensions

Each railing girder was supported on temporary piles driven adjacent to the existing structure (Figure 6-10). Railing girders under the old bridge were supported on temporary columns

located on the existing spread footings (Figure 6-11). As shown in Figure 6-11, the existing spread footings were widened to ensure abutment stability against the backfill pressure and the eccentric loading due to temporary columns of the railing girder. Also, the backfill was removed a few feet to reduce the lateral load on the abutment.



Figure 6-10. Temporary substructure with driven piles and the railing girder



(a) Existing footing with dowel bars for extension.



(b) Widened footing with formwork for grout pads.



(c) Railing girder and temporary columns on the widened footing with grout pads.

Figure 6-11. Widened footing with temporary columns supporting the railing girder

In the new superstructure, the permanent bearings were located at 1.17 ft from the girder ends (Figure 1–10). The contractor’s survey indicated that the abutment’s vertical wall surface was uneven. This required moving the railing girder supports an additional distance of 1/8 feet away from the abutment walls (i.e., towards the inside of the span). After making the adjustments, the railing girders and sliding girders were placed 2.8 ft (towards the inside of the span) from the end of the new superstructure.

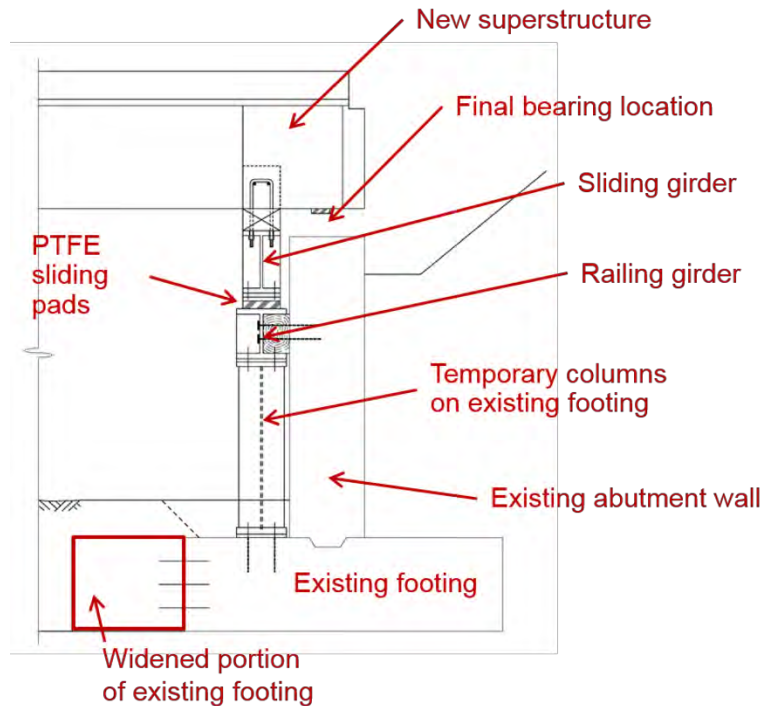


Figure 6-12. Section through an existing abutment with sliding accessories

Limited space between the temporary columns on spread footing and the abutment wall created difficulty for bolt installation. The contractor suggested rotating the columns by 90° (Figure 6-13). However, the suggested change was rejected after considering the potential impact of reduced capacity due to weak axis bending. The contractor still accomplished accessing and tightening the nuts between the columns and the wall. Only the rotation of the first column at the transition was allowed, as per the contractor request; while all the other columns on the spread footing were installed as designed (Figure 6-14). In addition to anchoring the temporary column bases to the abutment footing, the railing girder was anchored to the abutment wall using two adhesive anchors at each railing girder-column connection (Figure 6-15).



(a) Side view showing limited space between the column and the abutment wall



(b) Front view showing an adhesive anchor with a nut

Figure 6-13. Position of a temporary railing girder support column on the abutment footing



(a) Orientation of the temporary column at railing girder transition



(b) Orientation of typical temporary columns on the abutment footing

Figure 6-14. Orientation of temporary columns on the spread footing



Figure 6-15. Railing girder and abutment wall connection

6.3.1.3 Transition Girder

Geotechnical analysis indicated that there is a potential for uplift of the existing abutments once the existing superstructure is removed. The geotechnical report also indicated a total abutment settlement of 1 in. as the new superstructure slides onto the abutments from the temporary substructure supported on driven piles. To accommodate the settlement, transition girders with pin connections on each end were included between the railing girders on driven piles and railing girders on the abutment footing (Figure 6-16). Transition girders were expected to accommodate the differential movement between the existing abutments on the spread footing and the temporary substructure on driven piles, while preventing moment transfer between the railing girders during the slide. The transition girders were approximately 7 ft long, and included 6 in. diameter steel pins at both ends (Figure 6-17). Elastomeric bearings were placed in between the railing girder and the supports at the ends of each transition girder (Figure 6-18).

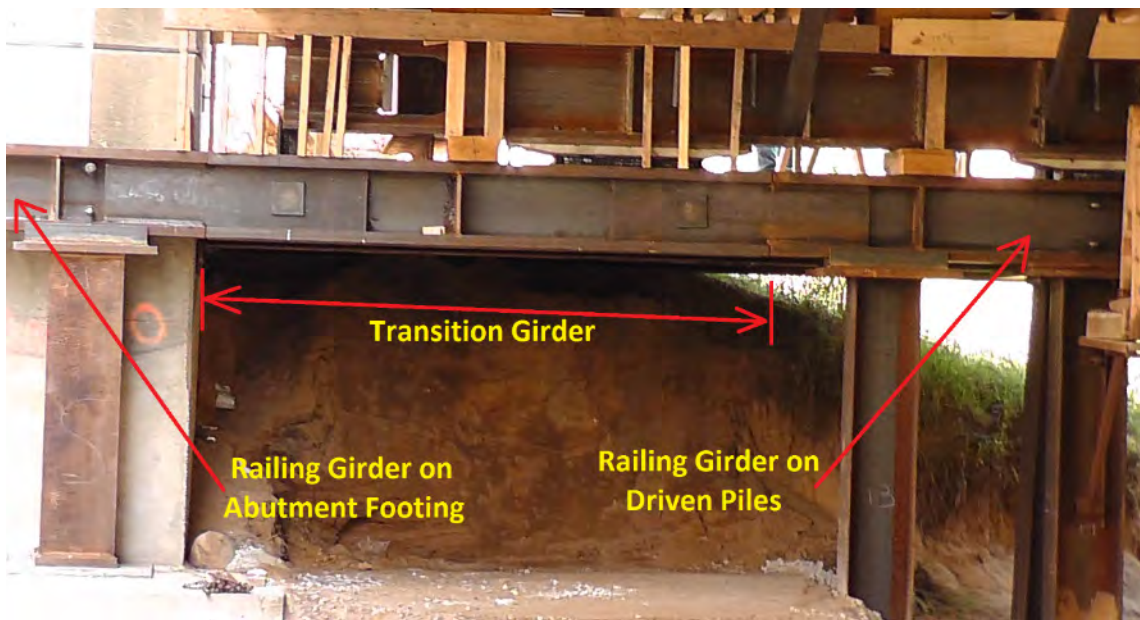


Figure 6-16. Transition girder



Figure 6-17. Transition girder and pin connection



Figure 6-18. Neoprene pads provided below each railing girder end at the transition girder connection

The transition girder concept and its design details were developed without performing a moving load analysis to check deflections and load transfer during the slide operation. After casting the deck at the temporary location and evaluating the load path under slide loads, it was realized that the pins at either end of the transition girder would create discontinuity in the railing girder (Figure 6-19). As a result of this discontinuity, significant deflection of the transition zone was calculated under the load of the superstructure. Displacement was large enough to have the superstructure jammed in the middle of the move. The analysis also showed a potential uplift of the railing girder away from the transition zone. In order to control the deflection and uplift forces, temporary foundation and two temporary supports were installed below each transition girder (Figure 6-19 and Figure 6-20).



Figure 6-19. Temporary foundation for supporting the transition girder



Figure 6-20. Temporary supports for the transition girder

6.3.1.4 Construction of Replacement Superstructures



Figure 6-21. New superstructure construction

Spread box beams of the replacement structure were supported by wooden blocks on the sliding girder (Figure 6-22). The sliding shoe under the fascia beam was positioned on the transition girder. In order to maintain the transition girder's elevation during construction the two supports under the obsolete transition girder were jacked-up to 10 kips before placing concrete for the backwalls and the 9 in. deck.

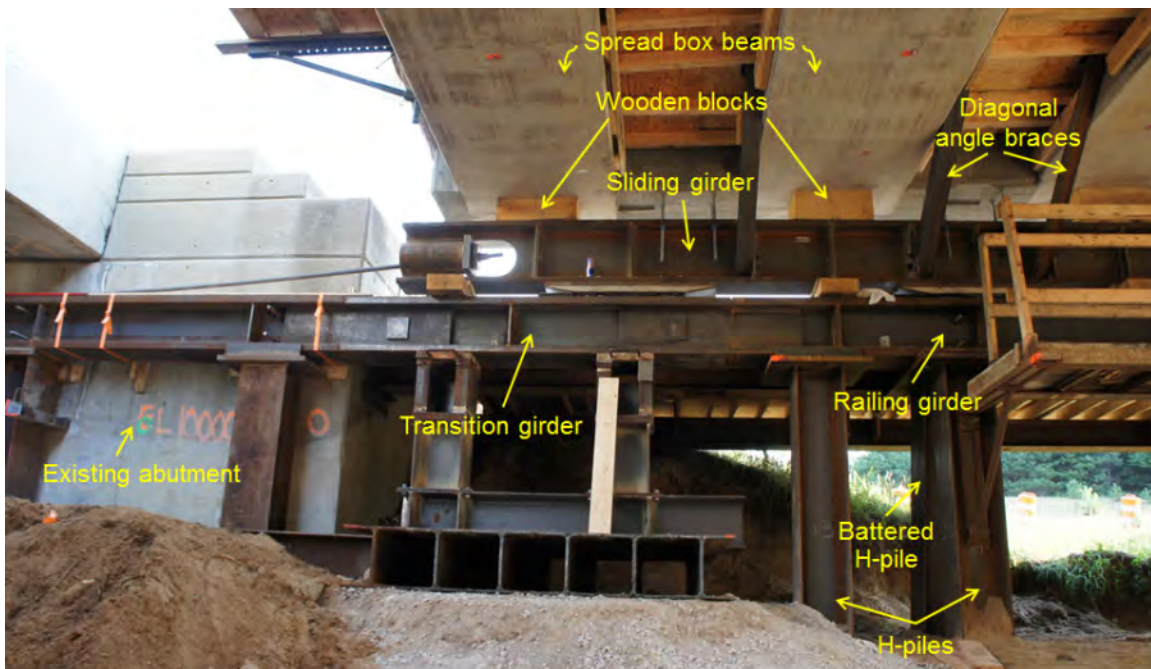


Figure 6-22. New superstructure on the sliding girder

The sliding beam was connected to the pile extensions to maintain stability during superstructure construction on temporary supports (Figure 6-23). The connection consisted of threaded sleeves welded to the slide beam and large threaded bars and nuts (Figure 6-24).



Figure 6-23. The sliding girder connection to the pile extension



(a) Threaded bars with threaded sleeves and nuts

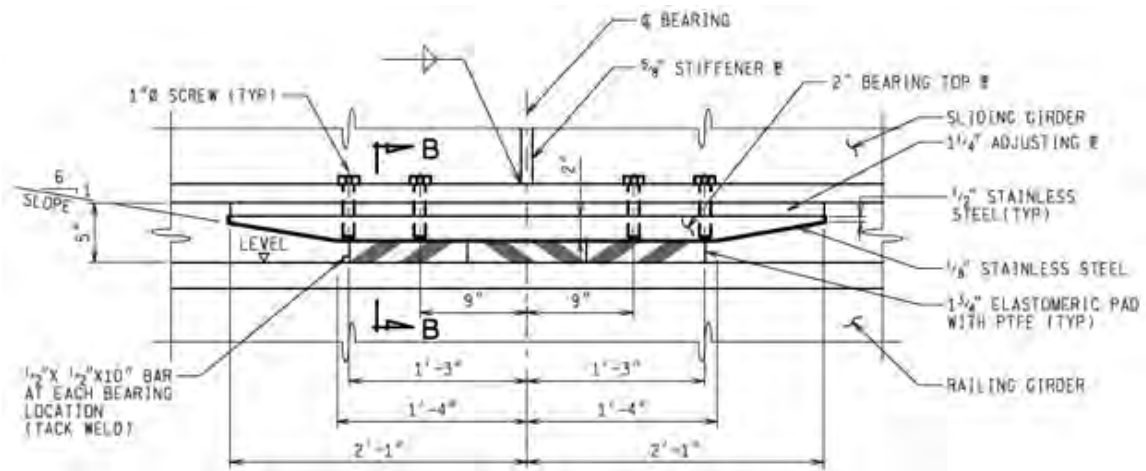


(b) Threaded bar-threaded sleeve connection

Figure 6-24. A close up view of the sliding girder-pile extension connection

6.3.1.5 NB Bridge Test Slide

During bridge superstructure construction and preceding the bridge slide (a duration of half-a-month), a series of three elastomeric pads with PTFE sliding surfaces were placed underneath each stainless steel sliding shoe (Figure 6-25 and Figure 6-26). Each pad was 1.75 in. thick, and had a plan area of 10 in. \times 10 in. Since the pads were loaded for a long duration, it was assumed that only a greater force than one required to overcome the static friction could break the bond. Hence, a test slide was planned with two objectives: (1) test all the equipment and sliding procedures, and (2) break the bond between sliding shoes and PTFE sliding surfaces.



(a) Elevation view of a sliding shoe and an elastomeric pad with PTFE sliding surface



(b) A sliding shoe and a bearing during bridge construction

Figure 6-25. Sliding shoe and elastomeric pad with PTFE sliding surface



Figure 6-26. An elastomeric pad with a PTFE sliding surface

The test slide was performed before the 5-day full closure. During the test slide, the deck was being cured. The bridge was pulled by two jacks powered by a hydraulic pump with a rated pressure of 2000 psi. The pressure to both jacks was kept equal. The sliding distance was monitored by using a tape measure against a small rod installed at the ends of each sliding girder as shown in Figure 6-27. The rod also showed the measure of the offset from the sliding alignment.

As was discussed earlier (Section 6.3.1.3), the moving load analysis indicated a potential uplift of the temporary piles during bridge move. The following three methods were considered to mitigate the potential uplift:

- Drive piles deeper to limit uplift.
- Construct safety barriers after the slide to minimize exterior girder dead loads (but may raise traffic safety concerns).
- Place temporary concrete barriers on the new superstructure as dead load and move it across the deck during bridge slide to prevent the uplift of temporary piles.

However, none of the above options was implemented. Pile driving deeper into the ground was not an option since the superstructure was already constructed. Placing safety barriers after moving the bridge superstructure was not an option due to traffic safety concerns. Placing a temporary barrier was not an option since the deck was being cured. Instead, the transition girder was supported with two temporary supports to prevent uplift.



Figure 6-27. A monitoring rod attached at the front end of a sliding girder

After jacking the temporary supports of the transition girder, the threaded rods connecting the sliding girder and the pile extensions were saw-cut (Figure 6-28). The new superstructure sliding operation was started after that.



Figure 6-28. Removal of bolts and nuts before sliding the new superstructure

The new NB superstructure was moved from east to west. Under the pulling force generated by the jacks, motion of the south sliding girder started first. Because of the unequal friction between the sliding surfaces, the bridge started drifting off the alignment. When the sliding girder was moved about 2 in. westward (i.e., longitudinal to the sliding direction), the front end of the girder drifted a ½ in. off alignment towards the north (i.e., lateral to the sliding direction) (Figure 6-29). Despite the drift from alignment towards the north, the sliding operation was continued. When the south railing girder was slid 4.25 in., the front end of the girder had drifted 1.5 in. towards the north. At that instance, the front end of the north railing girder had slid only 2.5 in. westward, but it drifted 1 in. towards the north. Thus, the hydraulic pressure for the jack pulling the south railing girder was turned off. The sliding force on the north girder was continued until the superstructure was realigned. Following the realignment, pulling of both sliding girders was resumed.

The sliding process continued with repeatedly realigning the bridge superstructure by jacking only one girder when both girders were misaligned. During the test slide, the transverse movement of the bridge superstructure movement was not constrained, and the alignment check was performed manually (Figure 6-30).

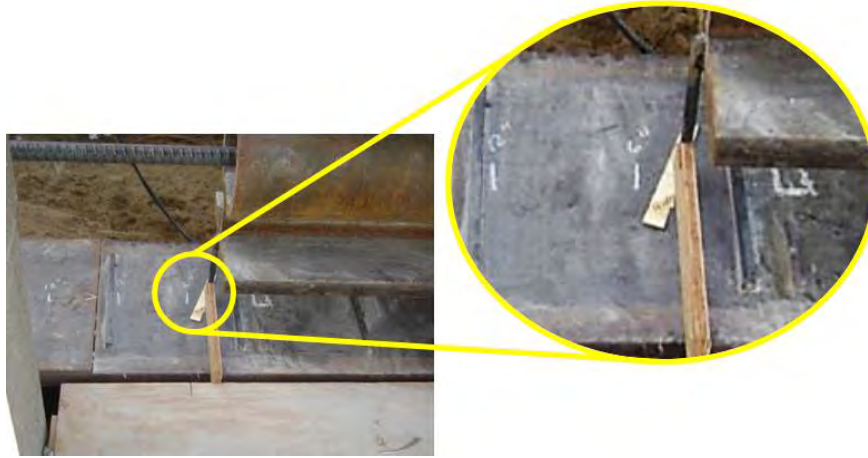


Figure 6-29. Off centered position of the south sliding girder



Figure 6-30. New superstructure brought back to centerline of slide

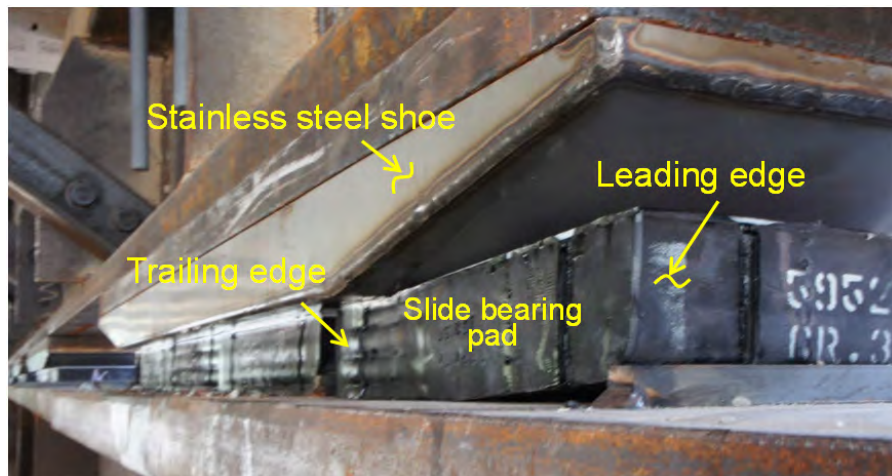
The sliding bearings were restrained by ten (10) inch long, 0.5 in. × 0.5 in. square steel rods, termed as keeper bars that were tack welded to the top of the railing girder at a spacing of 12 in. (Figure 6-25a and Figure 6-31). Twelve (12) inch long, elastomeric pads with PTFE were to remain between keeper bars during the slide. It was assumed that the keeper bars would restrain the bearing pads from moving with the superstructure.



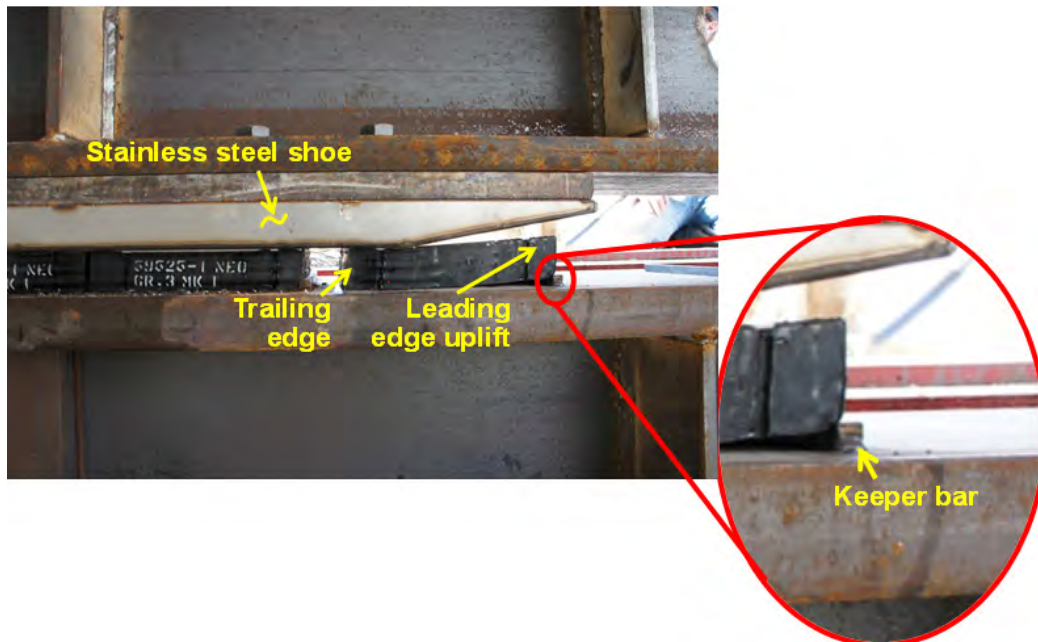
Figure 6-31. Keeper bars (or stopper rods) tack welded to the railing girder

During the slide operation, as the leading edge of the stainless steel shoe transitioned from one bearing pad to the next, the front of the pad lifted up due to the increased force on the trailing edge (Figure 6-32a). The uplift on the leading edge of the pad was significant enough that the pads were climbing over the keeper bars (Figure 6-32b).

During the test slide operation that lasted for about 1.5 hours, the bridge was slid about 7.5 in. (less than the planned test slide distance of 18 in.). After that, the new superstructure was pulled back to original position using jacks at the opposite ends of the sliding girders.



(a) Leading edge uplift due to the force from stainless steel shoe on trailing edge



(b) Slide bearing pad climbing on top of the keeper bar and dragging forward

Figure 6-32. Uplift of the slide bearing pad's leading edge

The observations from the test slide were as follows:

- The 0.5 in. tall keeper bars were not able to restrain the slide bearing pads..
- The bridge was not constrained against the transverse movement. Unequal friction between the sliding surfaces made it difficult to keep the slide in alignment. This required frequent adjustment of the sliding girder position to maintain the alignment.

6.3.1.6 Sliding Operations of NB Bridge

The following activities were completed before the NB bridge slide operation:

- August 03, 2014 – 9 in. thick cast-in-place concrete deck was placed.
- August 04, 2014 - Concrete barriers were cast.
- August 09, 2014 (Saturday) at 7 AM – 1-traffic lane was closed and wingwall demolition started.
- August 09, 2014 (Saturday) at 3:10 PM – the entire northbound was closed to traffic and superstructure demolition started.

The original plan was to remove 3 to 4 girders while the bridge was open to traffic. The intent was to minimize the traffic impact during the 5-day full closure of NB US-131. Due to the concern for the stability of the part-width structure, the plan for partial demolition was not executed, and the entire superstructure was demolished following full closure of NB US-131. Before the demolition, to protect the railing girder and the exposed spread footing from falling debris, plywood sheets were placed on top of it (Figure 6-33). Concrete and wooden blocks were stacked on top of the spread footing for supporting the girders to prevent direct impact to the footing (Figure 6-34). This also helped protecting the abutment from girder ends pulling off before cutting the position dowels.



Figure 6-33. Railing girder protected by placing wooden planks on top of it

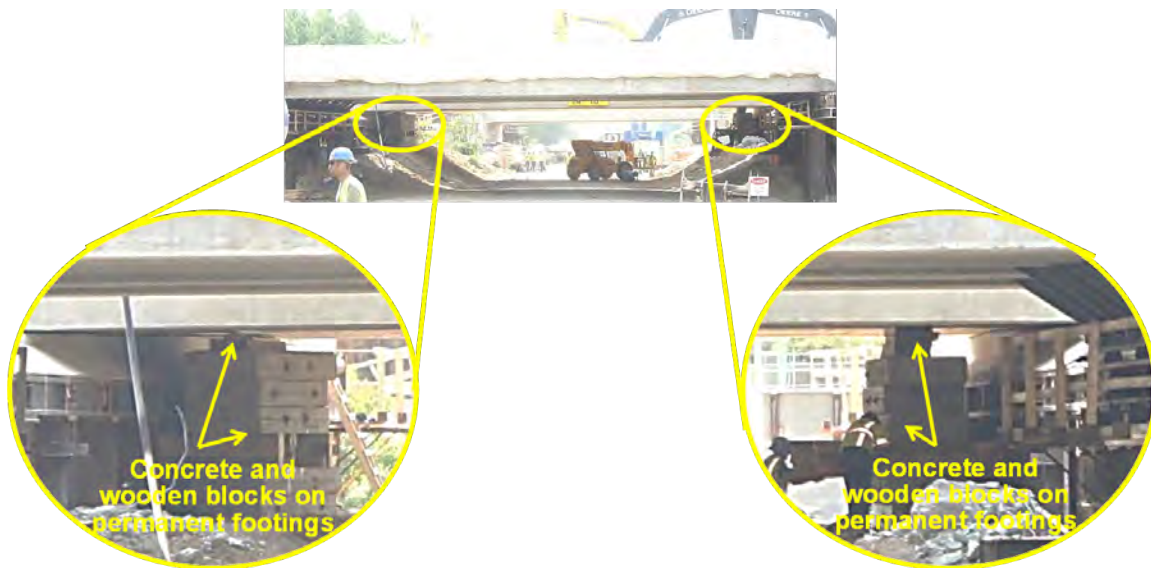


Figure 6-34. Concrete and wooden blocks on permanent footings to prevent damage from demolished girders

Bridge demolition and debris cleaning were performed simultaneously to accommodate the schedule, and to provide space underneath the bridge for continued operation of the activities (Figure 6-35). The demolition was completed at 10 PM. Workers continued cleaning debris until completion at around 3:30 AM on Sunday August 10. After demolishing the old superstructure, the sliding operation of the new superstructure started.



Figure 6-35. Parallel execution of bridge demolition and cleaning of debris

The NB superstructure sliding started at 12:45 PM on August 10, 2014. The sliding distance for the new superstructure was 65 ft towards west, and completion was expected within 4 to 6 hours duration. However, the sliding operation took much longer than planned due to several challenges.

Two posttensioning jacks with a maximum stroke of 2 in. and a capacity of 110T were mounted for the pulling operation (Figure 6-36). Both jacks were powered by a single hydraulic pump (Figure 6-37). Another hydraulic pump was kept as a spare. Also, two more pulling jacks were kept as spares in order to pull back the new superstructure, if needed. During the pulling operation, the pressure was kept equal on both jacks and adjusted manually when needed (Figure 6-38).



Figure 6-36. Posttensioning jack pulling the new superstructure



Figure 6-37. Hydraulic pump common for two jacks



Figure 6-38. Monitoring and adjusting the pressure on each pulling jack

During the slide operation, railing girder and deck displacements were monitored continuously using two total stations. Nine (9) targets located on the deck and 7 targets on each railing girder were used for this purpose (Figure 6-39).



Figure 6-39. Total station targets on railing girder

The sliding girders were pulled with threaded anchor bars (DYWIDAG bars) as shown in Figure 6-40. After each stroke, the nuts within the pulling jacks were tightened on the pulling rods using the lever, and the jacks were retracted (Figure 6-41). This process ensured that the tension in the pulling rod was intact while the jacks were being retracted. The manual jack retraction procedure, along with the limited stroke, extended the duration of the slide. The jacks needed to be retracted after approximately every 1.375 in. stroke.



Figure 6-40. Sliding girder being pulled using DYWIDAG bars



Figure 6-41. Pulling jack nut being tightened before retracting the jack

When the pulling force was at $2/3^{\text{rd}}$ of the calculated value based on the assumed friction between PTFE and stainless steel sliding shoes, the north-sliding girder moved about 1 in. (Note that the movement of south sliding girder was not being monitored; where motion started is uncertain). Based on the observations from the test slide, the sliding was halted, and additional keeper bars were welded on top of the existing keeper bars to increase their height. In addition, wooden blocks were placed on the leading edge of the bearing pads to prevent uplift (Figure 6-42). Additionally, wooden blocks were placed in between the keeper bars and slide-bearing pads at a few locations to prevent the slide bearing pads from dragging forward (Figure 6-43).

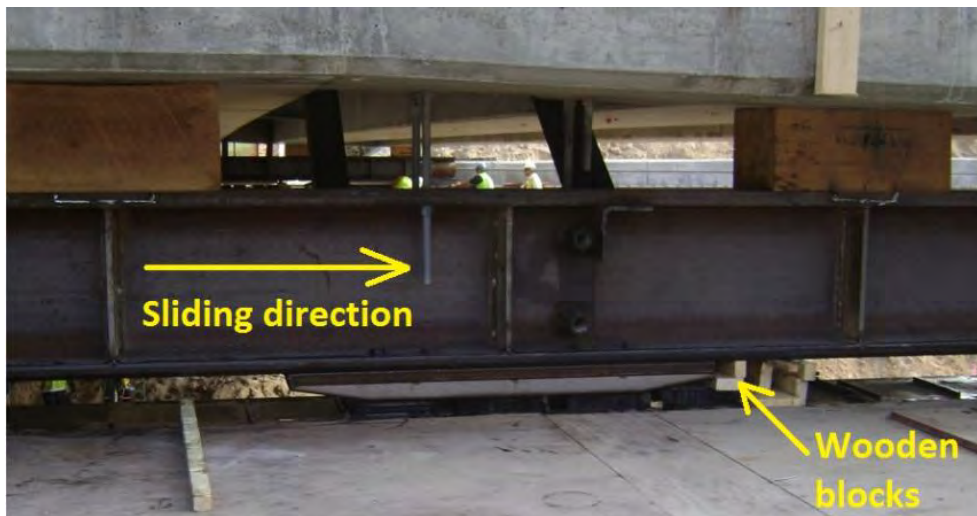


Figure 6-42. Wooden blocks placed on the leading edge of bearing pad to prevent uplift when the trailing edge is loaded as the sliding shoe moves on to the pad

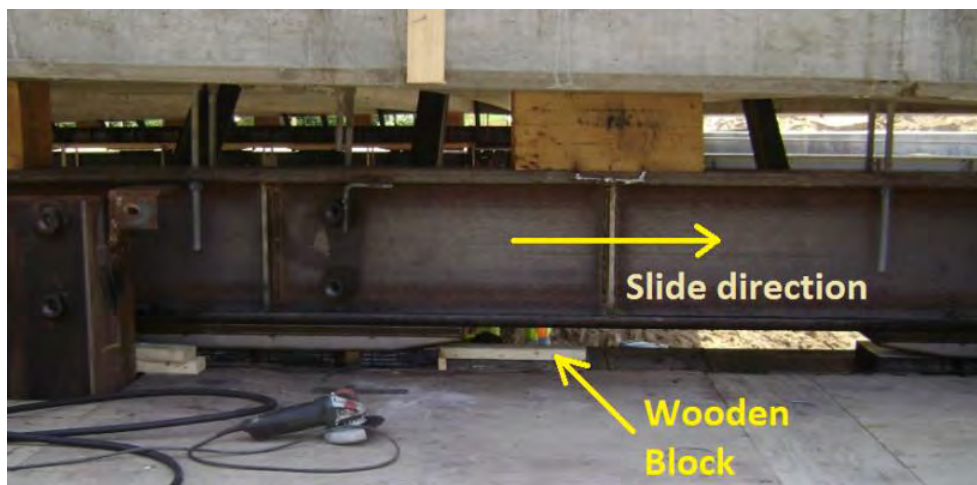


Figure 6-43. Wooden blocks placed in between keeper bars and bearing pads to prevent the pads from dragging forward

There were a limited number of bearing pads with PTFE, and the plan was to reuse as the sliding advanced; consequently, the pads from the rear end of the railing girders were removed and placed in front. This process encountered difficulties because a few pads did not fit in between the keeper bars. This required removing the keeper bars, placing the pads, and rewelded the bars. The slide operation progressed very slowly. The slide distances and corresponding times were recorded on August 10th:

- At 3:30 PM the total slide distance was 4 ft.
- At 5 PM the total slide distance was 6.75 ft.

In addition to the difficulties related to moving the pads forward, another issue came up with the use of PTFE without textured surface (as per the contract documents). During the lateral slide operation, Thermyl-Glyde[®] synthetic gear oil was applied on top of the pads as a lubricant to reduce the friction. The lubricant ran out of the surface and drained onto the railing girder below. This not only required a continuous clean up and work around, but it also lubricated the railing girder and, in several instances, pads slipped out from under the superstructure and fall off the railing girder.

The new superstructure movement was being tracked monitored in the slide (east-west) direction as well as transverse (north-south) direction. The north and south sliding girder movements in the direction of the slide were not equal. As a result, the structure lost alignment and drifted north. This was conjectured to be due to differential friction between the north and south sliding surfaces, or an elevation difference between the north and south sliding girders, along with a lack of any lateral restraint. The contract documents called for the superstructure to slide on top of the railing girder. The contract plans called for the top of the railing girder to be level, and they did not require a lateral restraint system. In addition to railing girder tolerances, there are additional parameters that cannot be accurately controlled to assure equal frictional forces on the sliding surfaces

To deal with the differential movement of the sliding girders, the pulling of the girder that is ahead was stopped to allow the other girder to catch up. The contractor tried to adjust the hydraulic pressure independently to each jack to achieve equal movement. However, the pressure control valve configuration on the hydraulic power supply limited the ability of the

operator to control pressure to the jacks. The solution was to stop the sliding operation periodically to adjust the sliding girder positions.

Even with the repeated adjustments of the jack, at a slide distance of 27 in. westward, the bridge had drifted 1.75 in. towards the north (i.e., transverse to the slide direction). The tolerance for the offset from the sliding alignment given in the special provisions was specified to 2 in. This tolerance was established considering the sliding girder flange width and bearing pad dimensions. Once that much transverse drift was observed, the sliding was halted, and the superstructure was pushed sideways from north to south by additional hydraulic jacks placed at the north end of the superstructure. Two jacks were placed against the 2nd and 4th pile extensions as seen in Figure 6-44 and Figure 6-45. After realigning the superstructure, wooden blocks and shims were placed in between the sliding girder and 1st and 3rd pile extensions on the north end of the superstructure to limit the drift (Figure 6-45). Shims were also installed in between the sliding girder and the north abutment (Figure 6-46).

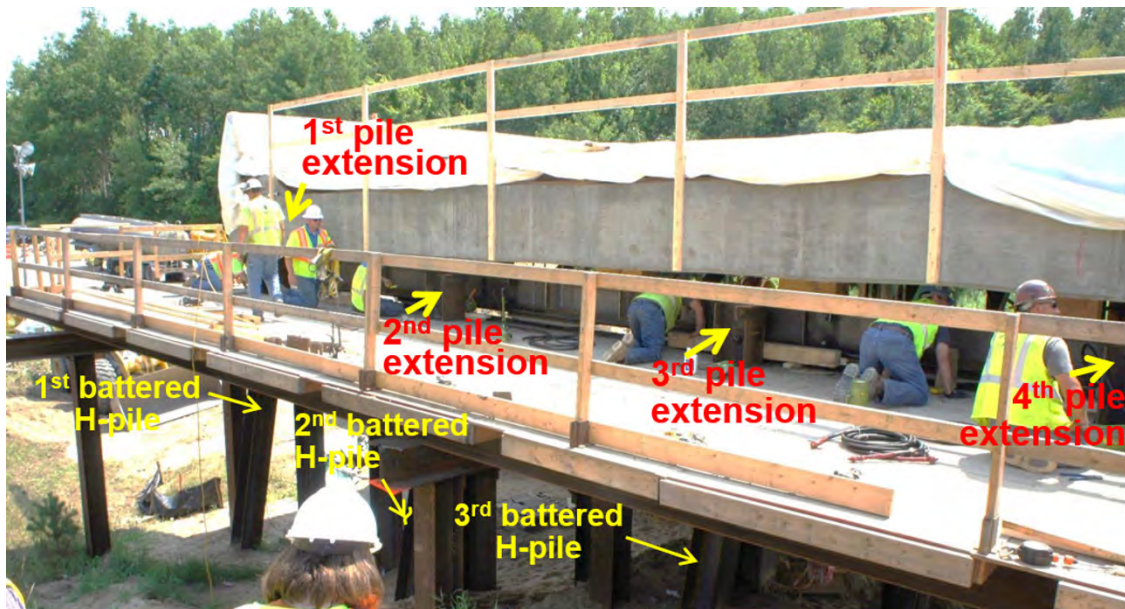


Figure 6-44. Battered H-piles and respective pile extensions at north end of the superstructure



Figure 6-45. Wooden block and shims at 1st pile extension, and jack at 2nd pile extension



Figure 6-46. Shims installed in between sliding girder and north abutment

The sliding was temporarily suspended to give the crew a break after the 2nd sliding shoe (from west) travelled over the transition girder. The primary reason was that the crew working on the sliding operation was already experienced with the slide, and bringing new crew for the night operation may have created more complexities, such as training the crew and distributing specific tasks.

The sliding was resumed by the same crew at 7 AM on August 11 (Monday) with repeated stops to reset the jacks. The sliding was completed on August 11 evening. The sliding of the NB superstructure took a total of 28 hours that included several halts for dealing with challenges. Once the superstructure was laterally slid into place, supports for permanent bearings were cast on the existing abutment wall and allowed to cure overnight. To place the bearings, each end of the superstructure was jacked separately to remove the wooden blocks from the sliding girder and lower it on to the permanent bearings. In this process, the superstructure was jacked up 7/16 in. using 7 synchronized jacks placed at the pockets in each backwall.

The following list summarizes the experience gained from the US-131 NB bridge slide and provides very useful advice for improving SIBC operations in future projects:

- If a bridge is planned to be slid onto an existing abutment, a detailed survey of the existing abutment is needed.
- Performing a review of slide operations and an associated analysis of the temporary structure under moving loads should be performed.
- Methods and means to control bridge alignment during a slide need to be discussed and analyzed.
- The uneven and unlevelled surface of the railing girders and differential friction on the railing girders resulted in lateral drifting of the superstructure towards north. This conclusion was a result of an intensive discussion between the designer and the contractor's engineers. However, there are numerous parameters controlling the friction of the sliding surfaces that cannot be accurately controlled. The methods and means for controlling slide alignment should not assume equal uniform friction of sliding surfaces.
- During this slide, the pulling jacks were powered using a single hydraulic power supply, and limited the operator capability of adjusting the force to each sliding girder. Even if each jack had an independent power system, it would not have been able to keep slide in alignment. The use of servo controlled hydraulic jacks with integrated force and displacement sensors is highly recommended.

- Limited stroke of the jacks required frequent interruptions to the pulling operation. Jacks with a longer strokes or a system that can be operated continuously is recommended to limit operation interruptions.
- If lubrication is specified using PTFE surfaces with dimples will be more effective for rheology.
- Evaluate and analyze sliding methodologies in addition to sliding girders used in this implementation. In analyzing the slide, the deformability of all sliding components needs to be included. The observed bearing pad uplift and associated jumping over the stopper bars is one of those events that could have been evaluated before the operation.

6.3.1.7 Railing Girder Reuse Plan for the SB Bridge

The original plan was to reuse the railing girders of the NB Bridge for the SB Bridge. The plan was to have the railing girder and the temporary columns connected before installing under the bridge. However, the space available under the bridge was limited, and the installation was deemed complicated. The plan was changed to reuse the railing girders on the temporary piles instead of the railing girders underneath the bridge. This change caused a delay in the new SB superstructure construction on the temporary substructure. This particular instance demonstrates the need of constructability analysis during the project planning stage.

6.3.1.8 Sliding Operations of SB Bridge

The sliding of the SB US-131 over 3 Mile Road Bridge was performed on September 09, 2014. The sliding operation started at 9:30 AM. The sliding direction of the new superstructure was from west to east with a sliding distance of 65 ft. Two total stations with 9 targets on the new superstructure and 6 targets on each railing girder were used to monitor the railing girder and deck displacements, during the slide operation. Based on the implementation of the NB bridge slide, the following changes were incorporated:

- To control the bearing pad uplift and related problems, longer pads of 24 in. length were used instead of the 12 in. pads used for the NB bridge slide. Also, to prevent the slide bearing pads from climbing over the 0.5 in. keeper bars, 1.0 in. keeper bars were installed.

- Pulling jacks with 60 T capacity and 6 in. stroke were specified. The pulling jacks were set to pull only 5 in. during each stroke. Each stroke was completed in 30 seconds. On average, the jack reset time was 5 seconds. The jacks were operated independently with hydraulic power supplies that provided control for the operator during the slide.
- To guide the bridge and keep it in alignment during the slide, rollers were attached to the temporary substructure at the pile extensions on both sides of the new superstructure (Figure 6-47). A 1 in. gap was provided in between the rollers and the sliding girder. The rollers provided adequate transverse constraint to the sliding structure while it moved over the temporary substructure on piles to control the transverse drift experienced during the NB bridge slide.
- PTFE rails were attached to each abutment wall to provide lateral sliding surfaces in case of horizontal drift of the superstructure (Figure 6-48). Approximately, a 1 in. gap was between the PTFE surface and the sliding girder.

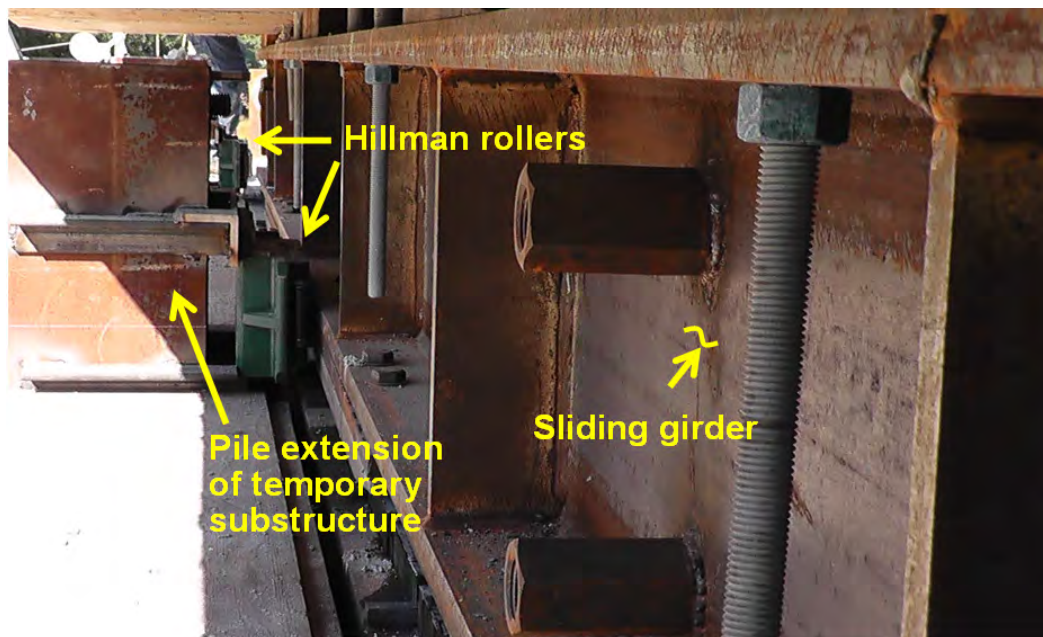


Figure 6-47. Hillman rollers attached to temporary substructure at the pile extensions

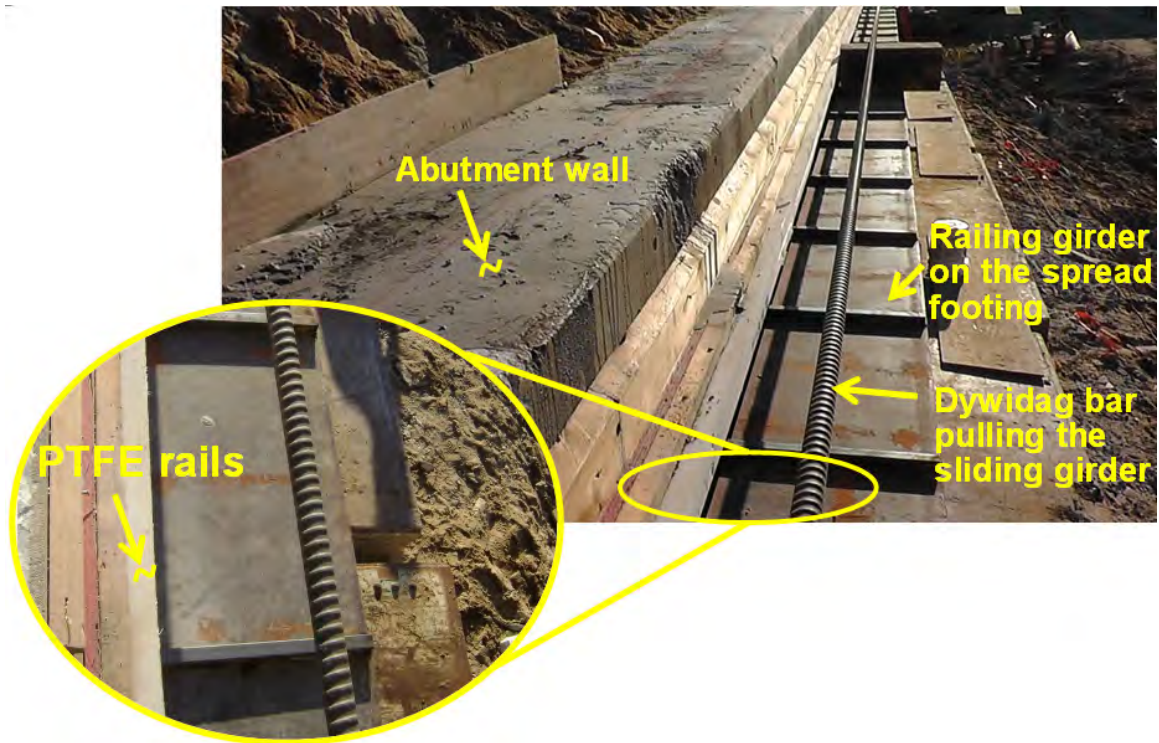


Figure 6-48. PTFE rails attached to the abutment wall to provide transverse constraint to superstructure

During sliding, the new superstructure also lost alignment and drifted south (i.e., transverse to sliding direction). There was an inch gap on each side of the superstructure; however, the total drift was measured as 1.75 in. This meant that the new superstructure pushed the temporary substructure about 0.75 in. southward. At this time, the rollers came in contact with the sliding girder. As the sliding operation progressed, for every 5 in. pull, an additional 0.125 in. lateral drift was measured southward. Thus, whenever the total drift reached or exceeded 1.75 in., the pulling operation was temporarily halted, and only the jack pulling the south sliding girder was activated until the total drift reduced to an inch. The slide operation was continued with periodic adjustments to remedy the lateral drift. When the new superstructure moved on to the temporary substructure attached to the abutment, the lateral drift stabilized to an inch. This was because the PTFE strips on the abutment walls were stiff enough to provide adequate restraint to keep the new superstructure in alignment.

At 12 PM on the same day, i.e., just 2.5 hrs from the starting time, the total slide distance was measured as 25 ft. The slide operation for the SB superstructure was completed in 7 hrs.

6.3.1.9 NB and SB Bridge Post Sliding Operations

After sliding into the final position, grout pads were formed at permanent bearing locations, and permanent bearings were placed on top of the grout pads. To form the grout pads, “MasterFlow 928 High-Precision Mineral-Aggregate Grout with Extended Working Time” was used. The grout pad length and width were 46.5 in. and 10 in., respectively. The grout pad thickness varied from 4.5 in. to 8 in. to match the existing road profile. The size of the grout pad required reinforcement to control shrinkage cracking. The grout was allowed to cure for 24 hrs before removing the formwork (Figure 6-49 and Figure 6-50).



Figure 6-49. Grout pad formwork and permanent bearing pads



Figure 6-50. Grout pads under permanent bearings

With the new superstructure at its final slide position, each end was vertically lifted by 7 hydraulic jacks placed at the preformed pockets in the backwall. Following lifting the permanent bearings for the wooden blocks were installed (Figure 6-51, Figure 6-52, and Figure 6-53). All 7 jacks, each with 100 T capacity, were synchronized using a single manifold (Figure 6-52 and Figure 6-53).



Figure 6-51. New superstructure at final slide position



Figure 6-52. Hydraulic jacks in backwall pockets



Figure 6-53. Hydraulic pump system with a manifold connecting all 7 jacks

An additional jack was placed under the fascia girder to support the weight of the barriers (Figure 6-54 and Figure 6-55). The jack under the fascia was operated independently with a hand pump from the other jacks. The process of lifting one end of the superstructure, removing the wooden blocks, and lowering the superstructure on permanent bearings was completed in 6 minutes (Figure 6-56).



Figure 6-54. Installing the jack under the fascia girder



Figure 6-55. The jack at fascia girder and the hand pump



Figure 6-56. Lifting up at one end of new superstructure using 7 synchronized jacks and a single jack under the fascia girder

Finally, a membrane was installed behind the permanent bearings before placing the fill underneath the approach slab as shown in Figure 6-57.



Figure 6-57. Installing membrane before placing the approach fill

6.3.1.10 Recommendations for Improving Bridge Slide Operations

The experience gained from monitoring the US-131 over 3 Mile Road bridge slide project allowed developing the following recommendations:

- For the sliding of new superstructure on to existing abutments, a detailed survey of the existing abutment is needed before the design process of the new superstructure.
- A test slide is essential for testing of all the equipment and sliding procedures before the full closure of the facility carried traffic. The test slide also helps to break the lock between sliding shoes and PTFE sliding surfaces. This is because the surface locks due to the PTFE pads being in contact with the sliding surfaces for the entire duration of superstructure construction.
- The railing girders and other sliding systems need to be protected during the demolition of the old bridge. Also, the substructure and abutments need to be protected from the impact of falling concrete.
- The slide distance of the superstructure needs to be monitored continuously along with its transverse movement (i.e., measure of offset from the sliding alignment). Manual monitoring requires coordination and communication. Monitoring using sensors would be simpler by showing bridge position during slide at the control site.

- Limited stroke of the jacks required frequent stops to the pulling operation. Jacks with a longer stroke are desirable. Most desirable is a servo controlled hydraulic system that can be operated continuously and provides feedback on position as well controls the alignment of the bridge during the slide.
- In case manual jacking will be used, the control of bridge alignment during slide needs to be considered. The lateral restraining system may include rollers with guide bearings set inside of a channel attached to the rail girder. Another option is to provide sliding surfaces along the sides of the superstructure.
- Bearing pad with Teflon surface can be effectively used for the slide. In this case, the deformability of the pad under load needs to be analyzed. An option is to use lager pads so that pressure is reduced and deformability is limited.
- Use PTFE surfaces with dimples to contain the lubricant within the surface during the slide. On the other hand, lubricant may not be required because jacks often have sufficient capacity to move the bridge without lubrication.
- Milling tolerances may result in variations in elevation at the top of railing girders (i.e., uneven and unlevelled surface), which could result in uneven contact of the sliding bearing. Regardless of specified tolerances, there will always be differential friction coefficient between the sliding surfaces. If not accounted for, the bridge will not remain in alignment during the slide.
- The vertical jacking of the superstructure to rest on permanent bearings needs to be with strict control. All the jacks need to apply equal displacements to the superstructure to prevent twisting. When the jacks are controlled to apply equal force during the lifting process, the portions of the structure (such as the fascia girder) that carry extra weight due to safety barriers cannot be synchronized with the other jacks. In order to lift one end of the structure uniformly, a servo controller is required to control the jacks.
- A constructability review is essential to prevent last minute changes. A constructability review would have identified the complications in reusing the railing girder from NB Bridge at the SB Bridge.
- Multiple crews need to be trained for the sliding operations, so that work stoppage is avoided when work duration is increased due to unforeseen issues.

6.3.1.11 Other Observations from US-131 Bridge Slide Project

The following observations were documented by MDOT during the project closure meeting:

- There were significant challenges related to the submittals from the contractor for the SIBC. The submittals were not given to MDOT in a timely manner, and MDOT's review had to be accelerated to meet the schedule. Thus, in future projects the contract documents, such as lateral slide special provision, need to emphasize that the contractor submittals are timely. Another solution is to include statements in the Progress Clause that the time specified for MDOT review of the contractor's submittal is important and not flexible: any delay resulting from late contractor submittals may result in liquidated damages to the contractor, should the contractor not meet the specified open to traffic dates.
- During the lateral slide in of the superstructure, vertical movement of the existing abutments was not monitored and recorded. On future SIBC projects where rebounding and/or settlement of the existing abutment is anticipated, MDOT will work to identify and design a system that will accommodate the potential movement while providing a continuous rail girder for the superstructure to move across. While several options have been suggested, no final decisions have been made to date.
- A check of deflections/loads as the superstructure moves across the temporary supports must be performed during the design. It should not be assumed that the contractor will do that: any delay of the check may create problems during the slide.

6.3.2 M-50 over I -96 Bridge Slide Project - Learning from Experience and Monitoring During the Move

The M-50 over I-96 bridge slide-in project activities and the related observations are documented in this section. The activities were described after reviewing the project documents (plans, special provisions, etc.), frequent site visits, and discussions with the MDOT engineers, consultants, and the contractor. During the slide operation, pier columns were instrumented, and the movements were recorded. Later, the monitoring data was analyzed, and models developed to calculate the forces acting on the pier and the associated stresses. The monitoring of the activities during this project contributed to the, recommendations in the report towards standardizing SIBC.

6.3.2.1 Site Characteristics and Selection of Construction Alternative

The M-50 (Alden Nash Highway) over I-96 project site is located 10 miles East of Grand Rapids in Lowell, Kent County, Michigan (Figure 6-58). Traffic data from 2012 shows that I-96 carries an average daily traffic (ADT) of 44,600 with an average daily truck traffic (ADTT) of 11%. Also, ADT on M-50 is given as 11,100 with an ADTT of 6%. An insufficient number of lanes, during peak traffic hours, caused severe backups on the ramps to M-50 spilling onto I-96 EB. Thus, the bridge was classified functionally obsolete. However, minimum disruption during bridge replacement was required because the M-50 interchange is the main access route to the nearby carpool parking lot, and I-96 is a heavily travelled interstate. Therefore, the SIBC technology was selected based on user delay costs following the evaluation of the site for SIBC suitability. The project consisted of full structure replacement and improvements to the ramps at the intersection.

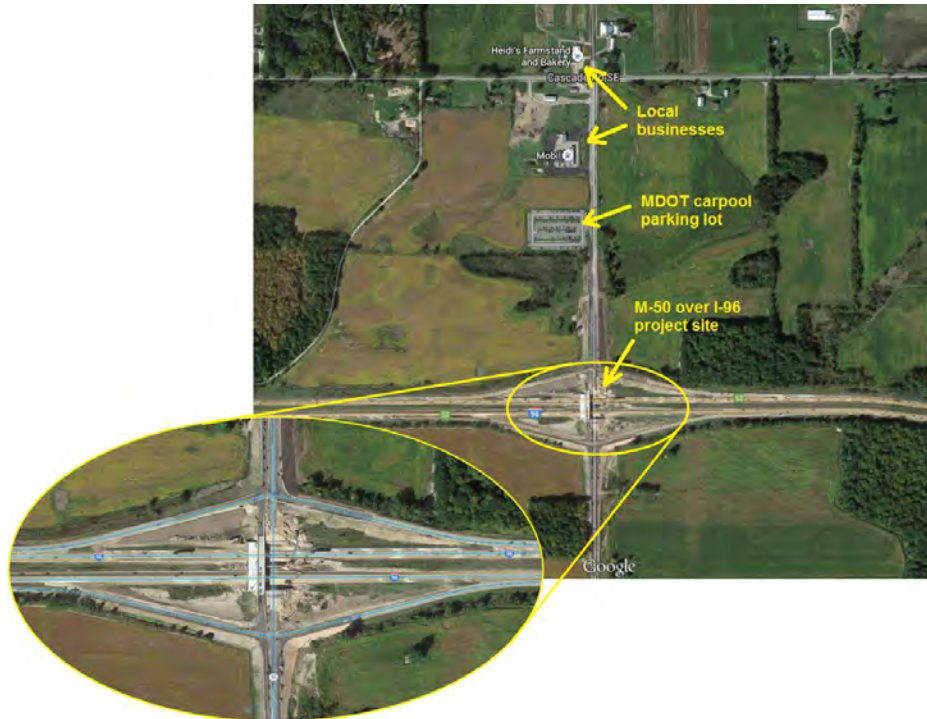


Figure 6-58. Bridge location (Source: Google map)

The Construction Manager/ General Contractor (CMGC) procurement method was utilized with Anlaan Corporation as the prime contractor. The bridge designer was the MDOT Bridge Design Division. The temporary substructure was designed by Parsons, Inc. Mammoet USA South, Inc. was the slide-in subcontractor.

6.3.2.2 Bridge Superstructure and Substructure Details

The old 4-span bridge was 227 ft long and 37 ft 5 in. wide. The new 2-span, 198 ft long and 71 ft 3 in. wide bridge (i.e., the replacement bridge) includes wide shoulders and two left turn lanes (Figure 6-59). The new bridge is a continuous for live load (CLL) structure with a jointless deck and independent backwalls (Figure 6-60). The cast-in-place concrete approach slab is supported on a sleeper slab on one end, and the other end is tied to the bridge deck. The approach slab concrete was cast following the move along with a closure pour (Figure 6-60).

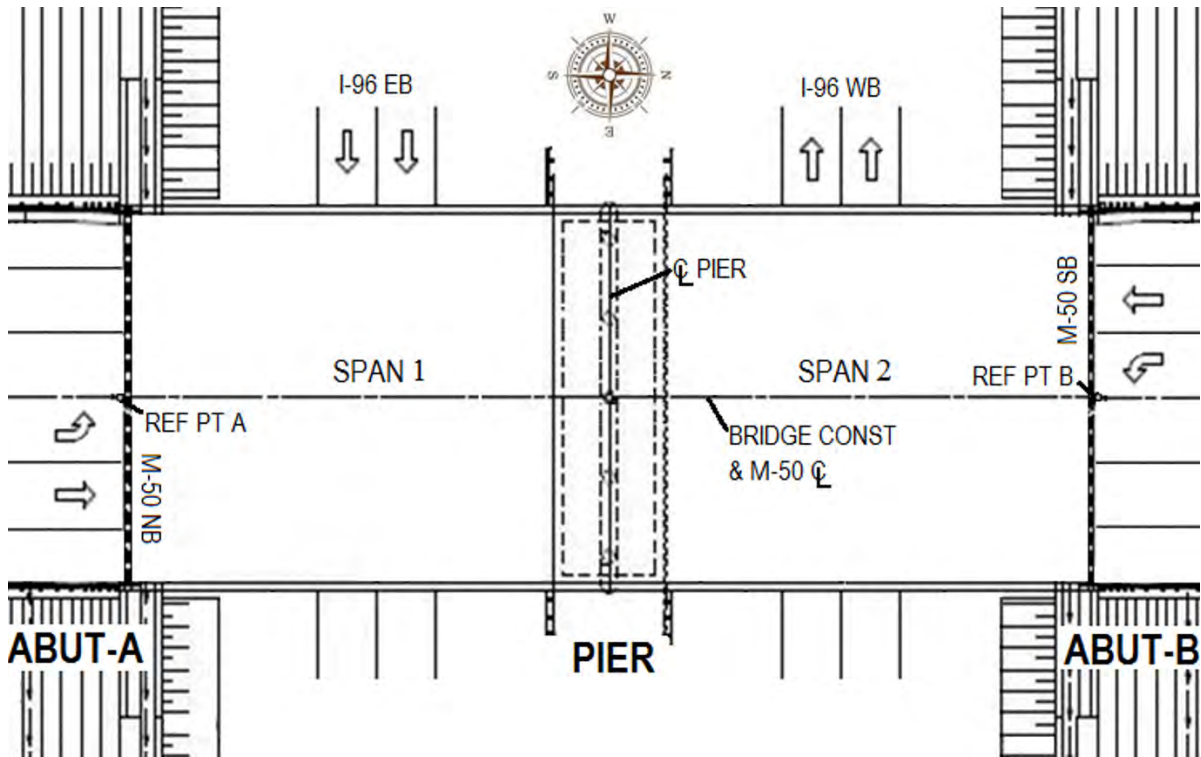


Figure 6-59. Plan of the new bridge

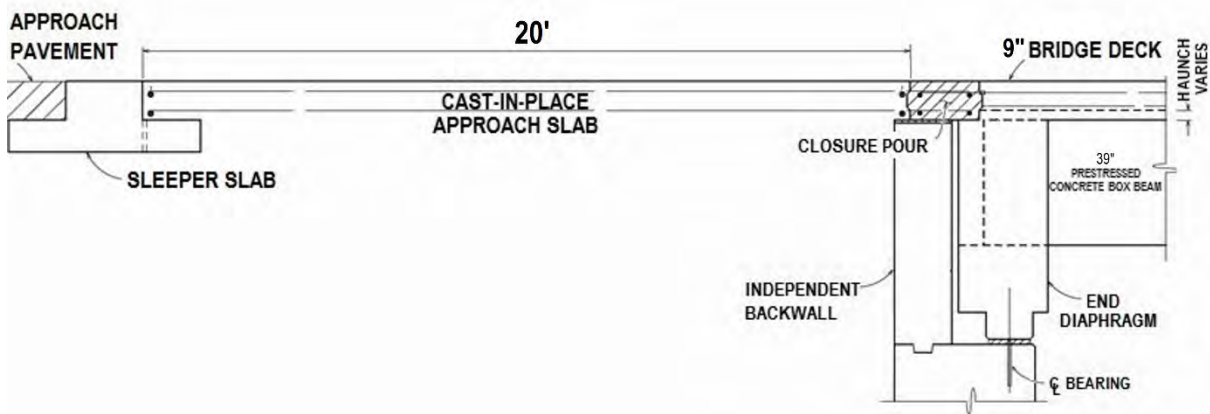


Figure 6-60. Section through approach slab and abutment with superstructure at final location

6.3.2.3 Bridge Construction and Maintenance of Traffic

The new superstructure was constructed on a temporary substructure on the west side of the old structure and adjacent to the permanent alignment of the bridge. The temporary substructure consisted of temporary abutments (abut-A and abut-B) and pier (Figure 6-61). The temporary substructure was built so that the new abutments and pier are aligned. The piles for the temporary substructure were specified to be at least 20 ft 4 in. away from the old structure.



Figure 6-61. Temporary structure under construction

Two spans of the new structure were slid using jacking locations at the two abutments and the central pier. At the pier and abutments, the sliding shoes were attached to half-depth precast diaphragms (Figure 6-62). The precast diaphragms were placed on the sliding tracks attached to cast-in-place temporary bents (Figure 6-62). Moreover, the temporary bents were supported on temporary steel piles. The box beam girders were placed on the half-depth precast diaphragms, and the remaining depth of diaphragms was cast-in-place following the move.

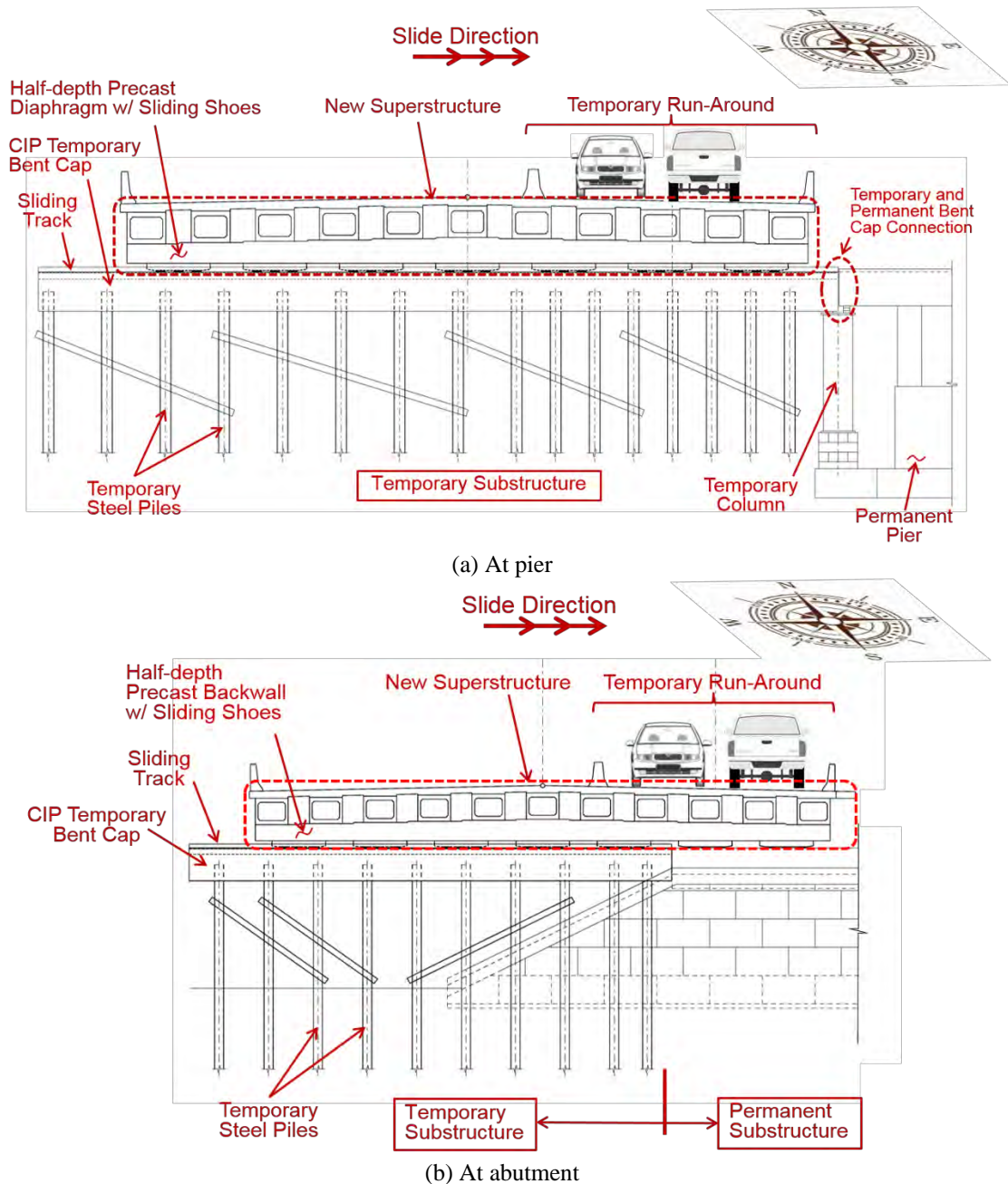


Figure 6-62. Cross-section view of the new superstructure on temporary substructure

The construction staging and maintenance of traffic (MOT) strategies of the project included the following:

- I-96 and M-50 had typical shoulder closures and minor traffic shifts in place for the entire project duration.
- During the bridge demolition and bridge slide, M-50 traffic was detoured to a portion of the new bridge, and only right turns from I-96 EB and WB to M-50 were allowed.

- I-96 was closed for two weekends with the duration of Friday 9 PM to Monday 5 AM. During the closure, I-96 traffic was routed through the M-50 entrance and exit ramps.
- Following the demolition of the old structure, two lanes of traffic were shifted to the new bridge, and M-50 was reopened (i.e., the new superstructure on temporary substructure was used as a temporary run-around).

Both lanes of I-96 EB and WB remained open except during the aforementioned durations. For M-50 traffic, a two-lane detour (one for each direction) was constructed over the new superstructure on temporary substructure, as a “temporary run-around” (Figure 6-62, and Figure 6-63). The temporary bridge approaches for the run-around were 25 ft long and 3.25 ft wide transversely posttensioned precast deck panels. The panels were supported by the end diaphragms of the new superstructure on one end and a temporary sleeper bent on the other end (Figure 6-64).



(a) Temporary run-around in preparation



(b) Temporary run-around ready for traffic
Figure 6-63. Temporary run-around



Figure 6-64. New superstructure at temporary location with temporary run-around in-place

Dowel bars connected precast panels to the end diaphragms and the sleeper bent. These dowels were not grouted. Even though the panels were lifted out-of-the-way during bridge slide, the contingency plan was to replace the panels and reopen the temporary run-around, in case the slide operation could not be completed as planned.

Temporary substructure was constructed in-line with the permanent substructure as shown in Figure 6-62. Since M-50 traffic was routed over the new superstructure before the move, the temporary substructure was designed according to AASHTO LRFD. The temporary substructure and the permanent abutments were supported on piles, while the permanent pier was supported on a spread footing (Figure 6-65).

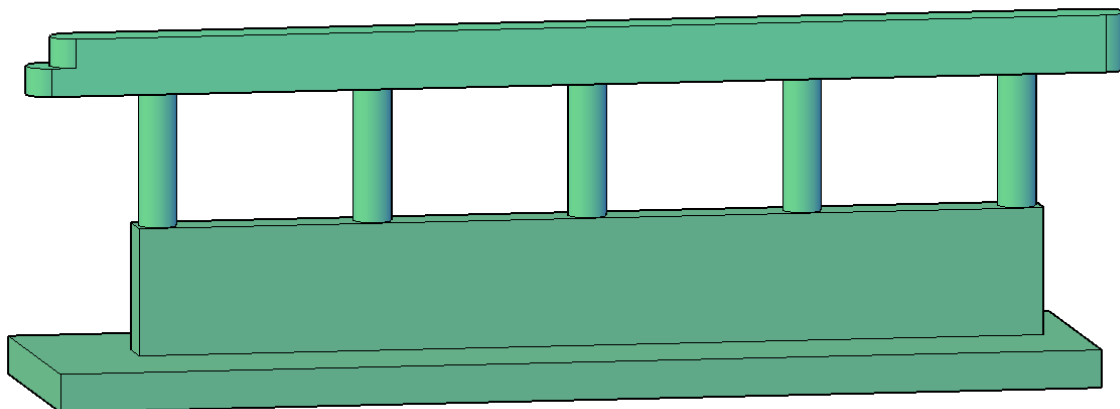


Figure 6-65. M-50 bridge pier

6.3.2.4 Bridge Slide Operation

The total sliding distance of the new superstructure was about 75 ft. Mammoet's skid tracks were utilized for the sliding operation. The skid tracks were anchored to the top of the temporary substructure. The superstructure, consisting of 7 stainless steel sliding shoes, was slid along the tracks directly onto the permanent bearings attached to new abutments and pier. The temporary substructure was accurately aligned with the permanent substructure and connected (Figure 6-66 and Figure 6-67). The transition zone from temporary substructure to permanent pier cap was supported by a temporary steel column as shown in Figure 6-67.



Figure 6-66. Temporary and permanent substructures connected at the abutment



Figure 6-67. Transition zone from temporary substructure to permanent pier cap

Each permanent bearing pad included a Teflon layer on top. The Teflon pads were also used as sliding surfaces inside the skid track and held in place with dowel rods as shown in Figure 6-68. The permanent pier cap included a groove to hold the sliding pads in place (Figure 6-69).



Figure 6-68. Teflon pads in skid track with dowel rods

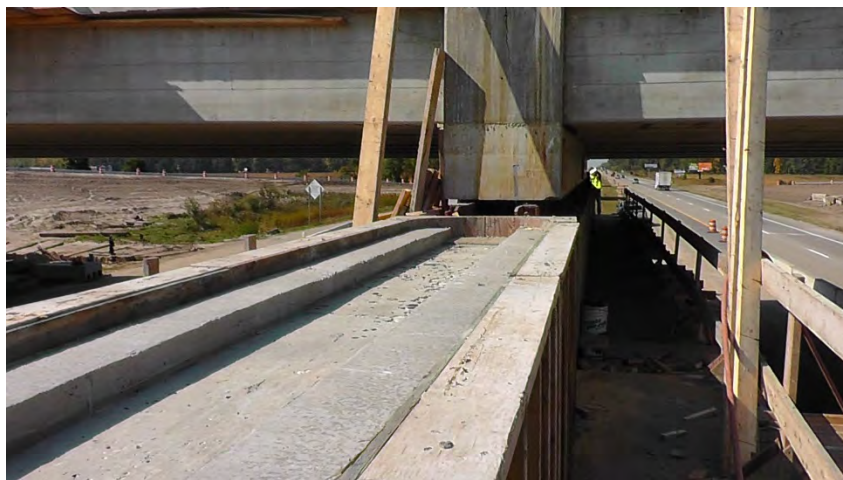


Figure 6-69. Permanent pier cap with a groove to place permanent bearing pads with Teflon layers

During the construction of the new superstructure at a temporary location, the top surfaces of Teflon sliding pads (in the skid tracks) were lubricated with Thermyl-Glyde® synthetic gear oil (commonly known as the Royal Purple). The prime objective of applying Royal Purple was to break the potential locking between the sliding shoes and the Teflon surface; hence, reduce the static friction force (i.e., reduce the breakout force). The force anticipated to overcome the initial static friction (breakout force) was applied using three push jacks (one at each abutment and another at the pier) along with a temporary pull jack at the leading face of the pier diaphragm.

To continue with the slide, three hydraulic push jacks moved the bridge superstructure to the two abutments and the pier. The pushing jacks were aligned along the centerline of the bearings to prevent eccentric loading. Rollers were attached to the superstructure end diaphragms' leading face (Figure 6-70) to maintain the horizontal alignment during the move.



Figure 6-70. Rollers at the end diaphragms' leading face to maintain sliding alignment

The push jack at the pier malfunctioned early during the move and stopped operating. The contractor decided to continue pushing the bridge using the remaining two push jacks, one at each abutment.

Another difficulty encountered during the slide was that the bridge was trying to rotate. Since the skid tracks restrained the rotation, lateral movement could be observed as the bridge moved on the permanent substructure beyond the tracks. Once off the skid tracks, the bearings started exerting pressure to push the substructure to the north side. In particular, it whenever a sliding shoe approached the transition (i.e., moving from temporary substructure to the permanent pier cap, Figure 6-71), the bridge superstructure was pushed northward. This also developed a substantial resistance for the sliding operation. In several instances, the sliding operation was stopped temporarily to lubricate the sidewalls of the skid tracks to reduce friction. The off-alignment deformations of the pier were also measured during the monitoring activity, which will be discussed next in Section 6.3.2.5.

The inability to maintain a precise horizontal alignment during a move is common and should be accounted for in every slide project. This is because of the variability of the friction force that develops on the sliding surfaces on the north and south abutments. With the jacks exerting equal force to the both sliding surfaces, the unequal incremental force developed from the difference with the friction force creates a couple. Depending on the direction of the couple, the front portion of the superstructure is either pushed south or north. In this case, it was pushed north, implying that the friction force over the south sliding surfaces was less than the north sliding surfaces.

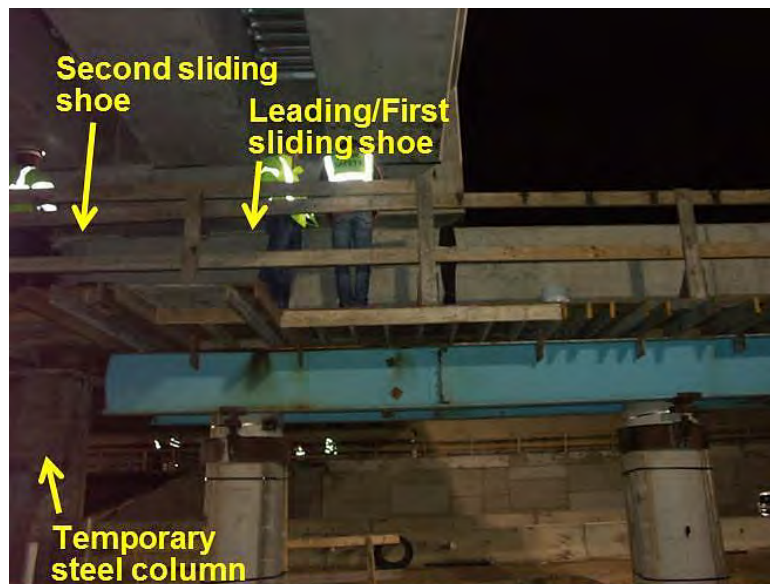


Figure 6-71. The second sliding shoe at the temporary to permanent pier cap connection (transition)

The weather was wet and cold, with below freezing temperatures during the night of the slide. As the night advanced, the temperature further dropped, and the Royal Purple lubricant started to coagulate on the sliding pads. A practical solution, dish washing liquid detergent, was agreed upon and procured from a nearby convenient store to use as a lubricant on the sliding pads. During this time, the slide was interrupted for over one hour.

6.3.2.5 *Monitoring Pier Deformations*

6.3.2.5.1 Equipment and Accessories

The bridge pier supporting the bridge in the middle was constructed over a shallow foundation. A quick analysis indicated that, as the bridge is being moved onto the pier, there might be measurable vertical deformations. The pier was instrumented with high precision crystal targets, and the movement during slide was measured with a *Laser Tracker*, a non-contact laser based equipment (Figure 6-72). The *Laser Tracker* measurement system consists of an Absolute Interferometer (AIFM), which is a combination of laser interferometer (IFM) and Absolute Distance Meter (ADM). According to the AIFM measurement, a half wavelength is $12.60 \mu\text{in}$ ($0.32 \mu\text{m}$). When the number of peak counts and the direction of beam movement are determined, the change in distance can be calculated by multiplying the number of counts with a half wavelength. Thus, the deformations are measured with a sensitivity of $.0000126 \text{ in}$

The ADM measures the absolute distance or a position of a target in a 3D coordinate system. The wavelength of the exiting beam, wave speed through air, and the modulation frequency are substituted into the formula to calculate the absolute distance. Since the wave speed through air is affected by the ambient conditions, temperature, relative humidity, and atmospheric pressure are monitored to perform necessary corrections to the wave speed. The calculation process involves identification of the minimum or null points in the modulated signal. Direct identification of the minimum point of a signal is not possible and requires using wobble measurement technique. The wobble measurement process requires some time as it involves making multiple measurements across a signal to identify the minimum value as the mean of multiple measurements.

Using ADM to calculate the absolute distance to a target is not possible when the target is not stationary. Combining ADM and IFM allows tracking the target in motion; while calculating the minimum point of the modulated moving signal determines the absolute distance. With a data acquisition rate of 3 kHz and an output rate of 1 kHz, the distance is calculated faster than the movement speed of the target. In addition to the AIFM, the *Laser Tracker* consists of high-precision horizontal and vertical angle encoders to measure laser beam orientation with respect to a right-handed coordinate system specific to the tracker. The vertical and horizontal angular resolution is 0.14 arc seconds (i.e., 6.8×10^{-7} radians). Ultimately, coordinates of a target are calculated by knowing the absolute distance to the target and horizontal and vertical angles between the laser beam and the coordinate axes (Attanayake et al. 2012; Ouyang et al. 2005).

Two types of targets (reflectors) are used with the *Laser Tracker* (Figure 6-73). The first one is a 0.5 in. diameter, glass prism reflector made of non-magnetic anodized aluminum; this is mounted in a cradle and attached to any surface with magnets or adhesive. The 0.5 in. reflector has an acceptance angle of $\leq \pm 50^\circ$. The second type is a 1.5 in. diameter red-ring-reflector (RRR) made of surface-hardened magnetic stainless steel. The 1.5 in. reflector has an acceptance angle of $\leq \pm 30^\circ$. The measurements can be performed using 0.5 in. reflectors alone. However, if the *Laser Tracker* cannot locate the 0.5 in. reflectors because of ambient conditions, then the RRR is utilized to direct the laser beam to the 0.5 in. reflectors.



Figure 6-72. Laser Tracker



(a) 0.5 in. glass prism reflectors



(b) 1.5 in. red-ring reflector

Figure 6-73. Laser Tracker targets (reflectors)

The *AT MetroStation* (Figure 6-74), a meteorological station with temperature, humidity and pressure sensors is attached to the tracker. A laptop is used to control the tracker and record the acquired data (Figure 6-75).



Figure 6-74. AT MetroStation

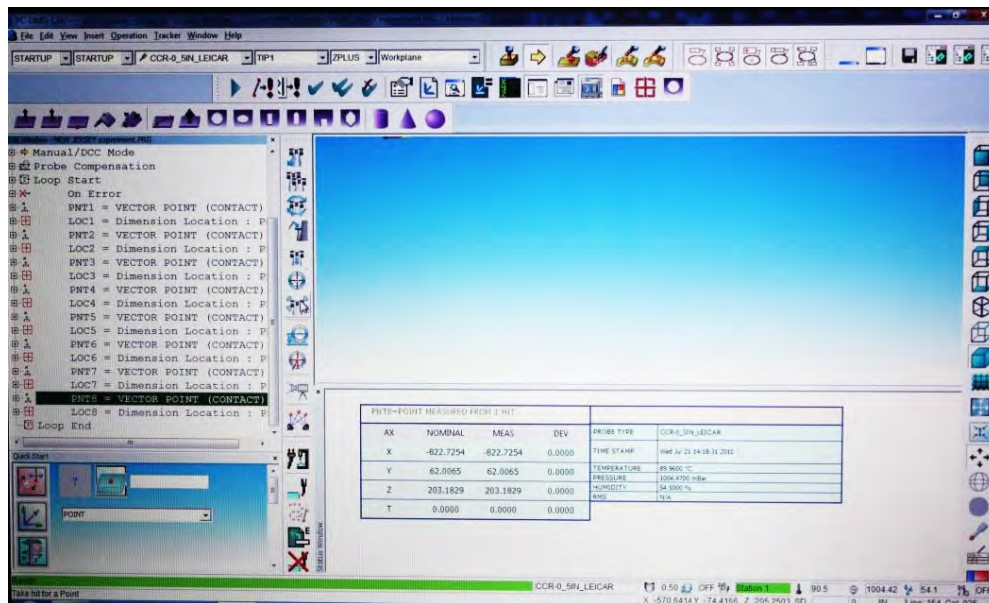


Figure 6-75. GUI to control the Laser Tracker

Monitoring bridge pier movement under the sliding forces requires mounting the targets on the bent cap or the columns. Magnetic bases with removable bolts mounted the reflectors on the pier-columns (Figure 6-76). Hot glue adheres to the bolt-heads. This specific mounting method provides the flexibility needed to orient the reflector towards the *Laser Tracker* after

mounting on a structure. In most applications, it is useful to define a structure specific coordinate system and use it as the reference coordinate system for all the measurements.



Figure 6-76. A reflector and a magnetic base

6.3.2.5.2 Reflectors and Equipment Setup

Reflector locations on five columns were labeled as PC-1, PC-2, PC-3, PC-4, and PC-5 (Figure 6-77 and Figure 6-78). First, metal plates were attached to each column using clamps and industrial strength epoxy adhesive (Figure 6-79). The adhesive was allowed to cure for 24 hours. On the day of the slide, the magnetic bases with reflectors were mounted on the metal plates (Figure 6-79).

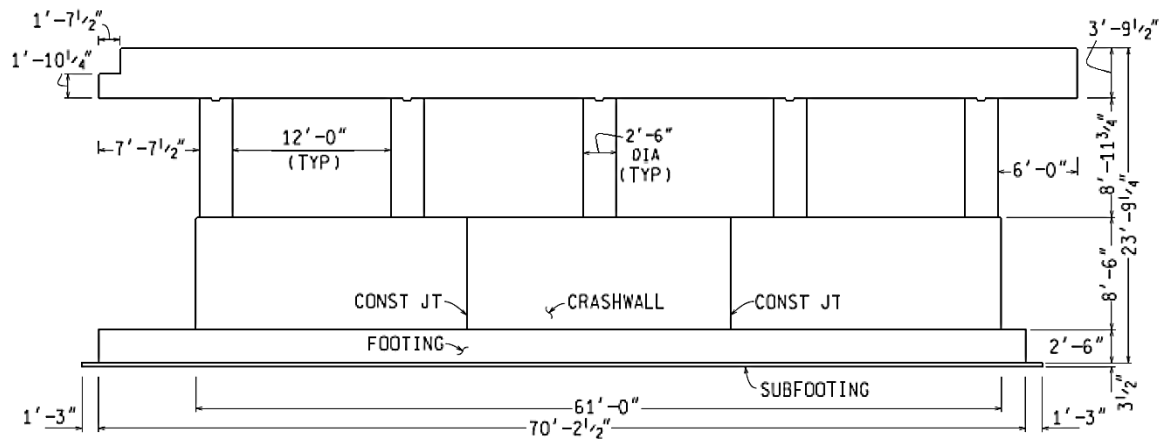


Figure 6-77. Elevation of the pier

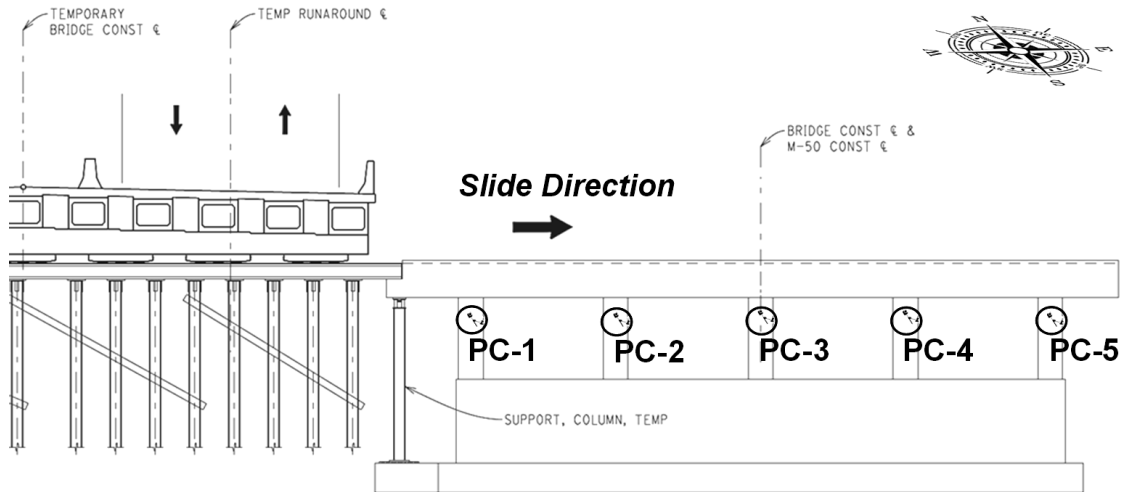


Figure 6-78. Labels of the measurement locations with respect to slide direction



Figure 6-79. Metal plates to attach magnetic bases with reflectors

The *Laser Tracker* was located with a view of all targets but away from the active construction zone and about 150 feet away from the targets (Figure 6-80). Before the slide, position coordinates of all the reflectors were measured with respect to the *Laser Tracker* coordinate system, and a structure specific coordinate system was defined.

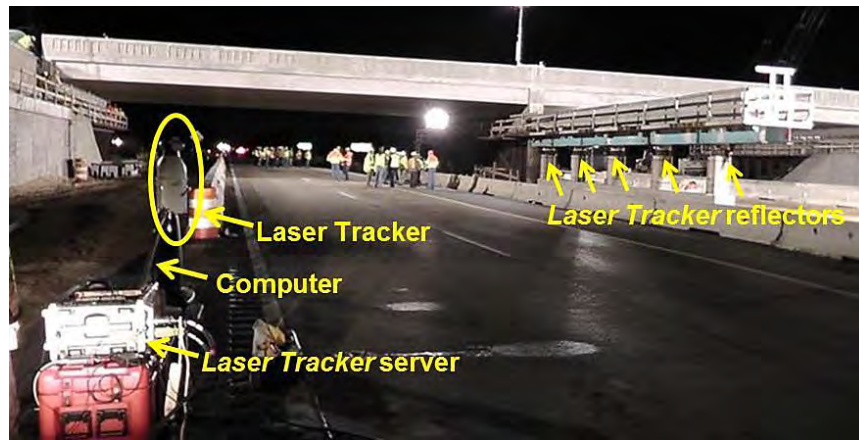


Figure 6-80. Laser Tracker, controller, and computer near the site

To keep track of pier movement, the following list provides the structure specific coordinate system (Figure 6-81):

4. X-axis → in the direction of slide, i.e., towards East
5. Y-axis → perpendicular to the slide direction, i.e., towards North
6. Z-axis → perpendicular to X-Y plane, i.e., upwards

After defining the coordinate system, and just before slide activity, reference measurements were taken.

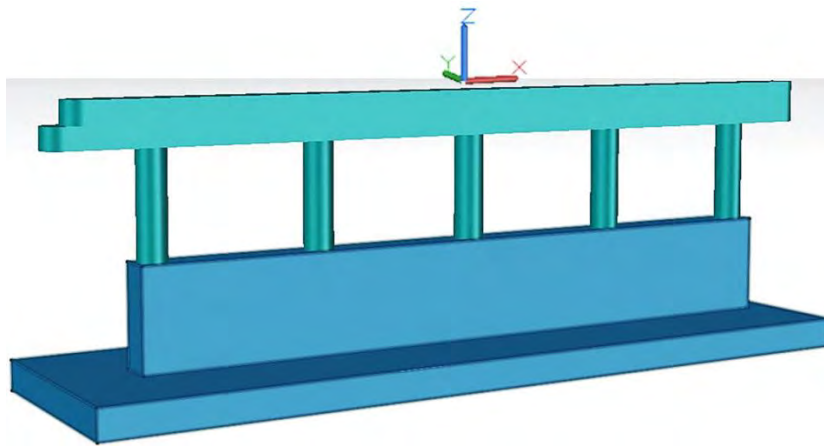


Figure 6-81. Coordinate system defined for pier monitoring

6.3.2.5.3 Data Acquisition

The data collection process was automated using the software and hardware available with the *Laser Tracker*. The automated process first requires manually executing the step-by-step measurement process. Following the manual execution of the measurement process, the *Laser Tracker* directs a laser beam to each target, one at a time, and records position coordinates with respect to the structure specific coordinate system that is defined before starting the data collection process. The laser beam is directed to each target sequentially. This process is repeated multiple times (i.e., called looping) to record a statistically sound data set, for a predefined number of loops. The automated process during bridge slide was designed to make measurements at all 5 targets (PC-1 to PC-5). The slide operation started at 11:59 PM on Oct. 17, 2014. During the measurement, the alignment of the target at PC-3 with the *Laser Tracker* changed; thus, it took longer to identify the target in order to make measurements. To expedite the process, the program was modified to skip the target and make measurements from the remaining targets.

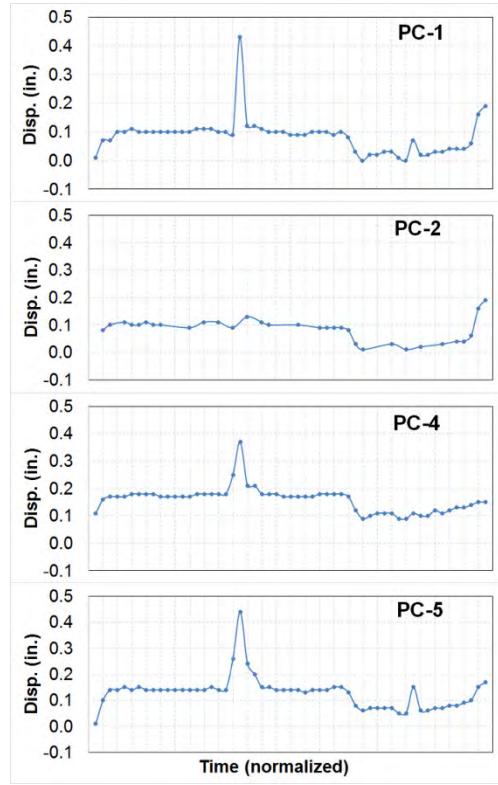
As mentioned in Section 6.3.2.4, the temperature was below freezing, and precipitation occurred during the night of the slide. This affected the measurements, because the laser beam was unable to locate the targets in a few instances. When the sliding was halted for more than an hour, the leading sliding shoe of the superstructure was on top of the fourth column (i.e., with PC-4 target), as shown in Figure 6-82. The *Laser Tracker* data collection was stopped.



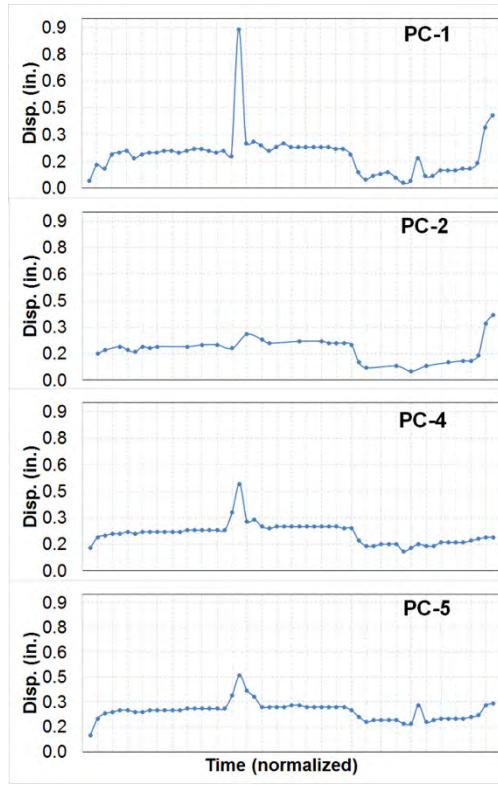
Figure 6-82. Leading sliding shoe at fourth column (*Laser Tracker* observation no. 55)

6.3.2.5.4 Data Processing

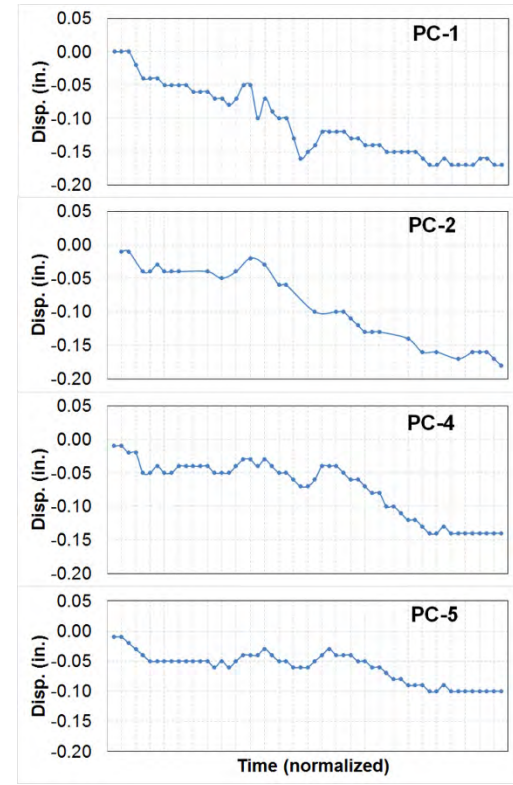
From the measured data, displacement of each target was calculated in X, Y, and Z directions with respect to the structure specific coordinate system. The displacements of PC-1, PC-2, PC-4, and PC-5 targets against time are shown in Figure 6-83.



(a) X-displacement



(b) Y-displacement



(c) Z-displacement

Figure 6-83. Measured displacements against time (a) in the direction of slide (X), (b) transverse to slide (Y), and (c) settlement or uplift (Z)

After evaluating the data presented in Figure 6-83, 18 measurements were identified to plot the displaced shape of the pier with respect to time and to calculate resultant translations and rotations. The observation number, time of observation, and the respective displacements are shown in Table 6–1. Note that a few data points from PC-2 are not available due to corrupted data files.

Table 6–1. Observations Showing Displaced Shape of the Pier

Obs. no.	Time	PC-1 [in.]			PC-2 [in.]			PC-4 [in.]			PC-5 [in.]		
		X	Y	Z	X	Y	Z	X	Y	Z	X	Y	Z
1	11:59 PM (Oct 17, 2014)	0.01	0.04	0.00				0.11	0.13	-0.01	0.21	0.20	-0.01
2	12:04 AM (Oct 18, 2014)	0.07	0.13	0.00	0.08	0.15	-0.01	0.16	0.19	-0.01	0.30	0.30	-0.01
5	12:24 AM	0.10	0.20	-0.04	0.11	0.19	-0.04	0.17	0.21	-0.05	0.35	0.35	-0.04
8	12:41 AM	0.10	0.19	-0.05	0.11	0.19	-0.04	0.18	0.22	-0.05	0.34	0.34	-0.05
16	1:07 AM	0.11	0.22	-0.07	0.11	0.20	-0.05	0.18	0.23	-0.05	0.34	0.36	-0.05
18	1:18 AM	0.10	0.20	-0.07	0.11	0.20	-0.04	0.18	0.23	-0.04	0.34	0.36	-0.05
20	1:24 AM	0.09	0.18	-0.05	0.09	0.18	-0.02	0.25	0.33	-0.03	0.42	0.44	-0.04
21	1:32 AM	0.43	0.89	-0.10				0.37	0.49	-0.04	0.53	0.56	-0.04
22	1:38 AM	0.12	0.25	-0.07	0.13	0.26	-0.03	0.21	0.28	-0.03	0.44	0.47	-0.03
25	1:48 AM	0.10	0.21	-0.10	0.10	0.21	-0.06	0.18	0.24	-0.05	0.35	0.37	-0.05
27	2:15 AM	0.10	0.25	-0.16				0.17	0.25	-0.07	0.34	0.37	-0.06
32	2:32 AM	0.10	0.23	-0.12	0.09	0.22	-0.10	0.18	0.25	-0.04	0.34	0.37	-0.04
38	2:52 AM	0.00	0.05	-0.14	0.01	0.07	-0.13	0.09	0.14	-0.08	0.26	0.28	-0.06
44	3:17 AM	0.00	0.04	-0.16	0.01	0.05	-0.16	0.09	0.13	-0.13	0.25	0.27	-0.09
45	3:21 AM	0.07	0.17	-0.17				0.11	0.15	-0.14	0.35	0.38	-0.10
49	3:37 AM	0.03	0.10	-0.17	0.03	0.10	-0.17	0.11	0.16	-0.14	0.27	0.30	-0.10
52	3:46 AM	0.04	0.11	-0.16	0.04	0.11	-0.16	0.13	0.17	-0.14	0.29	0.31	-0.10
55	3:57 AM	0.19	0.41	-0.17	0.19	0.37	-0.18	0.15	0.19	-0.14	0.37	0.39	-0.10

6.3.2.5.5 Pier Displacements during Bridge Slide

The X-, Y-, and Z- displacements presented in Table 6–1 were used to plot the displaced position of the pier. As an example, the position of the pier at 11:59 PM on October 17, 2014 (with respect to its unloaded position) is shown in Figure 6-84. Similarly, the position of the pier at every observation is given in Appendix G.

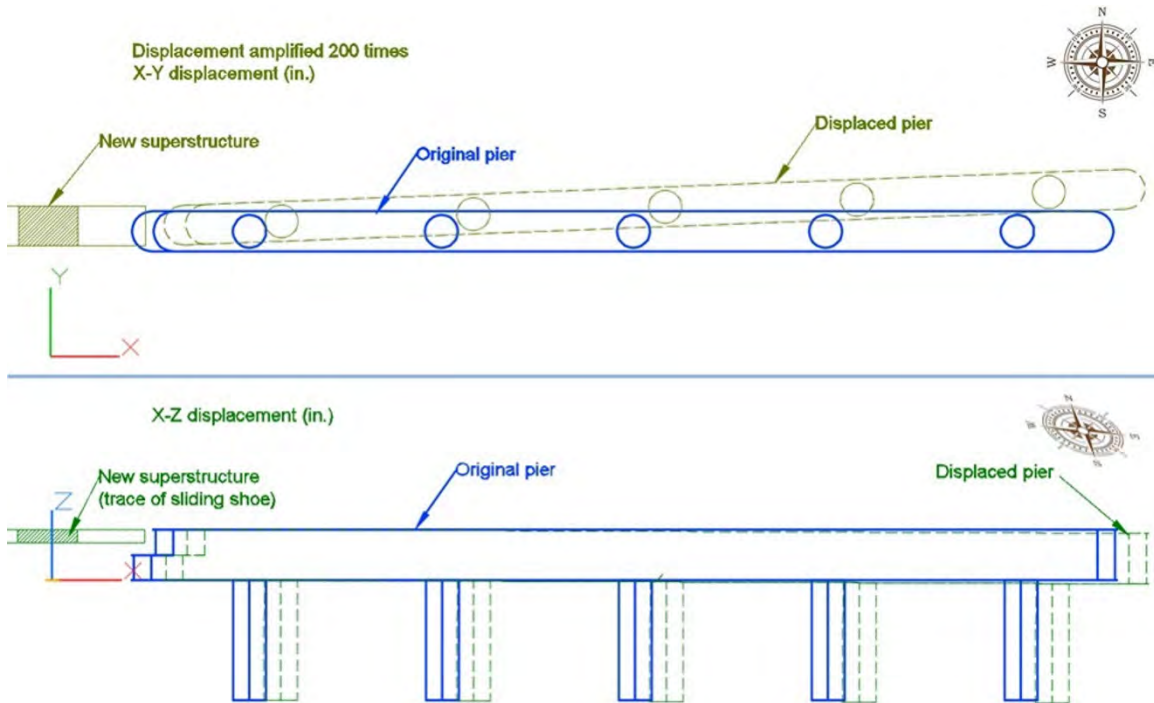


Figure 6-84. Exaggerated displaced position of the pier at time of observation no. 1

The pier is represented as a rigid body. Using the displaced positions of the pier from the 18 observations, the rigid body displacements, similar to Figure 6-85, were plotted for each observation. The rigid body displacements in X, Y, and Z directions (Δ_x , Δ_y , and Δ_z) were calculated for each observation at the centroid of the pier cap as shown in Table 6-2.

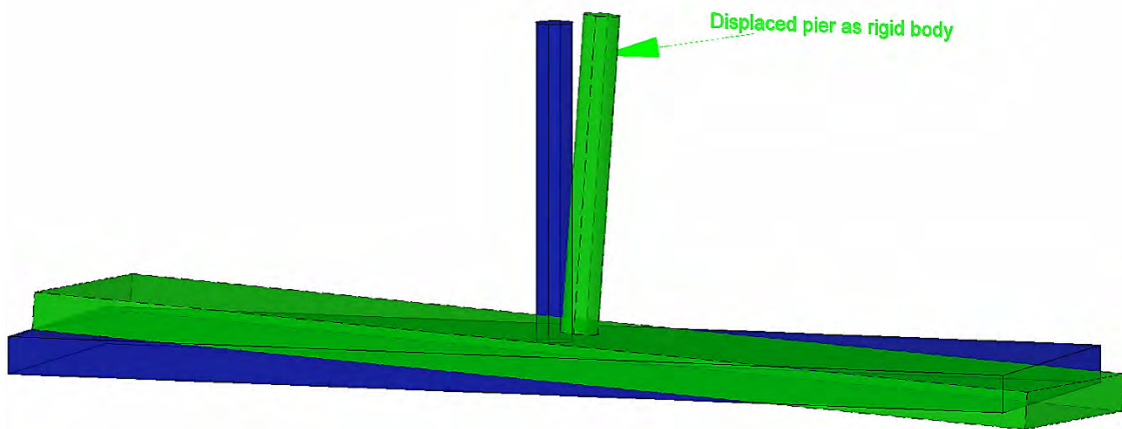


Figure 6-85. Displaced position of the pier as a rigid body

Table 6–2. Rigid Body Displacements of the Pier

Observation No.	Measured Displacement at Centroid			Rotational Direction (+ve or –ve)		
	Δ_x (in.)	Δ_y (in.)	Δ_z (in.)	θ_x	θ_y	θ_z
1	0.14	0.11	-0.01	+ ve	+ ve	– ve
2	0.16	0.17	-0.01			
5	0.19	0.25	-0.05			
8	0.20	0.24	-0.05			
16	0.20	0.26	-0.06			
18	0.19	0.24	-0.05	ve		+ ve
20	0.23	0.27	-0.04			
21	0.43	0.60	-0.06			
22	0.27	0.30	-0.05			
25	0.19	0.25	-0.08			
27	0.19	0.27	-0.11			
32	0.19	0.26	-0.08			
38	0.09	0.13	-0.10			
44	0.09	0.12	-0.14			
45	0.18	0.22	-0.15			
49	0.12	0.16	-0.15	– ve		
52	0.13	0.17	-0.15			
55	0.19	0.34	-0.16			

The rigid body displacements (i.e., Δ_x , Δ_y , and Δ_z) are the resultants of translations of the pier in X, Y, and Z directions (δ_x , δ_y , and δ_z) and rotations of the pier about X- and Y- axes (θ_x , and θ_y) as represented in Eq. 6-1 below.

$$\begin{aligned}
 \Delta_x &= \delta_x \pm \theta_y h \\
 \Delta_y &= \delta_y \pm \theta_x h \\
 \Delta_z &= \delta_z
 \end{aligned}
 \tag{6-1}$$

where: h is the height to the location of reflectors on the pier.

The rotational direction of the pier, positive or negative, was identified from the displaced shapes of the pier and shown in Table 6–2 above. The forces associated with the deformations are unknown. All *Laser Tracker* targets on the pier-columns were at approximately equal heights; thus, the average distance from the footing centroid to the targets can be used for “ h .” The “ \pm ” sign in Eq. 6-1 is included because the pier rotations about X and Y axes can be positive (clockwise) or negative (anticlockwise); the applicable one for a particular observation is taken based on the pier rotation direction identified from the displaced shapes.

6.3.2.6 Estimating Forces Associated with the Measured Pier Deformations

Bridge pier movements were monitored during bridge slide and recorded (see Section 6.3.2.5.5). Then, the pier cap translations and rotations were calculated. Using the pier cap translations and rotations, the force acted on the pier during bridge slide will be estimated. The force on the pier will be estimated from inverse analysis by first calculating the stiffness properties of the soil substrate. The force will then be calculated from the stiffness multiplied by the associated displacement. The methodology and results are described in this section.

6.3.2.6.1 Force – Deformation Relation

The force-deformation (stiffness) relationship is shown in Eq. 6-2, in terms of associated stiffness coefficients (K), translations (δ), and rotations (θ).

$$\begin{Bmatrix} F_x \\ F_y \\ F_z \\ M_x \\ M_y \\ M_z \end{Bmatrix} = \begin{bmatrix} K_{11} & K_{12} & K_{13} & K_{14} & K_{15} & K_{16} \\ K_{21} & K_{22} & K_{23} & K_{24} & K_{25} & K_{26} \\ K_{31} & K_{32} & K_{33} & K_{34} & K_{35} & K_{36} \\ K_{41} & K_{42} & K_{43} & K_{44} & K_{45} & K_{46} \\ K_{51} & K_{52} & K_{53} & K_{54} & K_{55} & K_{56} \\ K_{61} & K_{62} & K_{63} & K_{64} & K_{65} & K_{66} \end{bmatrix} \begin{Bmatrix} \delta_x \\ \delta_y \\ \delta_z \\ \theta_x \\ \theta_y \\ \theta_z \end{Bmatrix} \quad (6-2)$$

As mentioned before, the pier is considered to act as a rigid body. This means that all measured deformations are assumed to be due to the elasticity of the soil. Soil below and around the footing provided the resistance to pier movement and rotation. Also, assuming the stiffness terms in Eq. 6-2 are uncoupled, only the diagonal terms in the stiffness matrix are required to calculate the forces on the pier. Hence, Eq. 6-2 is rewritten as shown in Eq. 6-3.

$$\begin{Bmatrix} F_x \\ F_y \\ F_z \\ M_x \\ M_y \\ M_z \end{Bmatrix} = \begin{bmatrix} K_x & & & & & \\ & K_y & & & & \\ & & K_z & & & \\ & & & K_{\theta_x} & & \\ & & & & K_{\theta_y} & \\ & & & & & K_{\theta_z} \end{bmatrix} \begin{Bmatrix} \delta_x \\ \delta_y \\ \delta_z \\ \theta_x \\ \theta_y \\ \theta_z \end{Bmatrix} \quad (6-3)$$

where: K_x , K_y , and K_z are translational stiffness; K_{θ_x} , K_{θ_y} and K_{θ_z} are rotational stiffness.

From the uncoupled translations, the forces on the pier during bridge slide are as follows:

$$\begin{aligned} F_x &= K_x \delta_x \\ F_y &= K_y \delta_y \\ F_z &= K_z \delta_z \end{aligned} \quad (6-4)$$

The moments about X-axis (M_x) and Y-axis (M_y) result from the forces in Y direction (F_y) and X direction (F_x) respectively. Since the sliding forces are acting on top of the pier cap, the moment arm (H) is the distance from the footing centroid to the top of pier cap. Therefore, from Eq. 6-3, the moments are:

$$\begin{aligned} \rightarrow M_x &= F_y \times H = K_{\theta x} \theta_x \\ \rightarrow M_y &= F_x \times H = K_{\theta y} \theta_y \end{aligned} \quad (6-5)$$

Incorporating Eqs. 6-4 and 6-5 in the Eq. 6-1, Eq. 6-6 is derived:

$$\begin{aligned} \Delta_x &= \frac{F_x}{K_x} \pm \frac{F_x H}{K_{\theta y}} h \\ \Delta_y &= \frac{F_y}{K_y} \pm \frac{F_y H}{K_{\theta x}} h \\ \Delta_z &= \delta_z \end{aligned} \quad (6-6)$$

As shown in Eq. 6-7, Eq. 6-6 is rearranged to represent the forces acting on the pier in X, Y, and Z directions.

$$F_x = \frac{\Delta_x}{\left(\frac{1}{K_x} \pm \frac{Hh}{K_{\theta y}} \right)}; \quad F_y = \frac{\Delta_y}{\left(\frac{1}{K_y} \pm \frac{Hh}{K_{\theta x}} \right)}; \quad F_z = K_z \Delta_z \quad (6-7)$$

As per the Eq. 6-7, K_x , K_y , K_z , $K_{\theta x}$, and $K_{\theta y}$, are required to calculate the forces (F_x , F_y , and F_z) acting on the pier. While Δ_x , Δ_y , and Δ_z are displacements measured during the slide monitoring, K_x , K_y , K_z , $K_{\theta x}$, and $K_{\theta y}$ will be calculated from soil mechanical properties.

6.3.2.6.2 Translational and Rotational Stiffness Formulation

The translational and rotational stiffness coefficients are K_x , K_y , K_z , K_{θ_x} , and K_{θ_y} . Again, the entire pier (footing, columns, and the cap) is assumed as a rigid body, and the movements and rotations of the pier are only due to the elastic deformation of the soil around the footing. The coordinate system and the sign convention for the forces and moments acting on the pier are shown in Figure 6-86.

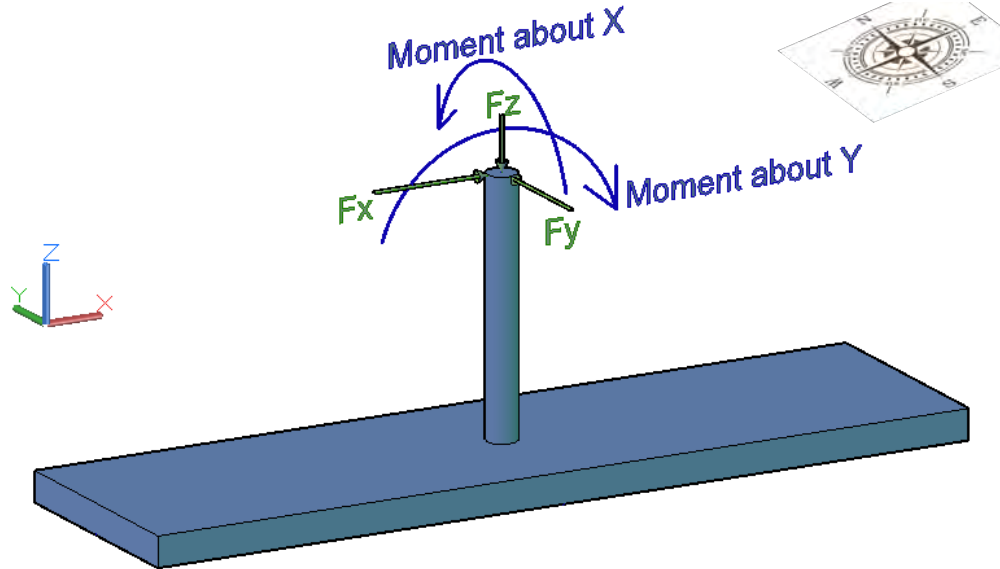


Figure 6-86. Forces and moments on the pier

6.3.2.6.2.1 Translational Stiffness in X-, Y-, and Z Directions

The foundation is embedded in the soil; thus, the translation of the pier, as a rigid body, is the elastic compressibility of the soil in the respective direction. The equation for elastic settlement of a foundation (δ) under a uniform pressure is given below (NCHRP 1991):

$$\delta = \mu_0 \times \mu_1 \times \frac{p \times B}{E} \quad (6-8)$$

where: p is the uniform pressure acting on the soil, B is the width of the footing, E is the undrained modulus of the soil, and μ_0 and μ_1 are the influence factors that depend on the geometric parameters of the foundation.

The Eq. 6-8 is rewritten as follows:

$$\delta = \mu_0 \times \mu_1 \times \frac{\left(\frac{P}{A}\right) \times B}{E} \quad (6-9)$$

where: P is the applied force and A is the cross-sectional area perpendicular to the load.

The Eq. 6-9 can be rearranged to calculate the applied force, P , in terms of δ , as shown below:

$$P = \frac{A \times E}{\mu_0 \times \mu_1 \times B} \times \delta \quad (6-10)$$

By definition, the translational stiffness (K) in the direction of translation (δ) is equal to the force (P) that generates unit translation (i.e., $\delta = 1$). The translational stiffness formulation becomes what is shown below:

$$K = \frac{A \times E}{\mu_0 \times \mu_1 \times B} \times 1 = \frac{AE}{\mu_0 \mu_1 B} \quad (6-11)$$

Eq. 6-11 is used to calculate K_x , K_y , and K_z , by substituting corresponding values for A , B , E , μ_0 , and μ_1 . The soil modulus of elasticity, E , is estimated from the properties of each soil layer and layer thickness. The influence factors (μ_0 and μ_1) in Eq. 6-11 are estimated from charts developed in an NCHRP study and shown in Figure 6-87. The influence factors are based on the length of the footing, L , depth of embedment, D , and H_t which is the least of the distance from bottom of the footing to a very hard strata or four times width ($4B$) (Bowels 1997).

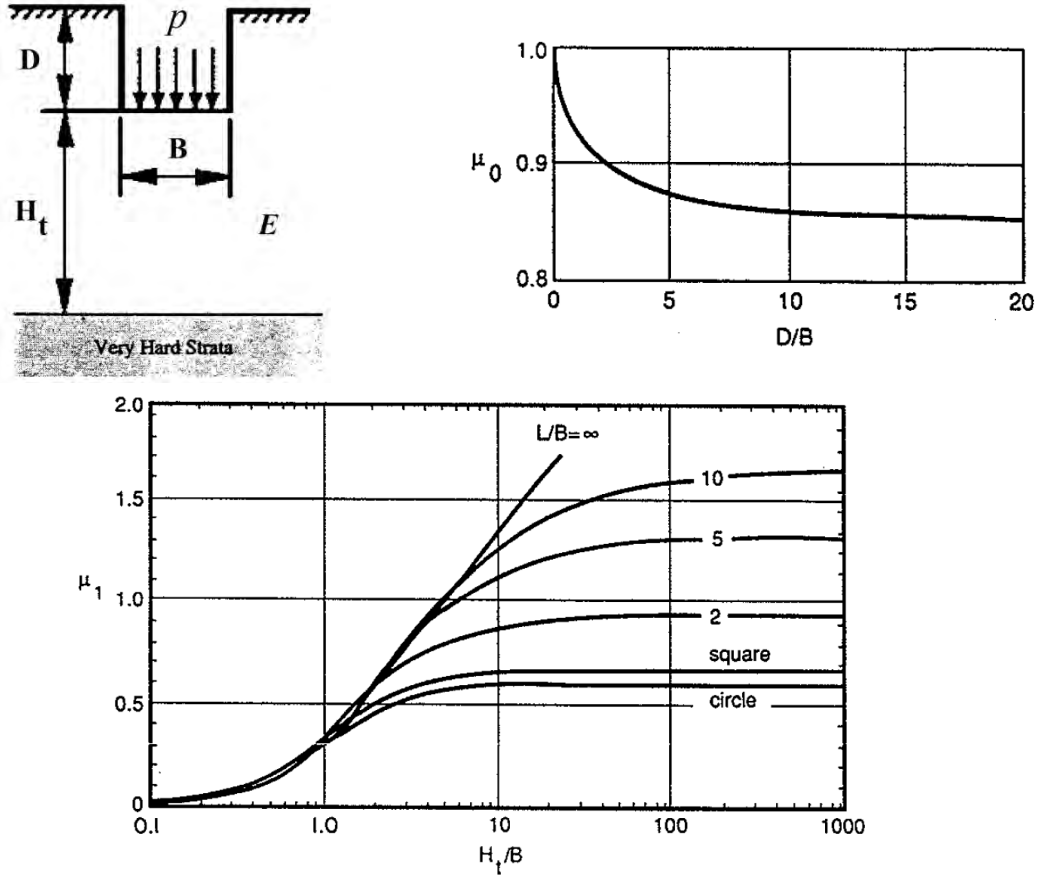


Figure 6-87. Settlement influence factors μ_0 and μ_1 (Source: NCHRP 1991)

6.3.2.6.2.2 Rotational (Rocking) Stiffness about the X-axis (K_{θ_x})

By definition, the rotational stiffness about an axis is the moment that generates a unit rotation about that axis. Thus, the rotational stiffness about the X-axis (K_{θ_x}) is as shown below:

$$K_{\theta_x} = \frac{M_x}{\theta_x} \quad (6-12)$$

where: θ_x is the rotation about X-axis as shown in Figure 6-88.

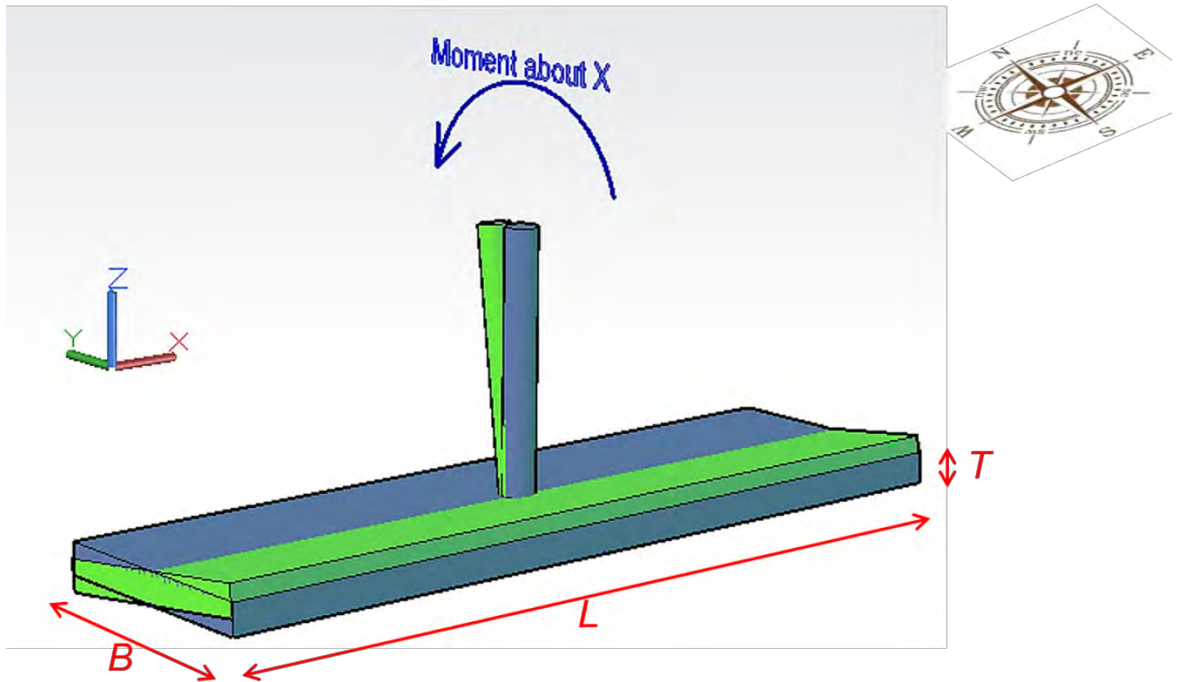


Figure 6-88. Pier rocking about X-axis

The rotation θ_x is represented below:

$$\theta_x = \frac{\delta_N}{B/2} \quad (6-13)$$

where: δ_N is the maximum differential elastic settlement across footing width.

Then, substituting Eq. 6-13 in Eq. 6-12, K_{θ_x} is formulated below:

$$K_{\theta_x} = \frac{M_x \times B/2}{\delta_N} \quad (6-14)$$

The foundation rotation about X-axis develops a linear pressure distribution on the soil. Therefore, the settlement expression for the shallow foundations subjected to eccentric loading is used (Algin 2009).

The settlement expression is based on Hooke's Law and linear pressure distribution as shown in Figure 6-89. Also, the expressions for special cases where an edge of the shallow foundation undergoes settlement are shown in Figure 6-90.

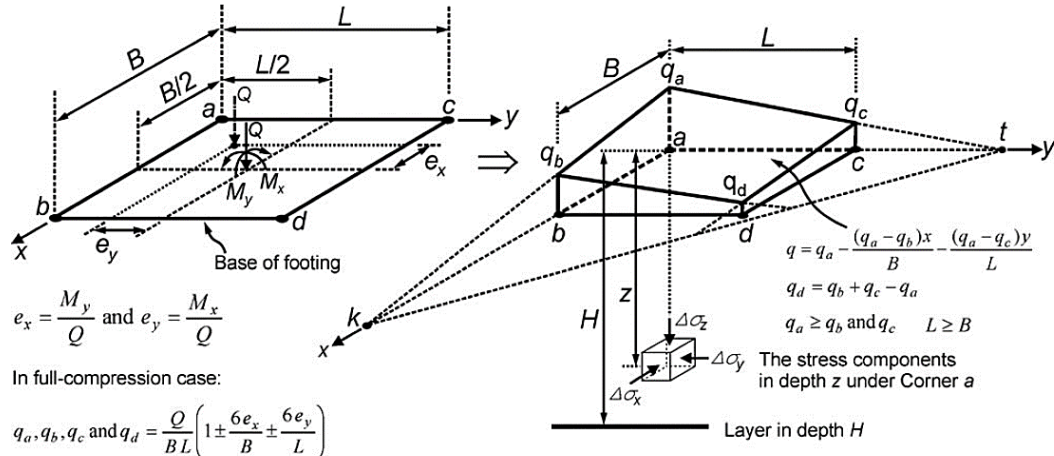


Figure 6-89. Pressure distribution under two-way eccentricity (Source: Algin 2009)

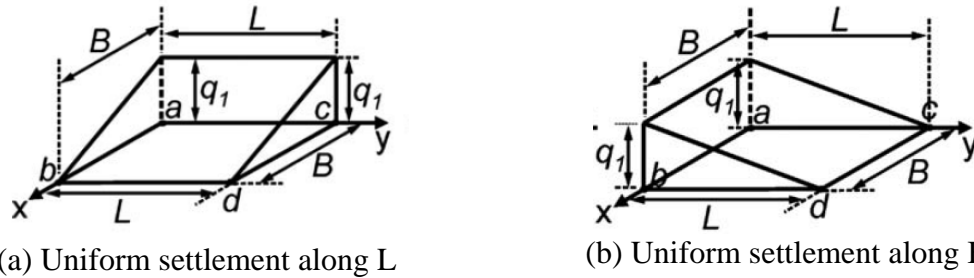


Figure 6-90. Special cases: uniform settlement along an edge of a shallow foundation (Source: Algin 2009)

The foundation settlement due to the moment about the X-axis is similar to the case in Figure 6-90a. The settlement expression for this case is given below (Algin 2009):

$$\delta_N = \frac{B q (1+\nu)}{E m (2\pi)} \left\{ \begin{array}{l} (1-2\nu)mn \tan^{-1}(u_5) + \nu n^2 \ln(u_6) \\ + (1-\nu) \left[1 - u_2 + m^2 \ln(u_8) + 2m \ln(u_9) \right] \end{array} \right\} \quad (6-15)$$

where: B is footing width, q is the stress, ν is Poisson's ratio of soil, E is soil modulus of elasticity, $m = L/B$, L is footing length, $n = H/B$, H is the least of depth to a very hard strata H_t or four times width ($4B$), and the u parameters are defined in the relations below:

$$u_m = \sqrt{1+m^2}; \quad u_n = \sqrt{1+n^2}; \quad u_1 = \sqrt{1+m^2+n^2};$$

$$u_2 = u_m + u_n - u_1; \quad u_3 = \sqrt{m^2+n^2}; \quad u_4 = u_m + u_3 - u_1; \quad u_5 = \frac{m}{nu_1}; \quad u_6 = \frac{u_3(1+u_n)}{n(1+u_1)};$$

$$u_7 = \frac{u_n(m+u_3)}{n(m+u_1)}; \quad u_8 = \frac{u_3(1+u_m)}{m(1+u_1)}; \quad u_9 = \frac{u_n(m+u_m)}{(m+u_1)}; \quad u_{10} = \frac{nu_n}{(u_1-m)(m+u_3)}$$

The pressure distribution on the soil is calculated considering M_x or the product of P and eccentricity e_x (Figure 6-89) as shown below:

$$q = \frac{P}{BL} \left(\frac{6e_x}{B} \right) = \frac{6M_x}{B^2L} \quad (6-16)$$

The rotational stiffness about the X-axis (K_{θ_x}) is calculated by substituting Eq. 6-15 and 16 for Eq. 6-14, and rearranging the terms as shown below:

$$K_{\theta_x} = \frac{E B^2 L m \pi}{6 (1+\nu) \left\{ \begin{array}{l} (1-2\nu)mn \tan^{-1}(u_5) + \nu n^2 \ln(u_6) \\ + (1-\nu) \left[1 - u_2 + m^2 \ln(u_8) + 2m \ln(u_9) \right] \end{array} \right\}} \quad (6-17)$$

6.3.2.6.2.3 Rotational (Rocking) Stiffness about the Y-axis (K_{θ_y})

The rotational stiffness about the Y-axis (K_{θ_y}) is the moment that generates unit rotation about the Y-axis, as shown below:

$$K_{\theta_y} = \frac{M_y}{\theta_y} \quad (6-18)$$

where: θ_y is the rotation about Y-axis as shown in Figure 6-91.

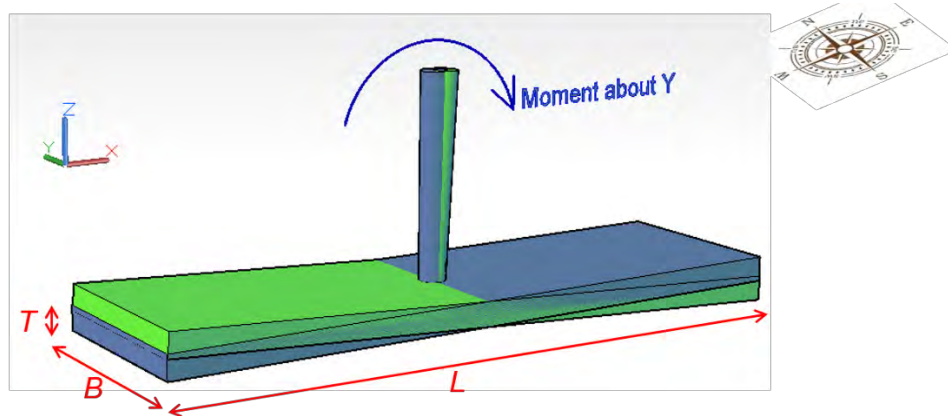


Figure 6-91. Pier rocking about Y-axis

The rotation θ_y is calculated using Eq. 6-19 as shown below:

$$\theta_y = \frac{\delta E}{L/2} \quad (6-19)$$

where: δE is the maximum differential elastic settlement across footing length.

Thus, substituting Eq. 6-19 in Eq. 6-18, $K_{\theta y}$ is calculated as shown in Eq. 6-20 below:

$$K_{\theta y} = \frac{M_y \times L/2}{\delta_E} \quad (6-20)$$

The foundation rotation formulation and the associated stiffness relation derivation are similar to the derivation shown above for rotation about X-axis. Again, the corresponding settlement expression is derived as follows (Algin 2009):

$$\delta_E = \frac{B q (1 + \nu)}{2 E \pi} \left\{ \begin{array}{l} (1 - 2\nu)n \tan^{-1}(u_5) + \nu n^2 \ln(u_7) \\ + (1 - \nu)[m(m - u_4 + 2 \ln(u_8)) + \ln(u_9)] \end{array} \right\} \quad (6-21)$$

where: the variables are defined similar to Eq. 6-15.

M_y relation with P and eccentricity e_y (Figure 6-89) is then:

$$q = \frac{P}{BL} \left(\frac{6e_y}{L} \right) = \frac{6M_y}{BL^2} \quad (6-22)$$

The rotational stiffness about the Y-axis ($K_{\theta y}$) is derived below:

$$K_{\theta y} = \frac{E L^3 \pi}{6 (1 + \nu) \left\{ \begin{array}{l} (1 - 2\nu)n \tan^{-1}(u_5) + \nu n^2 \ln(u_7) \\ + (1 - \nu)[m(m - u_4 + 2 \ln(u_8)) + \ln(u_9)] \end{array} \right\}} \quad (6-23)$$

The geometric parameters of the pier footing and the soil properties below the foundation are used to calculate the parameters in Eqs. 6-17 and 6-23.

6.3.2.6.3 Geometric and Geotechnical Parameters for Stiffness Formulation

From M-50 bridge plans, the length (L), width (B), and thickness (T) of the pier footing are 70.2 ft, 19.5 ft, and 2.5 ft, respectively. From the project geotechnical report, the boring test holes TH103 and TH108 were the closest to the pier as shown in Figure 6-92. The property data from these boring logs (Figure 6-93 and Figure 6-94) is utilized. The base of the pier spread footing is at an elevation of 831 ft, and very dense sand stratum is indicated at an elevation of 808 ft. The soil properties above the elevation of 808 ft will be controlling the stiffness expressions.

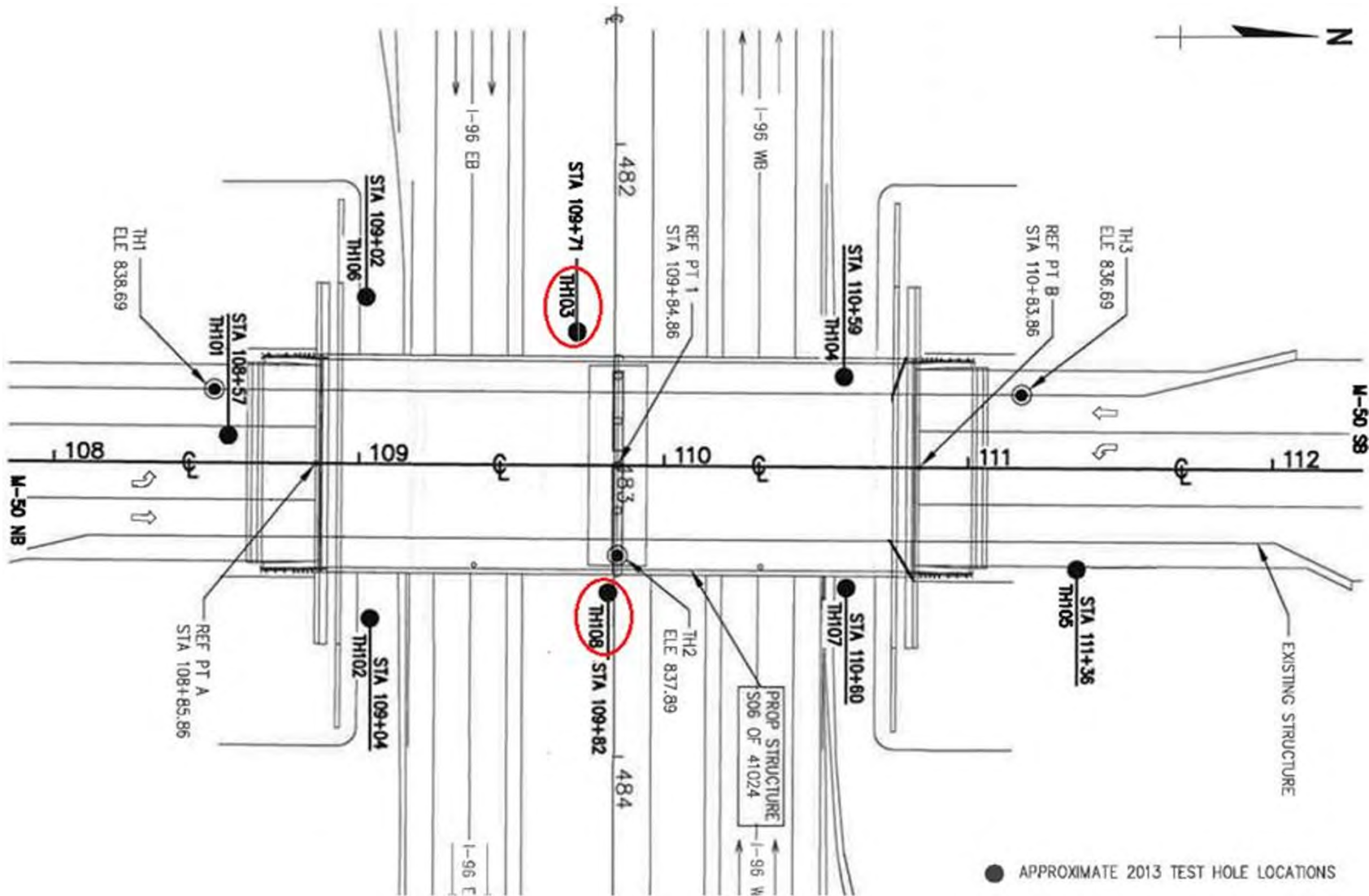


Figure 6-92. Test hole locations at the M-50 bridge site



Ground Surface

BORING TH108 LOG

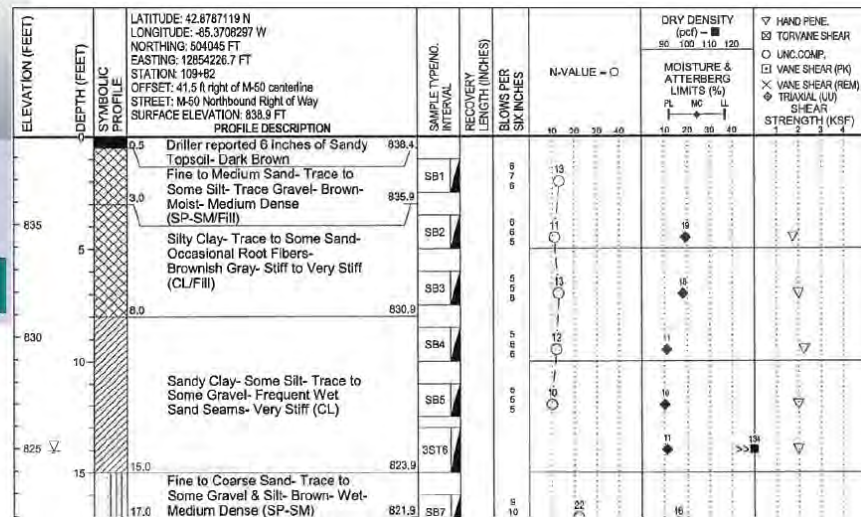


Figure 6-94. Pier and boring TH 108 log

6.3.2.6.4 Influence Factors for Settlement

The length (L) and width (B) of the footing for the Z direction settlement (δ_z) are 70.2 ft and 19.5 ft, respectively. Thus, the affected cross-sectional area A is 1368.9 ft². The footing is 8 ft below the ground surface; hence, $D = 8$ ft. Also, H_t is the least of the distance from the base of footing to very dense stratum (i.e., |EL. 831 – EL. 808| = 23 ft) and 4B (i.e., 4×19.5 = 78 ft). Based on this data, the influence factors (μ_0 and μ_1) in Eq. 6-11 for K_z are estimated from charts in Figure 6-87 as shown below (Figure 6-95):

$$\frac{D}{B} = \frac{8}{19.5} = 0.4; \quad \frac{H_t}{B} = \frac{23}{19.5} = 1.2; \quad \frac{L}{B} = \frac{70.2}{19.5} = 3.6 \quad (6-24)$$

$$\therefore K_z \rightarrow \mu_0 = 0.95; \quad \mu_1 = 0.32$$

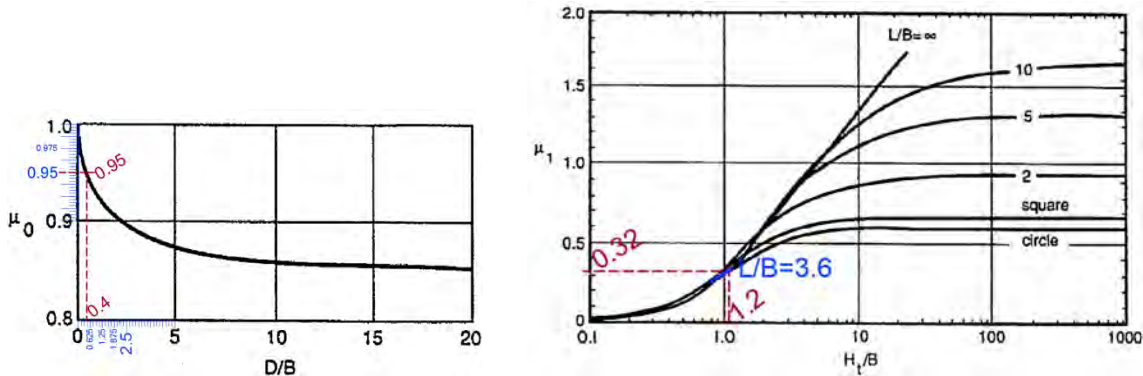


Figure 6-95. Influence factors for K_z

6.3.2.6.5 Influence Factors for X-translation

The length (L) and width (B) of the footing for calculating the stiffness coefficient for X-translation (δ_x) are 19.5 ft and 2.5 ft, respectively. In this case, the embedment length, D, is taken as zero (0 ft) because of the unbraced cut above the footing, and H_t is taken as least of the distance to the hard stratum (i.e., ∞) and 4B (i.e., 4×2.5 = 10 ft). Based on this data, the influence factors in Eq. 6-11 for K_x are estimated below from charts in Figure 6-87:

$$\frac{D}{B} = \frac{0}{2.5} = 0; \quad \frac{H_t}{B} = \frac{10}{2.5} = 4; \quad \frac{L}{B} = \frac{19.5}{2.5} \approx 7.5 \quad (6-25)$$

$$\therefore K_x \rightarrow \mu_0 = 1.0; \quad \mu_1 = 0.95$$

6.3.2.6.6 Influence Factors for Y-translation

The length (L) and width (B) of the footing for calculating the stiffness coefficient for Y-translation (δ_y) are 70.2 ft and 2.5 ft, respectively. The embedment length, D, is taken as zero (0 ft), and H_t is taken as least of the distance to the hard stratum (i.e., ∞) and 4B (i.e., $4 \times 2.5 = 10$ ft). The influence factors for K_y are estimated below from charts in Figure 6-87:

$$\frac{D}{B} = \frac{0}{2.5} = 0; \quad \frac{H_t}{B} = \frac{10}{2.5} = 4; \quad \frac{L}{B} = \frac{70.2}{2.5} = 28 \quad (6-26)$$

$$\therefore K_y \rightarrow \mu_0 = 1.0; \quad \mu_1 = 0.95$$

6.3.2.6.7 Soil Modulus of Elasticity (E)

The stiffness coefficients are related to soil modulus of elasticity, E. In estimating the modulus of elasticity, the properties of the soil layer below the footing taken from boring logs (i.e., at EL. 831 in Figure 6-93 and Figure 6-94) are:

- Soil type: Sandy clay with some silt (CL/Fill)
- Moisture content (w) = 11%
- Dry density (γ_d) = 146 pcf
- Undrained shear strength (S_u) = 1.75 ksf
- SPT test N-value at the bottom of the footing (i.e., at 8 ft from the ground) = 13

The SPT data was reported for successive 6 in. increments using a 140 lb automatic hammer with a 30 in. drop.

Estimating the soil elasticity modulus is not a straightforward process. Numerous methodologies are presented in the literature resulting in a spectrum of values. Here, two of the methodologies are utilized, and the results are compared.

The first methodology is based on the chart developed by Duncan and Buchignani (1976). For this, Plasticity Index (PI), overconsolidation ratio and undrained shear strength (S_u) of the soil are required. Sandy clay with some silt (CL/Fill) represents the soil below the footing. The project geotechnical gives the liquid limit (LL) and the plastic limit (PL) as 15% and 12%, respectively. Thus, PI is 3%. To account for the variability of moisture

content at the footing, a range for PI needs to be established (i.e., upper bound of PI). To establish the range, Casagrande's plasticity chart shown in Figure 6-96 is used. For the CL soil classification in Figure 6-96, the maximum allowable PI of 38% and the minimum PI from the geotechnical data of 3% are used (Holtz and Konacs 1981).

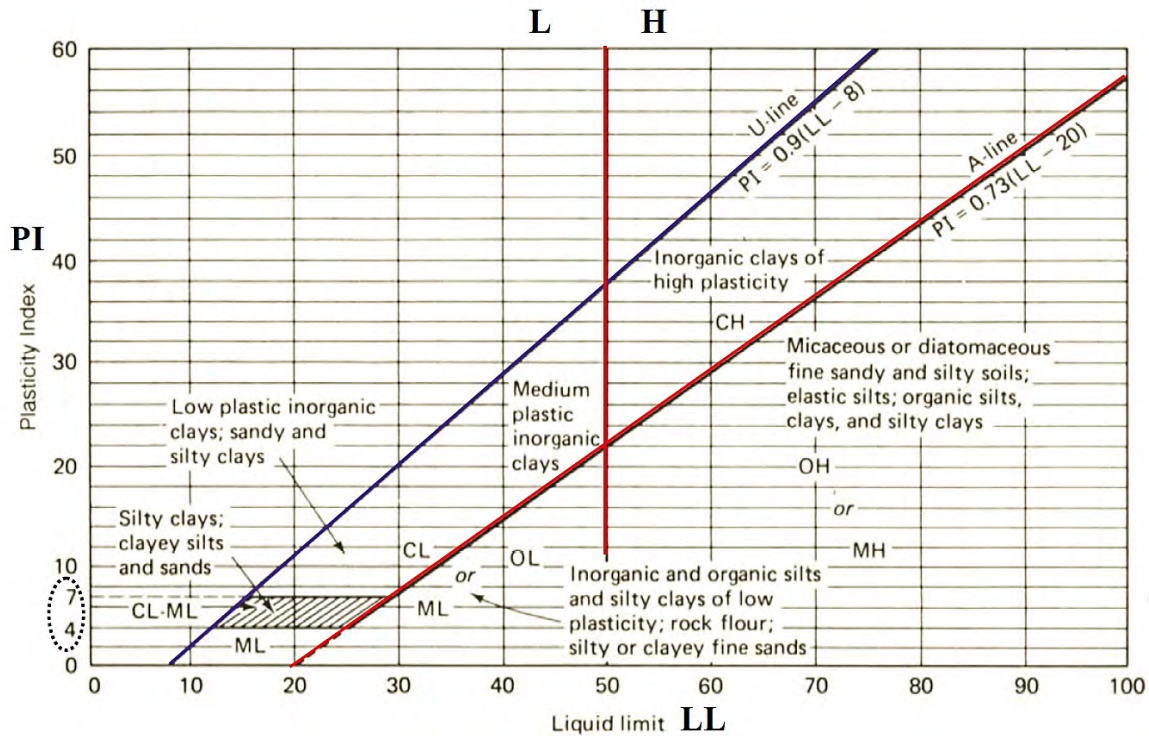


Figure 6-96. Casagrande's plasticity chart (Source: Holtz and Kovacs 1981)

The overconsolidation ratio (OCR) is also needed for estimating the elasticity modulus as formulated below:

$$(OCR) = \frac{\sigma'_c}{\sigma_o} \quad (6-27)$$

where: σ'_c is the preconsolidation pressure, and σ_o is the effective overburden pressure. Preconsolidation pressure (σ'_c) and the overburden pressure (σ_o) of the soil just below the footing are 4500 psf and 1438 psf, respectively giving an OCR value of 3.13. With an OCR of 3.13, the PI_{max} of 38%, and PI_{min} of 4%, the E/S_u ratio was estimated as depicted in Figure 6-97.

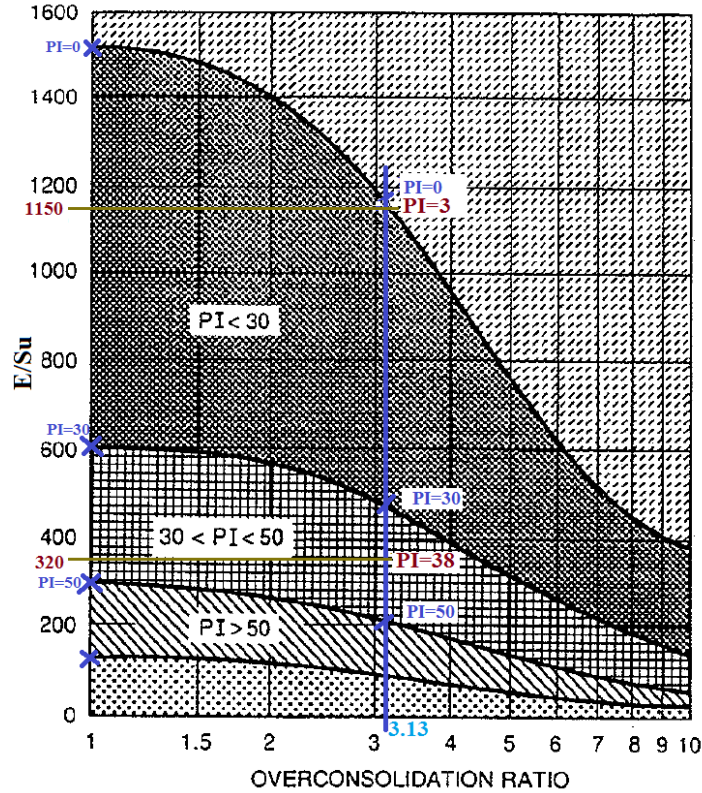


Figure 6-97. E/S_u calculation using PI and OCR (Chart Source: NCHRP 1991)

With an undrained shear strength (S_u) of 1.75 ksf, E_{min} and E_{max} values are calculated as:

$$\begin{aligned} \text{For } PI_{max.} = 38\% \rightarrow \frac{E}{S_u} &= 320 \rightarrow \mathbf{E_{min.(clay)}} = 560 \text{ ksf} \\ \text{For } PI_{min.} = 3\% \rightarrow \frac{E}{S_u} &= 1150 \rightarrow \mathbf{E_{max.(clay)}} = 2013 \text{ ksf} \end{aligned} \quad (6-28)$$

The second methodology for estimating the elasticity modulus is the relation by Bowels (1997) for clayey sand as given below:

$$E = 6.4 (N + 15) \text{ ksf} \quad (6-29)$$

where: N is to be estimated as N_{55}

The use of an automatic hammer provided the SPT data. The *SPT Correction* research report by Aggour and Radding (2001), gives the efficiency of the automatic hammer as around 80%. The boring log data indicates the uncorrected SPT N -value of the soil just below the

footing as 13. This SPT N-value is converted to N_{55} (i.e., SPT N-value for 55% efficiency hammer) as shown below:

$$N_{55} = 13 \times \frac{80}{55} \cong 19$$

Considering that Bowels (1997) proposed Eq. 6-29 for foundation design and assuming a factor of safety of 3, E is estimated below:

$$E_{(clay)} \approx 653 \text{ ksf} \quad (6-30)$$

The modulus estimate is within the range of clay modulus estimated in Eq. 6-28. It is appropriate to assume that the range of E provided in Eq. 6-28 as the soil elasticity modulus range.

As mentioned, boring logs show very dense Fine to Course Sand between EL. 808 ft and EL. 760 ft. The minimum and maximum values of modulus for that soil layer are calculated using the data provided in Bowels (1997) and Subramanian (2010) as shown below:

$$\begin{aligned} E_{\min.(sand)} &\approx 1003 \text{ ksf} \\ E_{\max.(sand)} &\approx 1692 \text{ ksf} \end{aligned} \quad (6-31)$$

The last parameter required to calculate the stiffness coefficients is Poisson's ratio (ν). The Poisson's ratio range for sandy clay is also estimated from the data given in Bowels (1997) and Subramanian (2010) as:

$$\begin{aligned} \nu_{\min.(clay)} &= 0.2 \\ \nu_{\max.(clay)} &= 0.3 \end{aligned} \quad (6-32)$$

Similarly, the Poisson's ratio range for very dense fine to course sand is again estimated as:

$$\begin{aligned} \nu_{\min.(sand)} &= 0.3 \\ \nu_{\max.(sand)} &= 0.4 \end{aligned} \quad (6-33)$$

6.3.2.6.8 Stiffness Coefficients

The soil layer around the footing provides the resistance to horizontal translation of the footing. For this particular footing, the soil layer located in between EL. 831 ft and EL. 833.5 ft is considered for translation in the X-direction. As per the information in the project geotechnical report, the soil type is clay (CL/Fill). Based on the soil properties, footing dimensions, and the influence factors, the K_x range is calculated as follows:

$$K_{x(\min.)} = \frac{AE_{\min.}}{\mu_0 \mu_1 B} = \frac{(19.5 \times 2.5) \text{ ft}^2 \times 560 \text{ k/ft}^2}{1.0 \times 0.95 \times 2.5 \text{ ft}}$$

$$\rightarrow K_{x(\min.)} \cong 958 \text{ k/in}$$

$$K_{x(\max.)} = \frac{AE_{\max.}}{\mu_0 \mu_1 B} = \frac{(19.5 \times 2.5) \text{ ft}^2 \times 2013 \text{ k/ft}^2}{1.0 \times 0.95 \times 2.5 \text{ ft}}$$

$$\rightarrow K_{x(\max.)} \cong 3443 \text{ k/in}$$

Similarly, the soil layer located in between EL. 831 ft and EL. 833.5 ft provides the resistance to translation in the Y-direction. From the soil properties, footing dimensions, and the influence factors, the K_y range is calculated as follows:

$$K_{y(\min.)} = \frac{AE_{\min.}}{\mu_0 \mu_1 B} \cong 3448 \text{ k/in}$$

$$K_{y(\max.)} = \frac{AE_{\max.}}{\mu_0 \mu_1 B} \cong 12396 \text{ k/in}$$

The soil layer below the footing generates the resistance to settlement (i.e., translation in Z-direction) of the footing. In this case, the soil layers are clay, from EL. 837 ft to EL. 808 ft, and sand from EL. 808 ft to EL. 760 ft. Based on the depths of clay and sand layers, and modulus of clay and sand estimated, the effective modulus range is calculated as shown below:

$$E_{(\min.)} = \frac{\sum(E_i Z_i)}{\sum Z_i} = \frac{560 \times 29 + 1003 \times 48}{77} = 836 \text{ ksf}$$

$$E_{(\max.)} = \frac{\sum(E_i Z_i)}{\sum Z_i} = \frac{2013 \times 29 + 1692 \times 48}{77} = 1813 \text{ ksf}$$
(6-34)

From the soil properties, footing dimensions, and the influence factors, the K_z range is calculated as:

$$K_{z(\min.)} = \frac{AE_{\min.}}{\mu_0\mu_1B} \cong 16088 k/in$$

$$K_{z(\max.)} = \frac{AE_{\max.}}{\mu_0\mu_1B} \cong 34888 k/in$$

The pier rotation about the X-axis causes uniform settlement along length L of the footing. In this case, the soil layer below the footing provides resistance to the settlement. Therefore, the settlement formulation from Algin (2009) can be implemented, and K_{θ_x} can be calculated using the formulation derived (Section 6.3.2.6.2.2). Effective modulus and effective Poisson's ratio of the soil layers below the footing need to be considered. Based on the project geotechnical report, the soil layers, clay and sand, are considered and the effective modulus is calculated as shown in Eq. 6-34: i.e., the same as the translation in the Z-direction. Similarly, based on the depths of clay and sand layers, and Poisson's ratio of clay and sand (Section 6.3.2.6.7), the effective Poisson's ratio range is calculated as shown below:

$$v_{(\min.)} = \frac{\sum(v_i Z_i)}{\sum Z_i} = \frac{0.2 \times 29 + 0.3 \times 48}{77} = 0.26$$

$$v_{(\max.)} = \frac{\sum(v_i Z_i)}{\sum Z_i} = \frac{0.3 \times 29 + 0.4 \times 48}{77} = 0.36$$
(6-35)

The variables defined in the δ_N settlement formulation (Eq. 6-15) are calculated using L = 70.2 ft, B = 19.5 ft, and H = 23 ft, as shown in Table 6-3 below:

Table 6-3. Parameter for Estimating Stiffness Coefficients using Algin (2009) Formulation

Parameter	Value
m	3.60
n	1.18
u _m	3.74
u _n	4.22
u ₁	5.55
u ₂	2.41
u ₃	5.46
u ₄	3.65
u ₅	0.16
u ₆	1.06
u ₇	1.02
u ₈	1.10
u ₉	3.39
u ₁₀	0.98

Substituting the effective modulus, effective Poisson's ratio, and variables from Table 6-3 in Eq. 6-17, the K_{θ_x} range is calculated as follows:

$$K_{\theta_x(\text{min.})} = 2.13 \times 10^7 \text{ k-in./rad}$$

$$K_{\theta_x(\text{max.})} = 6.69 \times 10^7 \text{ k-in./rad}$$

The K_{θ_y} is calculated from the formulation derived (Section 6.3.2.6.2.3). The effective modulus and effective Poisson's ratio of the soil layers below the footing is the same as calculated for K_{θ_x} (i.e., Eqs. 6-34 and 6-35). In addition, the variables defined in the δ_E settlement formulation (Eq. 6-21) are the same as shown in Table 6-3.

Substituting the effective modulus, effective Poisson's ratio, and variables from Table 6-3 in Eq. 6-23, the K_{θ_y} range is calculated as:

$$K_{\theta_y(\text{min.})} = 1.47 \times 10^9 \text{ k-in./rad}$$

$$K_{\theta_y(\text{max.})} = 3.71 \times 10^9 \text{ k-in./rad}$$

6.3.2.7 Force Acting on Pier during the Slide

As mentioned earlier, a total of 18 observations from the field measurements were selected for the analysis. For those observations, the range of force components acting on the pier is calculated using Eq. 6-7, and stiffness coefficients are calculated in Section 6.3.2.6.8 and shown in Table 6-4.

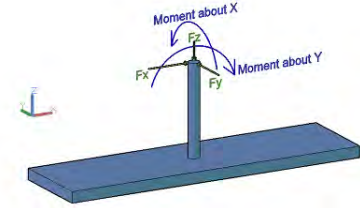


Table 6–4. Force Acting on the Pier during Bridge Slide

Obs. no.	Time	F_x		F_y		R (XY plane)		F_z	
		Min.	Max.	Min.	Max.	Min.	Max.	Min.	Max.
1	11:59 PM (Oct 17, 2014)	85	302	28	91	89	315	-56	-121
2	12:04 AM (Oct 18, 2014)	95	339	45	144	105	368	-82	-178
5	12:24 AM	113	402	65	210	131	454	-363	-794
8	12:41 AM	116	411	61	195	131	455	-400	-874
16	1:07 AM	125	455	66	213	142	503	-473	-1033
18	1:18 AM	120	438	63	203	136	482	-413	-902
20	1:24 AM	145	528	70	225	161	574	-325	-711
21	1:32 AM	271	986	155	501	312	1106	-518	-1131
22	1:38 AM	165	602	77	250	183	651	-403	-881
25	1:48 AM	117	424	64	207	133	472	-605	-1323
27	2:15 AM	116	422	71	228	136	480	-859	-1877
32	2:32 AM	116	423	67	217	134	476	-650	-1421
38	2:52 AM	58	209	33	108	67	236	-834	-1823
44	3:17 AM	55	201	31	100	63	225	-1122	-2451
45	3:21 AM	110	401	57	185	124	442	-1209	-2641
49	3:37 AM	73	266	42	134	84	298	-1225	-2677
52	3:46 AM	79	288	44	143	91	322	-1165	-2546
55	3:57 AM	118	430	87	281	147	514	-1263	-2760

The force components of F_x and F_y are combined to one resultant force applied horizontally to the pier as shown in Table 6–4 as R . Also, F_y in Table 1-4, which is the force acting transverse to the direction of the move, is from the couple formed by the mismatch of friction forces due to the differential friction between the north and south sliding surfaces.

The new superstructure was moved on seven sliding shoes. The first sliding shoe approached the permanent pier at the time of observation 5. At that time, the change in F_z between observations 2 to 5 in Table 6–4, is due to the weight of the superstructure moving on to the pier.

At the time of observation 21, a jump in F_x and F_y may be due to the sliding shoe jammed in the skid track and the pushing force exerted to the pier. The sliding shoe position on the permanent pier was tracked during the field measurements as shown in Table 6–5.

The large variation between lower bound and upper bound forces presented in Table 6–4 is due to the range of estimated E_{min} and E_{max} values. Table 6–5 shows the vertical load on the pier calculated based on the sliding shoe(s) position. For clarity, the modulus of elasticity was back-calculated, as shown in Table 6–5, by using the weight of the new superstructure as it moved onto the pier and the associated measured vertical displacement. The vertical load from new superstructure was calculated from the number of sliding shoes on the pier. It was assumed that all the sliding shoes over the pier equally share the load. From this analysis, the modulus of elasticity estimated for each observation, as shown in Table 6–5 using Eq. 6-36, more or less agrees with the lower bound value calculated from soil boring data:

$$F_z = K_z \Delta_z = \frac{A \times E}{\mu_0 \times \mu_1 \times B} \times \Delta_z$$

$$\rightarrow E = \frac{F_z \times \mu_0 \times \mu_1 \times B}{A \times \Delta_z} \quad (6-36)$$

Table 6–5. Soil Modulus of Elasticity Estimated from Superstructure Weight

Obs. no.	Time	Sliding shoe(s) position on the pier	Load on the pier [F_z] (kips)	Soil modulus of elasticity(ksf)
1	11:59 PM (Oct 17, 2014)	No sliding shoe on the pier.	0	0
2	12:04 AM (Oct 18, 2014)	No sliding shoe on the pier.	0	0
5	12:24 AM	First shoe at the transition, i.e., at the temporary column.	-307.14	351
8	12:41 AM	First sliding shoe completely on the pier before the first pier-column.	-307.14	320
16	1:07 AM	First sliding shoe at the first pier-column.	-614.28	540
18	1:18 AM	Second sliding shoe at the transition, i.e., at the temporary column.	-614.28	619
20	1:24 AM	First sliding shoe just after the first pier-column.	-614.28	785
21	1:32 AM	Second sliding shoe completely on the pier.	-614.28	493
22	1:38 AM	Second sliding shoe at the first pier-column.	-921.42	950
25	1:48 AM	Third sliding shoe at the transition, i.e., at the temporary column.	-921.42	632
27	2:15 AM	First sliding shoe at the second pier-column.	-921.42	446
32	2:32 AM	Fourth sliding shoe at the transition, i.e., at the temporary column.	-1228.56	785
38	2:52 AM	First sliding shoe partly on the third pier-column.	-1228.56	612
44	3:17 AM	Fifth sliding shoe at the transition, i.e., at the temporary column.	-1535.70	569
45	3:21 AM	Fifth sliding shoe completely on the pier.	-1535.70	529
49	3:37 AM	First sliding shoe between third and fourth pier-columns.	-1842.84	625
52	3:46 AM	Sixth sliding shoe at the transition, i.e., at the temporary column.	-1842.84	656
55	3:57 AM	First sliding shoe at the fourth pier-column.	-1842.84	606

The range of vertical load calculated in Table 6–4 is shown in Figure 6-98. Also, the Figure 6-98 shows the vertical load on the pier calculated based on the sliding shoe(s) position.

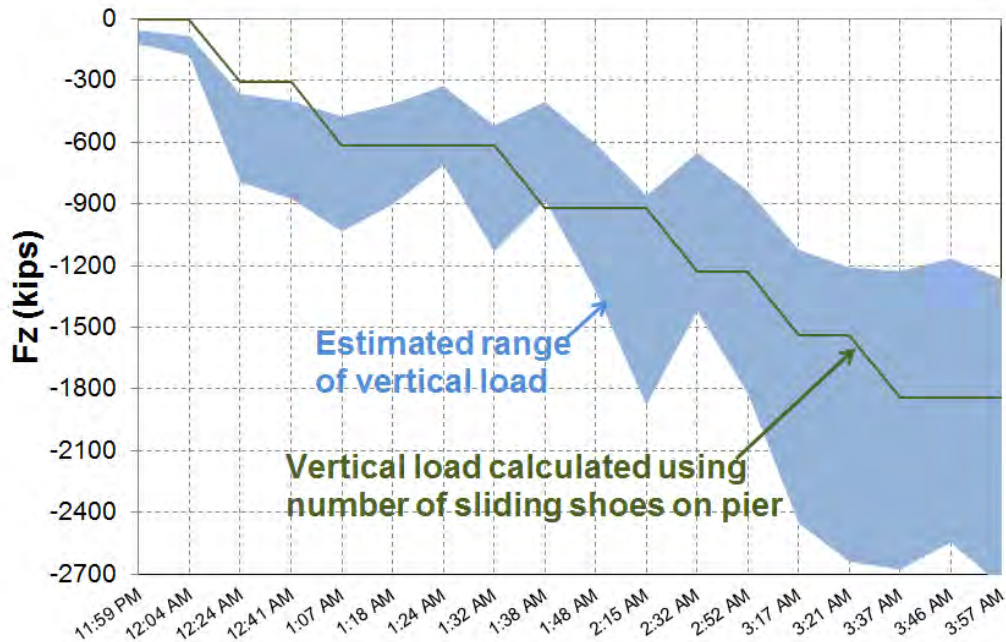


Figure 6-98. Vertical load acting on the pier during bridge slide

At the time of observations 49, 52, and 55, the superstructure was sitting on six sliding shoes on the pier. The vertical load represented by the superstructure weight and the settlements measured were used to estimate a range of soil modulus of elasticity. The estimated elasticity modulus values ranged between 606 ksf to 656 ksf. This range includes the modulus value estimated based on Bowels's (1997) model (i.e., Eq. 6-30, $E = 653$ ksf); furthermore, the maximum value of the range is close to the latter. This validates the elasticity modulus estimates above; thus, the force estimates are updated based on these modulus estimates. The most probable range of forces on the XY plane is shown in Table 6-6 for the group of measurements taken during the monitoring. As seen in Table 6-6, the transverse force developed during the slide was over 350 kips. Again, if the bridge remains in alignment during the move, horizontal force will not develop. However, it is unrealistic to assume that sliding friction will remain equal between the north and south sliding surfaces. The unequal friction coefficient generates unbalanced resistance that forms a couple forcing the superstructure off the alignment. Methods for retaining the slide in alignment will be discussed in Chapter 7.

Table 6-6. The Most Probable Range of Forces in the XY Plane

Obs. no.	Time	F_x (kips)		F_y (kips)		R [XY plane] (kips)	
		Min.	Max.	Min.	Max.	Min.	Max.
1	11:59 PM (Oct 17, 2014)	92	101	29	65	96	120
2	12:04 AM (Oct 18, 2014)	103	113	45	103	113	153
5	12:24 AM	122	135	66	149	139	201
8	12:41 AM	125	138	62	139	139	196
16	1:07 AM	136	145	67	152	151	210
18	1:18 AM	131	139	64	145	145	201
20	1:24 AM	157	168	71	160	173	232
21	1:32 AM	294	313	158	357	334	475
22	1:38 AM	179	191	79	178	196	261
25	1:48 AM	127	135	65	148	142	200
27	2:15 AM	126	134	72	162	145	211
32	2:32 AM	126	135	68	155	144	205
38	2:52 AM	62	67	34	77	71	102
44	3:17 AM	60	64	31	71	68	96
45	3:21 AM	120	127	58	132	133	183
49	3:37 AM	79	84	42	96	90	128
52	3:46 AM	86	92	45	102	97	137
55	3:57 AM	128	137	88	200	156	242

The range of forces acting on the pier in the XY plane during the slide (from Table 6-4) and the most probable range of forces (from Table 6-6) are plotted in Figure 6-99, Figure 6-100, and Figure 6-101.

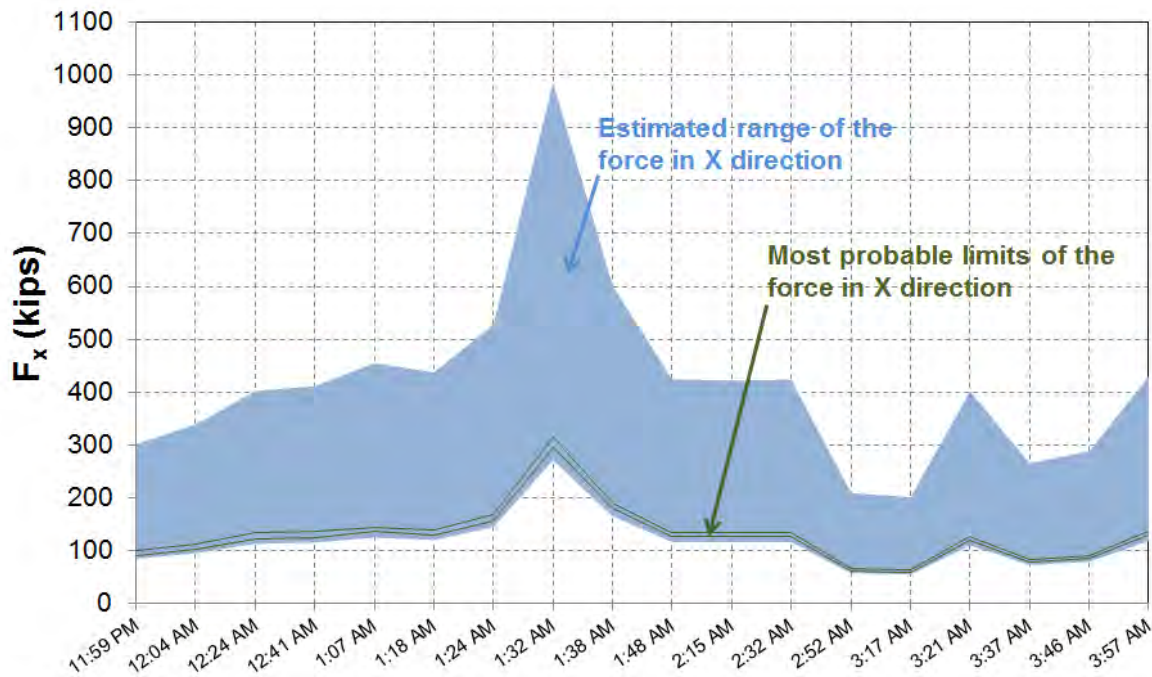


Figure 6-99. Range of force acting on the pier in X direction during bridge slide

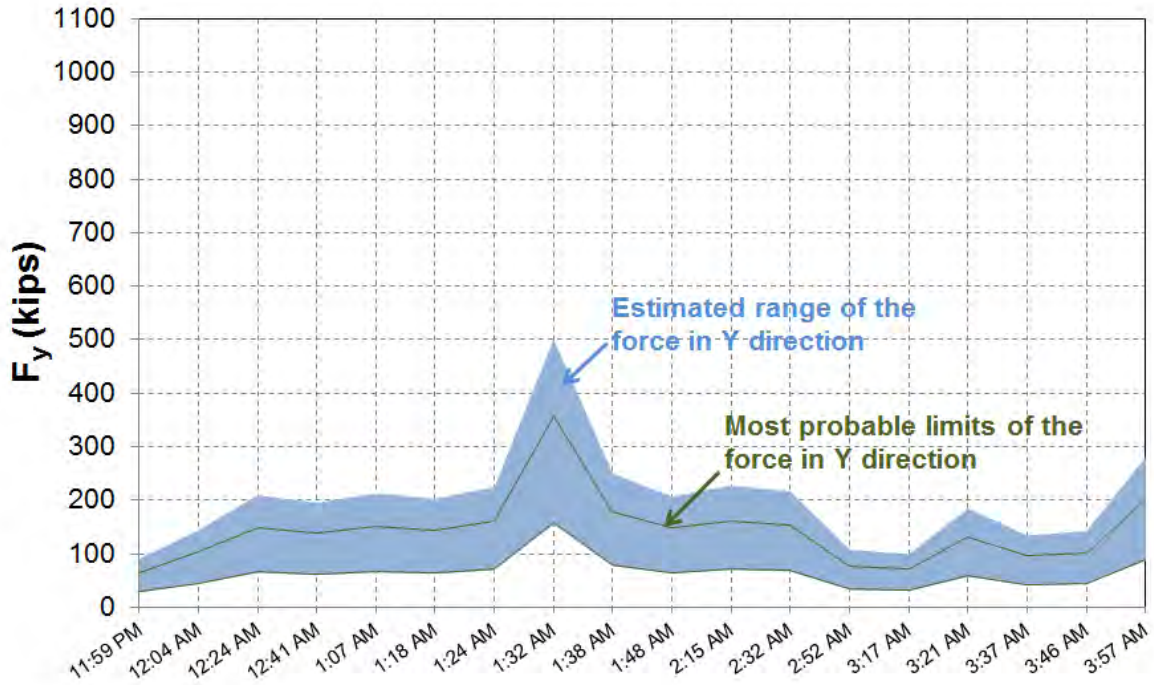


Figure 6-100. Range of force acting on the pier in the Y direction during bridge slide

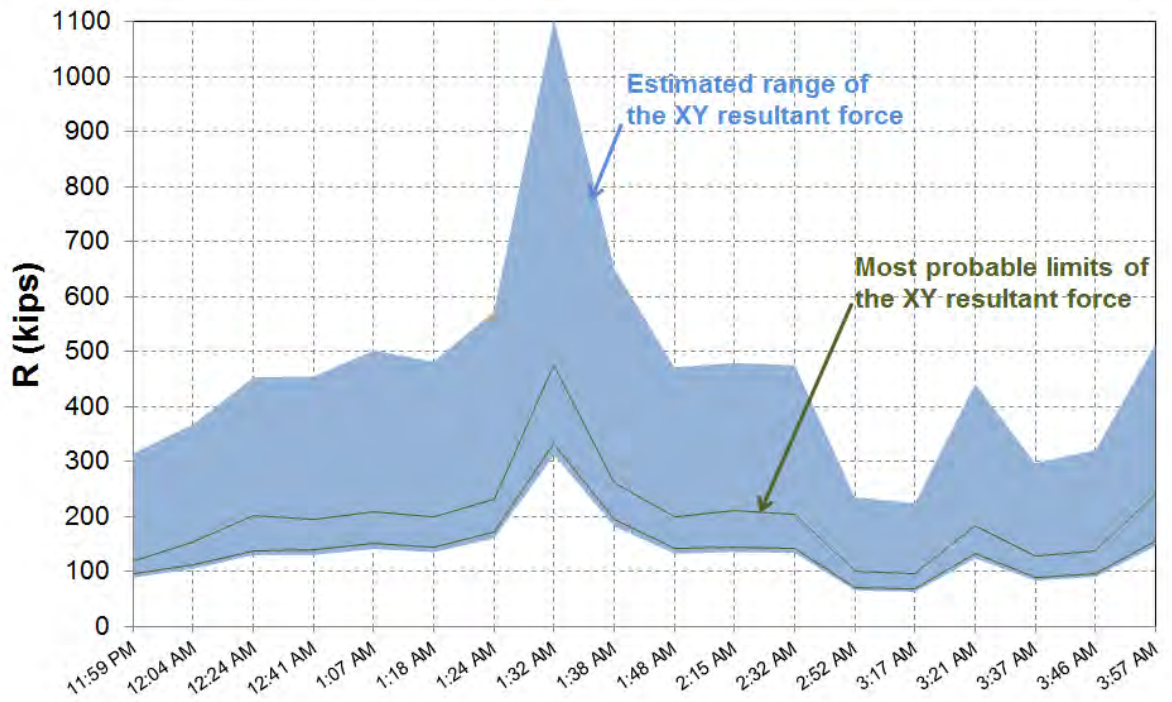


Figure 6-101. Range of the resultant force acting on the pier in the XY plane during bridge slide

6.3.2.8 Conclusions

6.3.2.8.1 Conclusions from the Field Monitoring and Data Analysis

The field measurements and analysis of forces on the pier during the sliding operation demonstrated complexities and shortcomings in the sliding methodology. The M-50 bridge being one of the first slides performed in Michigan, the observed shortcomings are considered among the following lessons learned to improve future slide operations:

- During the move, forces and deformations on the pier were expected in the sliding direction (X direction) because of friction, and in the normal direction (Z direction) due to the weight of superstructure. Monitoring data showed significant transverse deformations, which generated force in the lateral direction (Y direction). The force calculated in the slide direction is between 294 kips and 313 kips, and in the transverse direction, it is between 158 kips and 357 kips. These forces are from the superstructure being stuck in the skid track and groove in the pier (Figure 6-69.) With the superstructure stuck, forces generated by the jacks are transferred to the pier. The force developing in the transverse direction indicates that the bridge superstructure is being pushed transversely (discussed under Section 6.3.2.4). For future reference, skid tracks are not sufficient to keep the move aligned. In addition, monitoring forces and deformations need to be an essential component of the move operations. Additionally, jacks operating under pressure generated by manifolds are not appropriate for move operations. Servo jacks operating under set displacement targets are the appropriate hydraulics for keeping the move aligned.
- The reported capacity of the jack specified for the move at pier was 187 kips. With the malfunction of the jack, the superstructure was pushed from the abutments only without control at the pier. Comprehensive analysis needs to be performed in order to make procedural changes of the move operation. Additionally, the temporary substructure and the pier cap connection allowed force transfer from the temporary substructure to the pier. The temporary and permanent substructures need to include a key mechanism allowing vertical force, but not axial force, transfer to the permanent substructure.
- The resistance to sliding was partly due to lubricant performance in cold weather. The move operations need to standardize sliding surface materials and properties. Often

externally applied lubricant will create uncertain sliding friction and associated force imbalances between sliding surfaces. Surfaces with a reliable friction coefficient, such as oil impregnated linear bearings, need to be specified.

6.3.2.8.2 Observations Documented during the MDOT Post-Construction Meeting

The contractor needed to perform tasks for several months before the sliding weekend. The research team and MDOT performed field monitoring during that period. A few lessons learned from that monitoring and MDOT post-construction meeting are the following:

- It was identified that the soil near the temporary and permanent substructure was saturated. The water from superstructure curing, rain, and lack of drainage caused water to pond near the substructure. This may be one of the factors that led to the softening of the subgrade near the pier and contributed to pier displacements. The MSE wall also settled between 3 in. to 5 in. Additional temporary drainage measures need to be required in future projects to collect and channel the water away from the substructure. The settlement of the MSE wall was also accounted to driving piles in very close proximity. Non-displacement type piles are specified within the vicinity, or within 25 ft, of the permanent substructure.
- The M-50 traffic used the new superstructure on temporary supports as a temporary run-around, while the old structure was being demolished and the new substructure was being built. The temporary alignment (i.e., temporary run-around) was connected to the permanent alignment before the approach. There were some minor issues with elevations at and near the location where the permanent alignment and temporary alignments tied together. The issues were resolved with Hot-Mix-Asphalt wedging. For future projects, such areas need to be closely considered to ensure the elevations will work for the existing profile of the permanent alignment, the profile of the temporary alignment, and the proposed profile of the permanent alignment.
- The side slopes for the M-50 roadway were specified as 2:1. The project engineer suggested that shallower slopes need to be specified for future projects. The rationale for this is to keep the toe of slope location from the temporary alignment and to take the permanent slopes and tie them into that point once the temporary run-around is

removed. This procedure shallows up the slopes and minimizes the amount of material that needs to be removed.

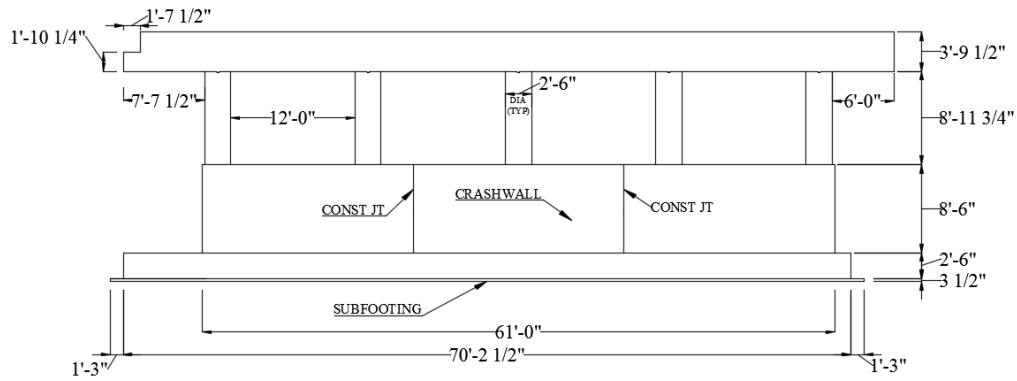
- Along the outside of the temporary roadway, the plans called for guardrail to be driven to protect the 2:1 slopes. For the temporary run-around, a temporary barrier was installed because the new superstructure was wider than the temporary roadway. It was impossible to attach a guardrail to the temporary barrier. The solution implemented was to run the temporary barrier off the new superstructure and onto the temporary approaches. Then, pin the barrier to the approaches and attach an impact attenuator to the end. Extend the guardrail a sufficient distance behind the impact attenuator and the barrier. Such a solution can be implemented to deal with similar difficulties in future projects.

6.4 STRUCTURAL IMPACT ON PIER DUE TO SLIDING FORCES

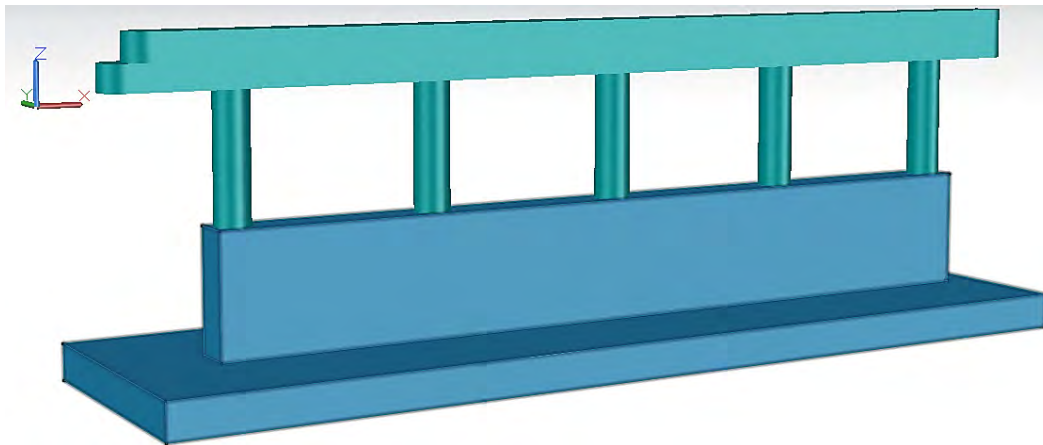
Structural impact on the M-50 Bridge pier was evaluated using an FE model. The pier is supported on a shallow foundation and soil-structure interaction was included in the model. During bridge slide, pier movements were recorded. The most critical movements were enforced on the model to calculate the stresses and to evaluate the potential for structural damage.

6.4.1 Pier Geometry and Modeling Parameters

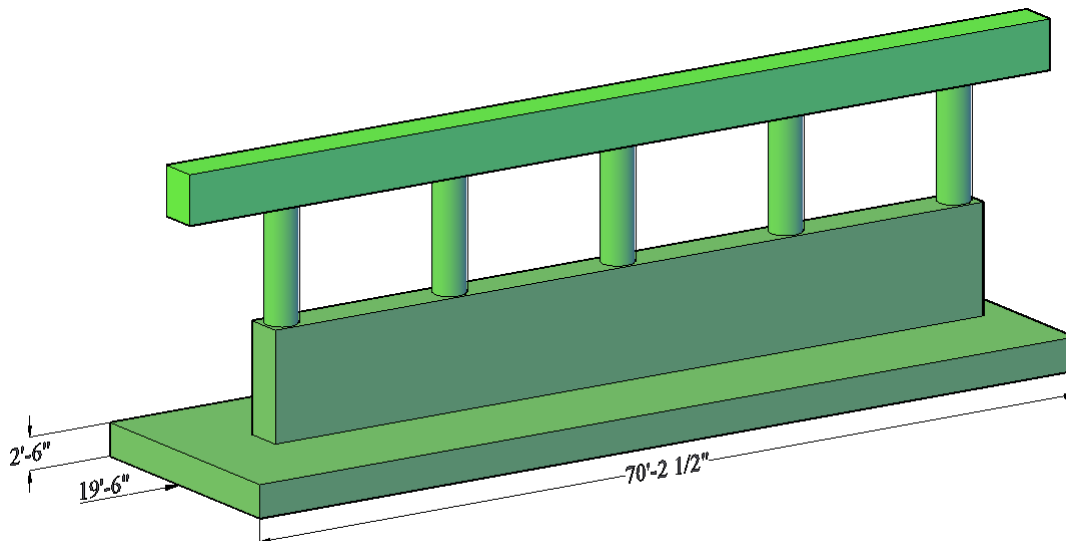
Pier geometry and dimensions are shown in Figure 6-102. Foundation, crash wall, and column geometries were not altered. Since curved ends of the pier cap have no structural significance, the end geometry was slightly modified by removing the curved geometry to enhance FE mesh quality.



(a) Dimensions of the pier



(b) 3D geometry and the coordinate system



(c) 3D geometry showing simplified pier cap ends

Figure 6-102. M-50 pier geometry and dimensions

The thickness of the soil layer around the footing was calculated based on the influence zone definition presented in Coduto (2001). According to Coduto (2001), when the length (L)/width (B) ratio is 1, the depth of influence is equal to 2B. Similarly, if the L/B ratio is equal to or greater than 10, the depth is 4B. When the ratio is in between 1 and 10, the value can be linearly interpolated between 2B and 4B. The depth of influence and the depth to hard strata are shown in Table 6-7. From these two dimensions, the lower value was used to represent the thickness of the soil layer around the footing.

Table 6-7. Depth of the Soil Layer Measured from Each Face of the Footing

Description	Length, L (in.)	Width, B (in.)	L/B	Depth of influence, Z_f (in.) ⁺	Depth to hard strata, H (in.)
Footing bottom surface	842.5	234.0	3.6	$2.6B \cong 608$	276
Surface perpendicular to X- axis	234.0	30.0	7.8	$3.5B \cong 105$	> 105
Surface perpendicular to Y- axis	842.5	30.0	28.1	$4B = 120$	> 120

+ Use the smallest from Z_f and H for modeling soil layer thickness

Flexural response of the pier under prescribed displacements was of interest. Hence, C3D8I elements were used to model the pier components including the foundation. The extent of soil is infinite. The boundary conditions need to be adequately defined so as not to influence the pier response to the loads. Linear infinite elements (CIN3D8) can be used to simulate the extent of soil beyond the zone of strain influence (Strömblad 2014). This modeling approach required defining near field and far field regions (Figure 6-103). The near field region dimensions were taken as the smaller of Z_f and H, as shown in Table 6-7 and modeled with C3D8 elements. The displacement tends to be zero at the boundary of the far field region. Hence, the infinite elements should be able to represent this behavior. Infinite elements are linear elements; hence, the displacement varies linearly within the element. This requires using a sufficiently large single layer of infinite elements to properly represent the boundary effects (Strömblad 2014). A parametric study was conducted, as discussed in Section 6.4.3, to evaluate effect of far field dimensions.

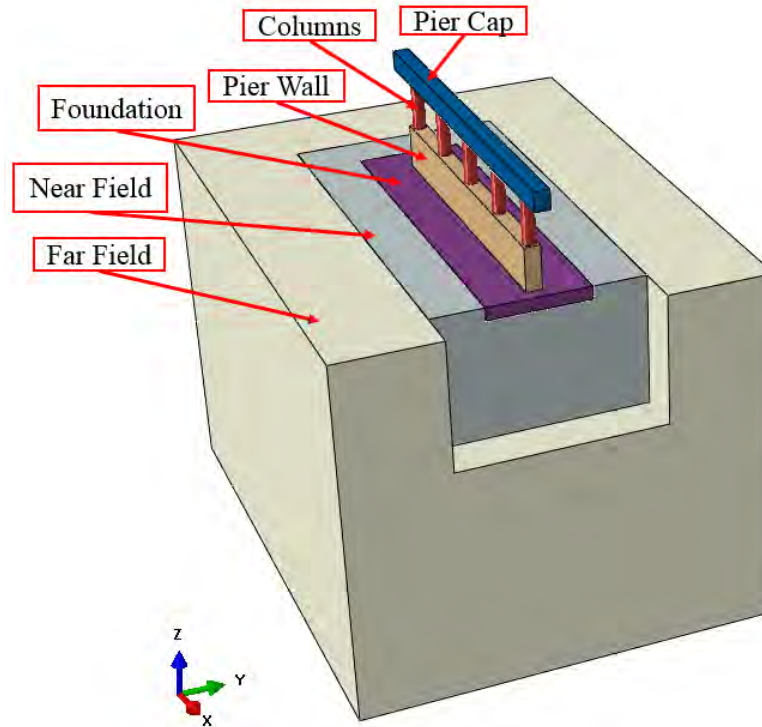


Figure 6-103. M-50 pier and soil profile definitions

Concrete design strength of 4000 psi given in the plans was used. Concrete unit weight of 0.15 kcf was used. Concrete modulus of elasticity was calculated using AASHTO (2014) Eq. 5.4.2.4-1. Concrete properties used in the model are shown in Table 6-8.

The soil around the footing was identified in the soil boring logs as sandy clay and silty clay (CL as per the Unified Soil Classification System). Since the undrained shear strength was greater than 1 ksf, both of these clay layers were identified as stiff to very stiff clays. The softening of the stiff clay was not considered in the continuum soil modeling, and a perfectly plastic behavior was assumed due to lack of field data to identify all the required modeling parameters. The following five parameters were used to model the soil that consists of a linear elastic model and a Mohr-Coulomb constitutive model for the inelastic behavior:

- Modulus of elasticity (E)
- Poisson's ratio (ν)
- Cohesion (c)
- Friction Angle (ϕ)
- Dilatation Angle (ψ).

Poisson's ratio and cohesion (c) were taken from Section 6.3.2.6.7. Modulus of elasticity was calculated as 154 ksf using the information given in Section 6.3.2.6.7. Friction and dilation angles for stiff clay were taken as 0° (Bowles 1997). A summary of all the material properties used in the model is shown in Table 6-8.

Table 6-8. Material Properties

Material	Modulus of Elasticity, E (psi)	Poisson's Ratio, ν	Cohesion, c (psi)	Friction Angle, ϕ (deg.)	Dilatation Angle, ψ (deg.)
Concrete	3.320×10^6	0.2	-	-	-
Stiff clay	1100	0.3	12.15	0	0

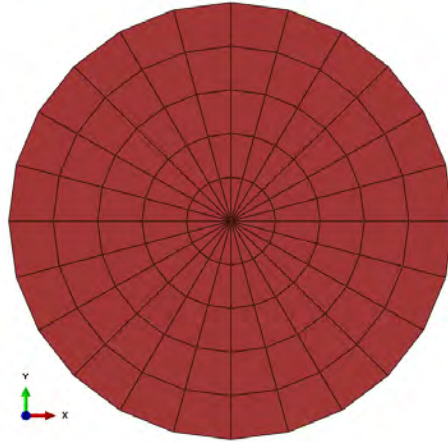
The contact and constraint definitions presented in Table 6-9 were used in the model. The coefficient of friction between stiff clay and concrete was defined as 30% (Coduto 2001).

Table 6-9. Contact and Constraint Definition Used in the Model

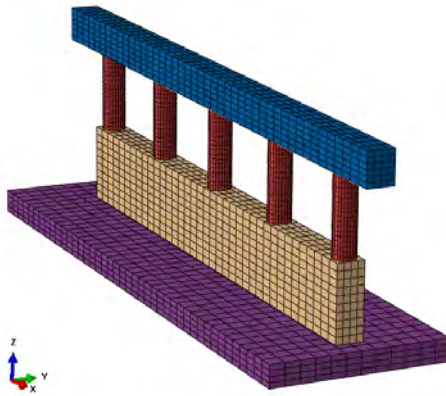
Option	Keyword	Notes
Contact Pair	*Contact Pair	<ul style="list-style-type: none"> • Contact pair option was used to define the interaction at the interface between the foundation and soil. • Penalty contact method was used. • Friction coefficient of 0.3 was at the interface.
Tie- Constraint	*Tie	<ul style="list-style-type: none"> • Surface-to-surface tie constraint tie constraint was used to define the interaction between all the members in the pier.

6.4.2 FE Discretization of the Pier

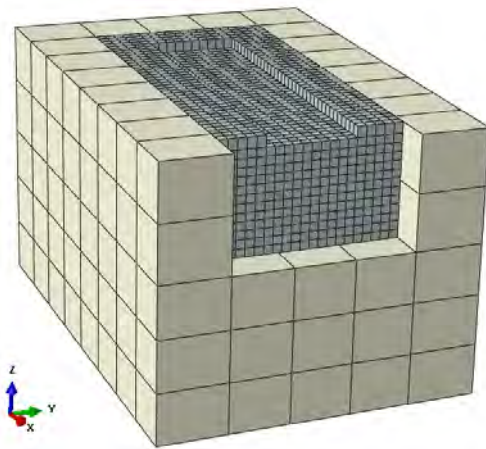
Figure 6-104 shows the FE representation of the model. Pier components were discretized into elements with aspect ratios that are suitable for stress calculation. Columns were discretized as shown in Figure 6-104a. Colum mesh includes a limited number of 6-node triangular prism elements (C3D6) in addition to C3D8I elements. Due to the element formulation, models developed with C3D6 are stiffer than the models developed with C3D8I. However, the increase in stiffness depends on the percentage of C3D6 elements in a model. Hence, a parametric study was performed as discussed below. Figure 6-104b shows the FE representation of the pier. Far field was represented with large infinite elements (Figure 6-104c).



(a) Column cross section



(b) Pier

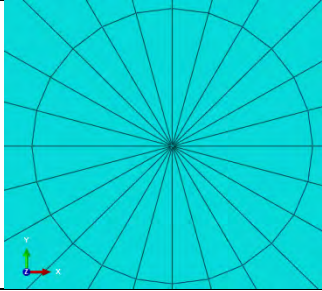
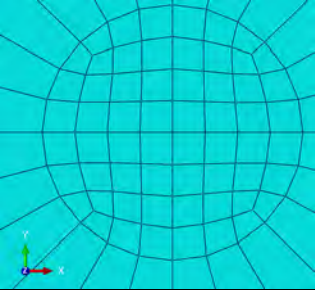


(c) Soil

Figure 6-104. FE representation of the model

In order to evaluate the impact of C3D6 elements in the pier columns, two different element configurations were used (Table 6-10). One cross-section was discretized primarily with C3D8I elements and a limited number of C3D6 elements. The other cross-section was discretized entirely using C3D8I elements. The columns were fixed at the bottom, and a 10 kips load was applied at the top of each column. As shown in Table 6-10, there is no significant difference in the analysis results; hence, a Case 1 mesh configuration was selected to represent the columns in the pier model due to ease in discretization.

Table 6-10. Sensitivity Analysis for Column Mesh Configuration

Analysis Case	Case 1	Case 2
Mesh Configuration		
Percent of C3D6 elements	4.2	0.0
Deflection at top (in.)	3.344×10^{-2}	3.346×10^{-2}
Moment at the base (k-ft)	M=83.9 k-ft.	M=84.0 k-ft.

6.4.3 Boundary Conditions

It was not necessary to define any other boundary conditions since the infinite soil elements (CIN3D8) were used to simulate the infinite extent of the soil layers. The dimensions of the far field regions can influence the analysis results. Hence, a parametric analysis was performed by varying the dimensions of the far field regions ranging from 0.5 to 2 times the near field dimensions. Concerning the loads, three concentrated loads of 100 kips were applied at the top of the bent cap and directly above the middle column. Then, the maximum tensile stresses developed at the bottom of the footing as well as the maximum footing settlement were compared as shown in Table 6-11. According to the analysis results, the ratio of the far field dimension to the near field dimension of 1.0 and 1.5 shows converging results. Hence, the ratio of the far field dimension to the near field dimension of 1.5 was selected, and the far field dimensions of 157.5 in., 180 in., and 414 in. around and at the bottom of the footing were used.

Table 6-11. Sensitivity Analysis for Far Field Dimensions

Ratio of the far field dimension to the near field dimension	Maximum stress at the bottom of the footing		Maximum footing settlement (in.)
	σ_{xx} (psi)	σ_{yy} (psi)	
0.5	32	32	0.108
1.0	33	37	0.183
1.5	33	37	0.183
2.0	44	51	0.541

6.4.4 Prescribed Displacement

The pier displacements were recorded during bridge slide. The displacements were monitored by mounting reflectors on three columns (1st, 4th, and 5th). The displacements

documented during the 21st observation presented in Table 6–1 were selected as an input displacement to the FE model. The displacements recorded during that particular observation are presented in Table 6-12. These displacements were prescribed at the respective locations on the model, and the response of the pier was documented.

Table 6-12. Displacements Used in the Analysis

	Column		
	1	4	5
X displacement (in.)	0.43	0.37	0.53
Y displacement (in.)	0.89	0.49	0.56
Z displacement (in.)	-0.10	-0.04	-0.04

6.4.5 Analysis Results

The deformed shape of the pier is shown in Figure 6-105.

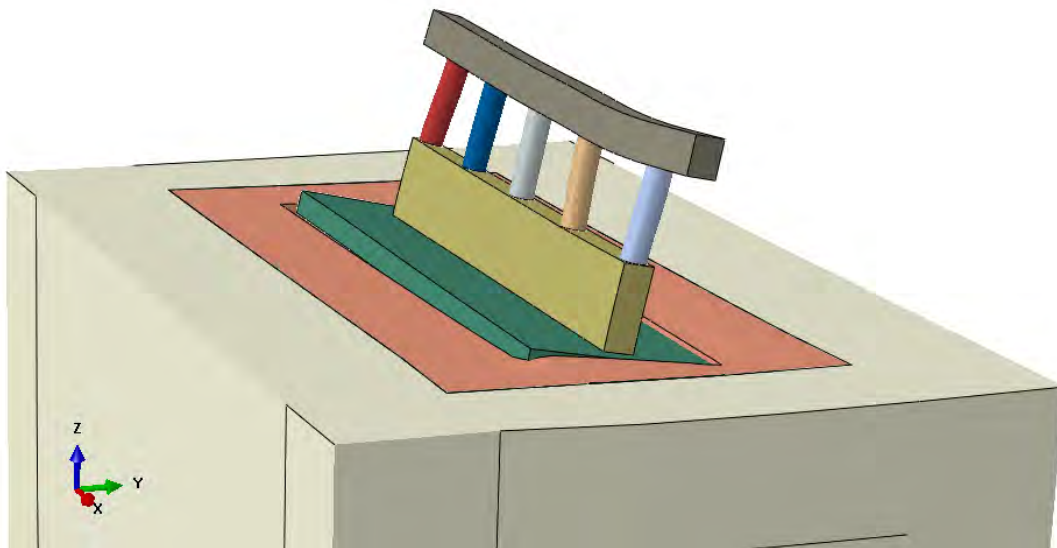
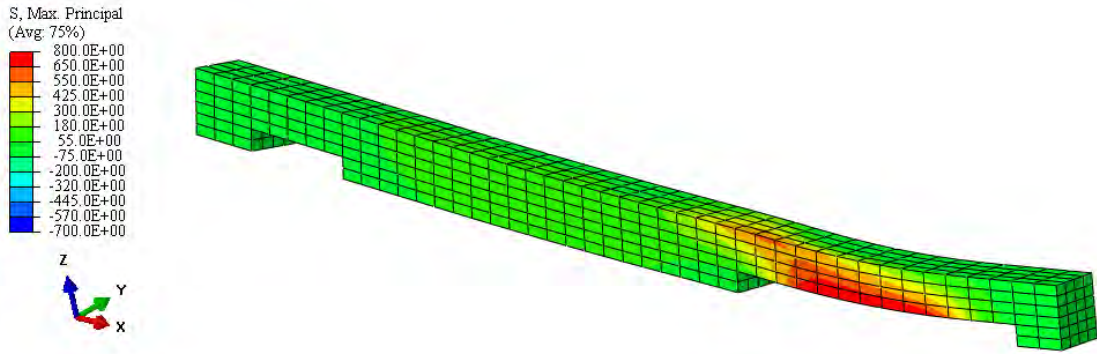
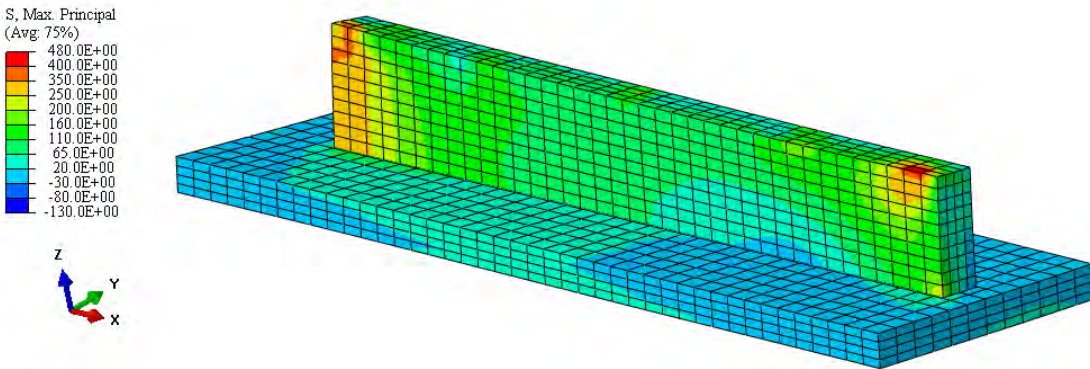


Figure 6-105. Deformed shape of the pier under prescribed displacements (100 times scaled)

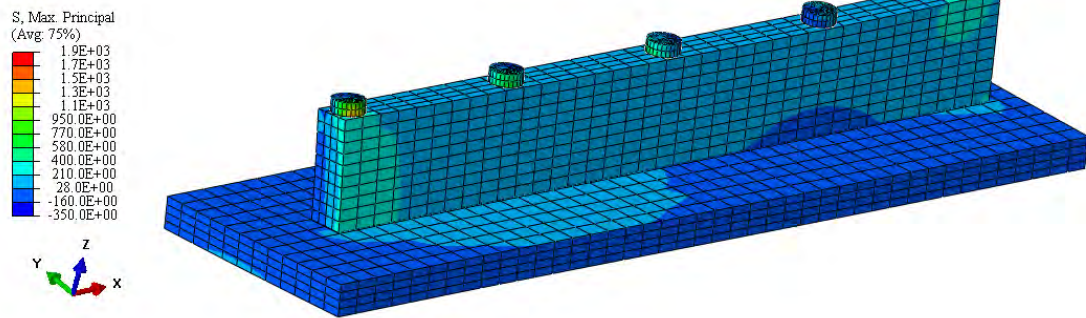
The maximum principal stresses were calculated. Figure 6-106a shows the maximum principal stress developed in the bent cap. Since displacements were applied on only one node in each of the three columns, excessive local stresses were developed around that node. Hence, the stresses developed around those nodes were disregarded. The maximum bent cap stress of 0.8 ksi was calculated. The maximum principal stress contours on the wall and the foundation are shown in Figure 6-106b. The maximum tensile stress of 0.443 ksi was developed in the crash wall close to the wall-column connection. The maximum principal stress contours on the column ends closer to the crash wall are shown in Figure 6-106c. The maximum tensile stress of 1.9 ksi was developed in the bottom of the 5th column.



(a) Maximum principal stress distribution in the bent cap



(b) Maximum principal stress distribution in the wall and the footing



(c) Maximum principal stress distribution in the column ends

Figure 6-106. The maximum principal stress contours

6.4.6 Summary and Conclusion on Structural Impact of Bridge Slide

M-50 over I-96 bridge pier movements were monitored during slide. The measured displacements were used as prescribed displacement in the FE model to evaluate the stresses developed in the pier. The following conclusions are derived from the analysis results:

1. Maximum tensile stress generated in the pier cap is 0.80 ksi, which is above the tensile strength of concrete. The measured displacements at columns 2 and 3 were

not available. Hence, the analysis was performed only using the displacements at columns, 1, 4, and 5. Further, the bridge superstructure's dead load was not included in the analysis. Since the stresses are closer to tensile strength of concrete, it is necessary to develop robust monitoring programs until the impact of sliding is clearly understood.

2. Maximum tensile stress generated in the wall and foundation is 0.44 ksi. The largest stresses are generated at the column wall connections. The weight of the superstructure will generate compressive stresses at those locations and decreases tensile stresses. No cracks are expected at the wall and foundation because of sliding.
3. Maximum tensile stress generated in the columns is 1.9 ksi. This stress is large enough to generate cracking in concrete. However, the weight of the superstructure was not included in the analysis since the measured displacements were used as prescribed boundary conditions. When the bridge superstructure is on the pier, the weight generates compressive stresses in the columns. As a result, the tensile stresses generated in the column ends decrease. However, the findings encourage developing robust monitoring programs until the impact of sliding is clearly understood.

6.5 SIMULATION OF SLIDE OPERATION

The US-131 Bridge over 3 Mile Road, described in Section 6.3.1, is used as the slide simulation example. As discussed in Section 2.5.2.3, PTFE-stainless steel interface friction is a function of many parameters making it unrealistic to assume uniform friction along the sliding path or between each sliding bearing surface. Simulations will help in understanding the impact of sliding path friction on the pulling or pushing forces, maintaining slide path alignment, and the stresses or stress resultants developed in the temporary structure.

Based on the bridge alignment between the abutments, the railing girders on each temporary substructure can be built at the same alignment (i.e., at grade) or at a different alignments. For example, as shown in Figure 6-107, the railing girder at abutment B of the US-131NB Bridge was located at a higher elevation than the railing girder at abutment A. The alignment change between the two railing girders was 0.31 ft. Simulation will also include cases with railing girders at the same alignment and railing girders at different alignments. Simulations will help evaluate the impact of different alignments on the sliding operation, maintaining slide path alignment, and the stresses or stress resultants developed in the temporary structures.

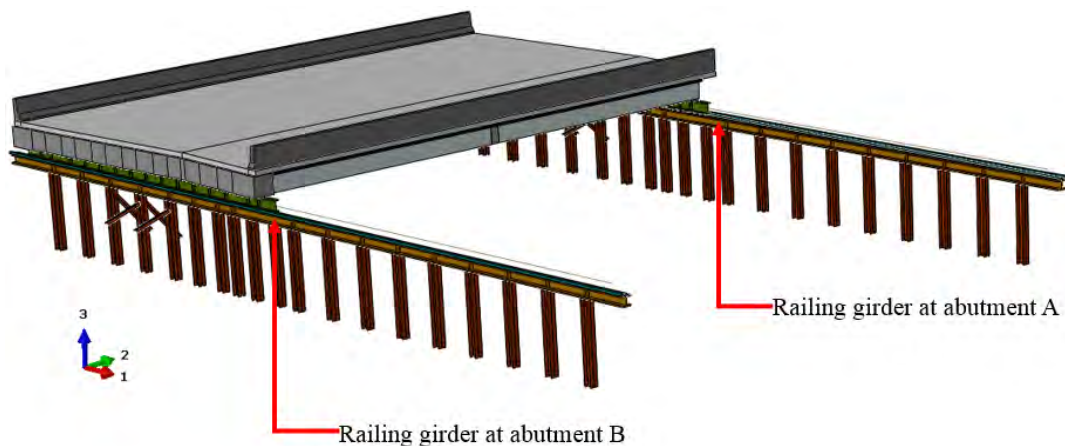


Figure 6-107. US-131 NB Bridge on the temporary structure

Pulling or pushing of a bridge superstructure is not a continuous operation. Depending on the stroke capacity of the jacks, the superstructure is pulled or pushed up to a certain distance, and the jacks need to be reset. Further, a structure can be slid into place by applying a force, or as described earlier, it can be moved by setting displacement targets. The move procedure that includes defining the force will be termed as force control; the

move that includes setting displacement targets will be termed as displacement control. Sections 2.5.2.1 and 2.5.2.2 describe the displacement and force control methods, respectively. Simulation of a sliding operation under displacement and force control methods is for demonstrating the impact on the sliding operation as well as the forces developed in the temporary structure.

The scope of the bridge slide simulation is presented in Figure 6-108. This scope will evaluate the impact of unequal friction, unequal alignment, continuous and discrete sliding, and displacement and force control sliding methods on the superstructure movement and the stresses or stress resultants developed in the temporary structures.

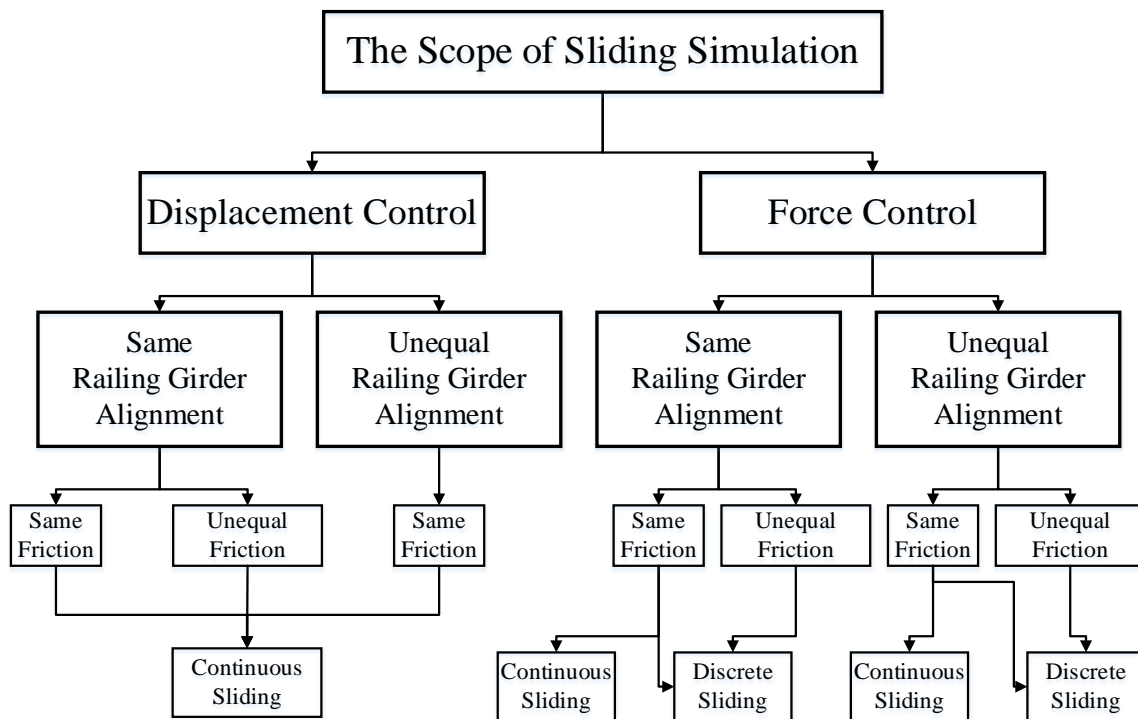


Figure 6-108. The scope of sliding simulation

Analysis is performed under displacement and force control methods. For each method, railing girders at abutment A and B are positioned at the same alignment; then they are placed in a different alignment with abutment B railing girder at 0.31 ft above the railing girder at abutment A. The alignment difference of 0.31 ft is determined based on the information provided in the bridge plans. The analysis is also performed with equal friction and unequal friction on the sliding surfaces. Section 6.5.1.3 presented the friction model and

the coefficients used in the analysis. Analysis is also performed in continuous and discrete modes. In the continuous analysis, the superstructure is slid from beginning to end without a pause. In the discrete mode, the superstructure is pulled and allowed to stop, more closely representing the slide operation. The stop and go move simulation will show the dynamic forces developed in the system.

6.5.1 Finite Element Model (FEM) Parameters

6.5.1.1 Geometry

The US-131 NB bridge geometry and the temporary structure and sliding mechanism details are closely replicated. Simple minor modifications to the bridge superstructure details are made to enhance the quality of finite element analysis results. Table 6-13 lists the components included in the model and remarks related to modifications.

Table 6-13. Components Included in the Model

Component	Remarks
Barrier	Cross-Section is modified for FE mesh quality.
Haunch	A 2 in. thick haunch is included in the model.
Interior Beam	Internal diaphragms are excluded.
Steel Diaphragm	Steel intermediate diaphragms are excluded.
Fascia Beam Deck Backwall Wooden Blocks Sliding Girder Sliding Girder Stiffeners Sliding Shoe Railing Girder Railing Girder Stiffeners Battered Piles Pile Bracing	Geometry is not altered.
PTFE	One continuous PTFE layer is used as the sliding surface instead of using discrete PTFE pads.
Extended Piles and Columns	Same cross-section is used. Equal heights for extended piles and columns are maintained even though the temporary structure column heights are different in the plans.

The bridge superstructure and temporary structure, including sliding and railing girders, are first modeled in AutoCAD. The components are imported to Abaqus CAE for pre-processing. Figure 6-109 and Figure 6-110 show the CAD model, and Figure 6-111 shows the geometry in Abaqus CAE environment. As shown in Figure 6-111a and b, direction 1, 2, and 3 define the sliding, transverse to sliding, and the vertical directions, respectively.

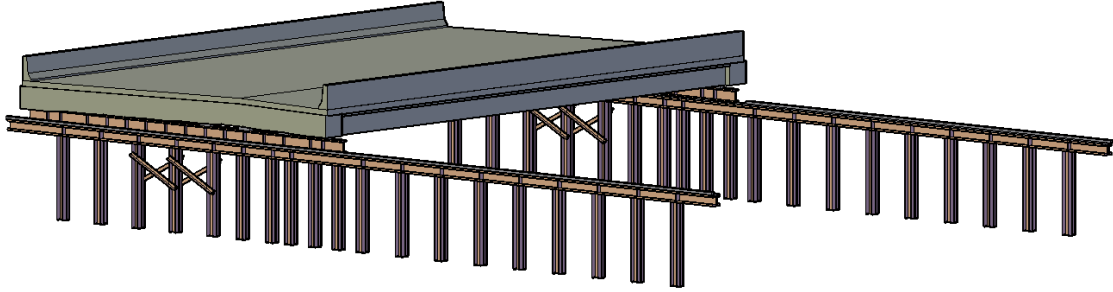


Figure 6-109. CAD model of the bridge superstructure and temporary structure

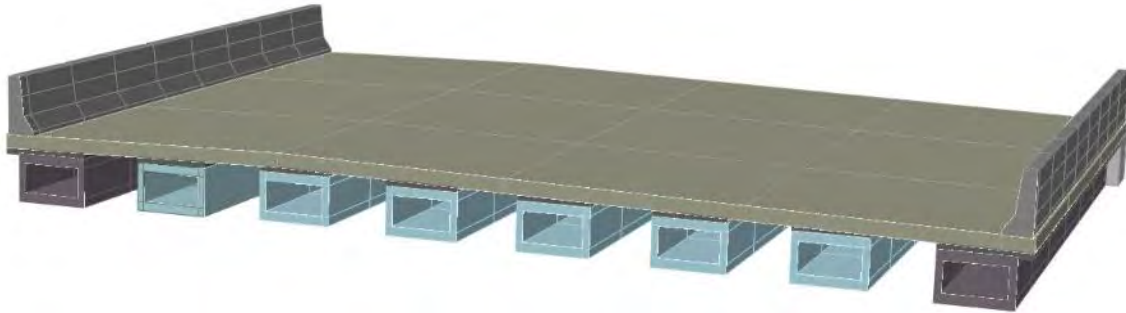


Figure 6-110. Cross section of the superstructure

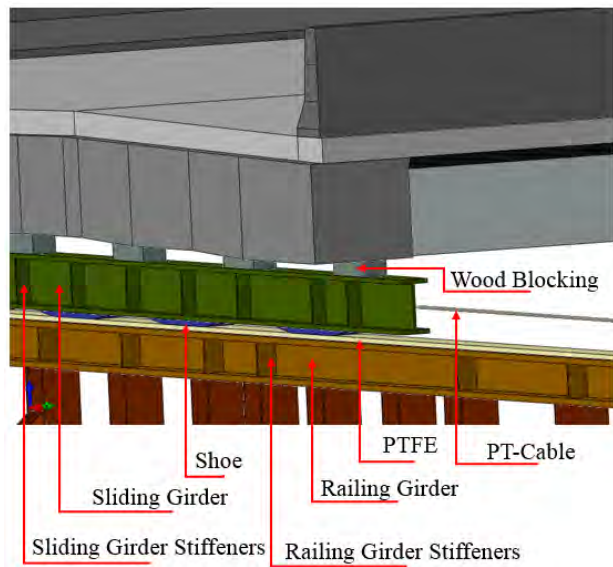
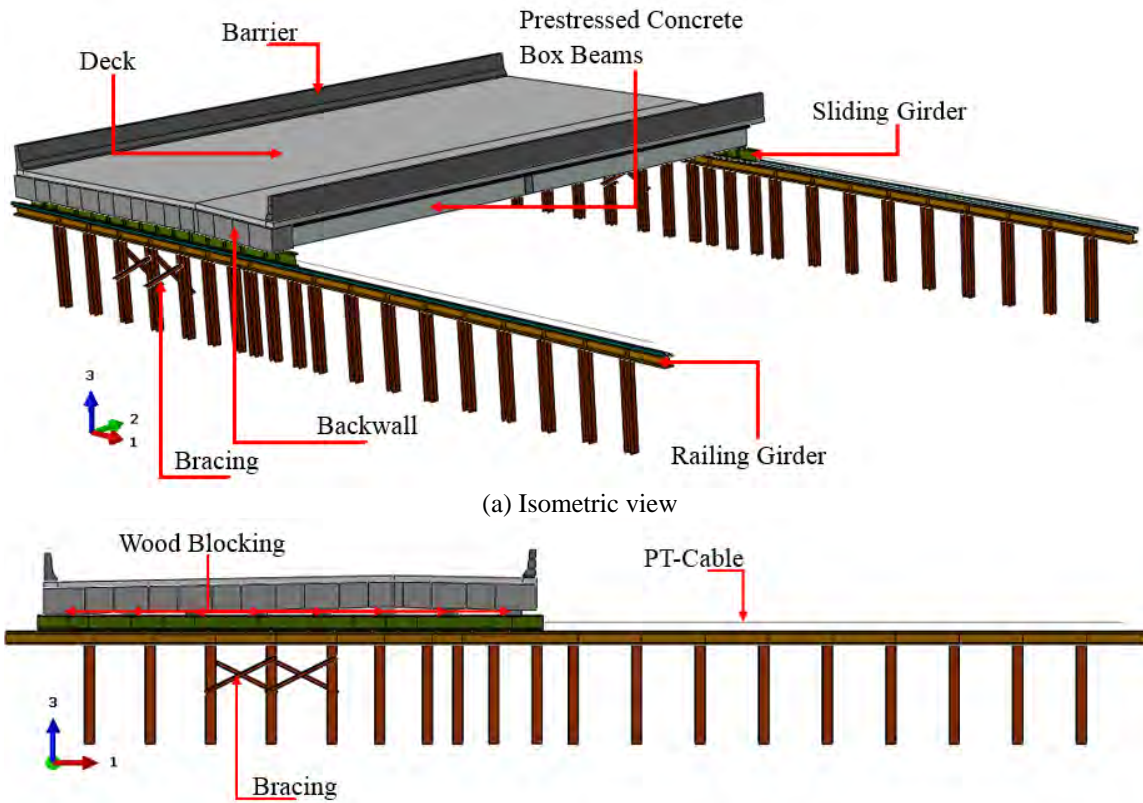


Figure 6-111. Superstructure, temporary structure, and sliding mechanism detail

6.5.1.2 Material Properties

Material properties given in the bridge plans are assumed. The modulus of elasticity is calculated using AASHTO (2014) Eq. 5.4.2.4-1. Moreover, the unit weight of concrete is taken as 0.15 kip/ft³.

Modulus of elastic (E), Poisson’s ratio (ν), and mass-density (ρ) are defined for each material. Since there is no unit definition in Abaqus, the American Standard Unit system is selected as shown in Table 6-14.

Table 6-14. Material Properties

Materials		Modulus of Elasticity, E × 10 ⁶ (psi)	Poisson’s Ratio, ν	Mass Density, ρ (lb ² ×s ² /in ⁴) × 10 ⁻⁴
Concrete	Grade D	3.834	0.20	2.25
	Fascia Beam	4.774		
	Interior Beam	4.696		
Steel		29.000	0.30	7.30
PTFE (Dupond® 1996)		0.073	0.46	2.02

6.5.1.3 Normal Pressure and Friction

According to the classical isotropic Coulomb friction model presented in Section 2.5.2.3, static and kinetic friction coefficients, as well as the decay rate, are needed to define friction behavior at the PTFE-stainless steel interface. The kinetic friction coefficient depends on the normal pressure at the interface. Assuming the superstructure weight is equally distributed to all the sliding shoes, the nominal pressure at the interface is calculated as 282 psi. Considering the data and the subsequent analysis given in Chapter 2, for the simulations performed in this study, the breakaway friction of 10% and kinetic friction of 5% are assumed. In order to define the decay rate, static friction, kinetic friction, and the sliding velocity are needed. During the US-131 over 3 Mile Road and M-50 over I-96 slide projects, sliding velocities of 2 in/min and 2.7 in/min were recorded from the total move duration. Note that the sliding process consisted of a collection of successive discrete sliding events. The sliding velocity is estimated from the periods when the bridge was in motion. With an average velocity ranging from 2 in/min to 2.7 in/min, much higher peak velocities are expected. Further, with experience, it is possible to achieve a peak slide velocity of at least two to three times the velocities that were estimated from the first two SIBC projects in

Michigan. Expecting a sliding velocity of 6 in/min (i.e., 0.1 in/sec) or greater during a discrete event is reasonable.

As shown in Figure 6-108, simulation is performed separately for both continuous and discrete slide events. During the continuous slide simulation, the bridge is pulled 62.5 ft (from start to the end) as a single event. Due to the complexity of the model, simulation of sliding at a very small velocity, such as 0.1 in/sec, is not practical, and the computational time will be excessive. In addition, the coefficient of friction does not change drastically once sliding initiates. For that reason, performing a continuous slide at a higher velocity does not affect the simulation results that are of interest. After considering the above facts and conducting exploratory analyses, a sliding velocity of 10 in/sec is used. Decay rate is defined to achieve 5% friction when the velocity reaches 10 in/sec, resulting in a decay rate of 0.4105. Based on the decay rate and the 5% kinetic friction coefficient, the variation of friction coefficient against slip rate is shown below in Figure 6-112:

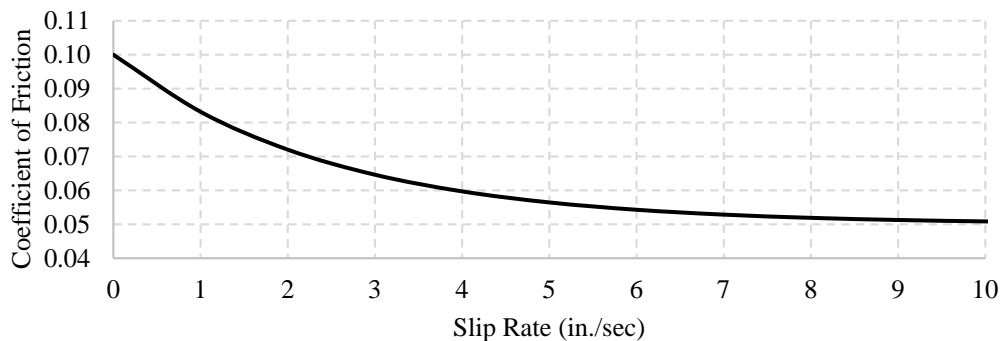


Figure 6-112. Variation of friction coefficient against slip rate

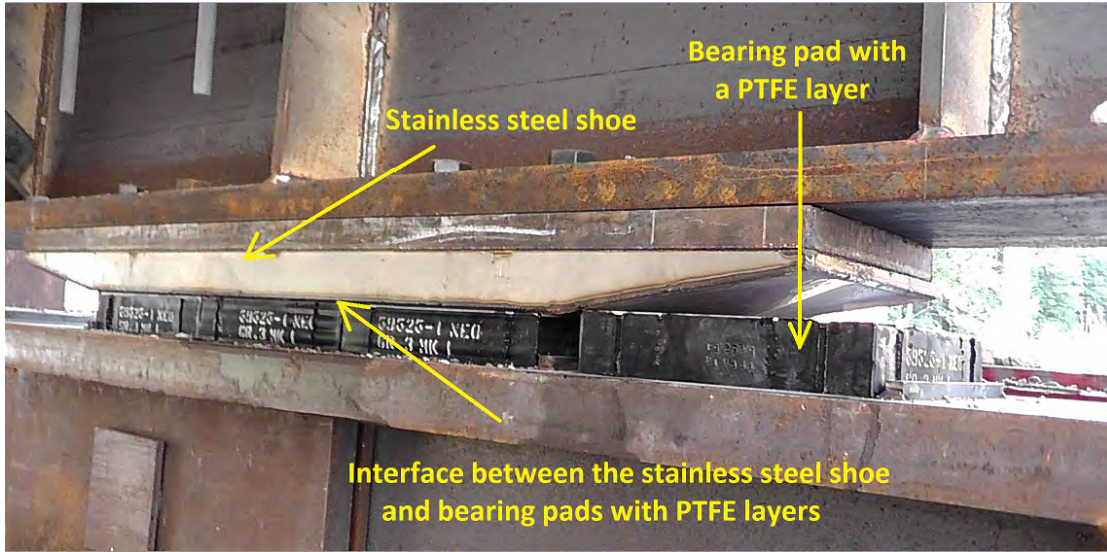
Analysis is also performed with unequal friction coefficients between two railing girders. In this case, the static friction is kept the same, and the kinetic friction of 2% and 5% is defined for the railing girder at abutments A and B, respectively. These values are chosen to show an extreme case of unequal friction on sliding girders.

6.5.1.4 Contacts and Constrains in Abaqus

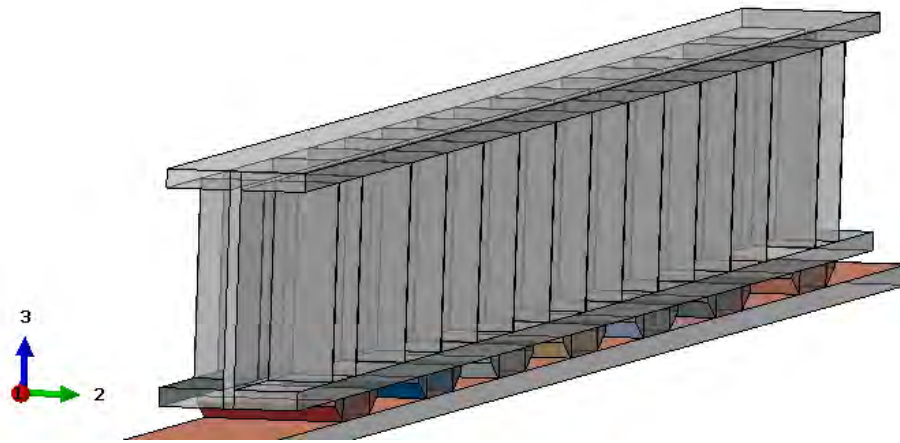
Abaqus CAE, the preprocessor, utilizes component geometry for FE discretization. Following the FE representation of each component, the interaction between the components is defined using contact surfaces or constrains. The contacts and constrains used in the model are shown in Table 6-15 below.

Table 6-15. Contact and Constraint Definitions Used in the Model

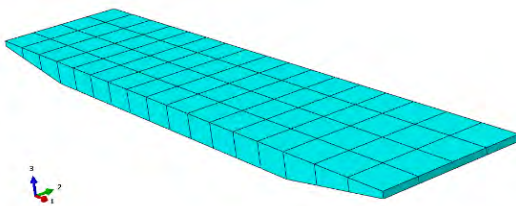
Option	Keyword	Notes
Contact Pair	*Contact Pair	<ul style="list-style-type: none"> • The contact pair option is used to define the interaction at the interface between the polished stainless steel shoe and the PTFE pads (Figure 6-113). • The contact pair option is also used to define the contact between transverse rollers and the sliding girder. • The penalty contact method is used. • 10% static and 5% or 2% kinetic friction coefficients are used as the interaction properties at the interface between polished stainless steel shoes and PTFE bearings. • Frictionless interaction is defined for the contact between transverse rollers and the sliding girder.
Tie-Constraint	*Tie	<ul style="list-style-type: none"> • Tie constraint is used to define the interaction between rigidly connected parts or members. • Surface-to-surface tie constraint is used since individual component FE discretization is different.
Multi-Point Constraint	*MPC	<ul style="list-style-type: none"> • A multi-point constraint is used to define the connection between the pulling rods and the sliding girder. • A pulling rod is modeled using 2-node truss elements. The node closer to the superstructure is tied to the front surface of the sliding girder.



(a) A stainless steel shoe sliding over bearing pads with PTFE layers



(b) Geometric representation of a sliding girder, stainless steel shoes, and the sliding surface in the model



(c) FE representation of the sliding shoe



(d) FE representation of the PTFE layer

Figure 6-113. A sliding shoe and PTFE pads (a) physical geometry, (b) geometric representation in the model, and (c) FE representation

6.5.1.5 FE Discretization of the Bridge Model

The primary objectives of the FE analysis are to demonstrate the impact of sliding path friction and unequal railing girder alignment on the pulling or pushing forces, maintaining slide path alignment, and calculating the stresses or stress resultants that develop in the temporary structures. The railing girder is supported on the extended piles or columns as a continuous member. This arrangement allows the girder to deflect in between the supports and remain rigid over the supports. Hence, it is critical to evaluate the stresses developed at the PTFE-steel sliding shoe interface, especially when the interface is being supported on a railing girder with changing stiffness.

Since the primary focus is on the interface stresses, bridge movement, and the stresses or stress resultants on the temporary structures, the bridge superstructure is discretized into a coarse mesh. The members of the temporary structures are discretized into elements with aspect ratios that are suitable for stress calculation (Figure 6-114).

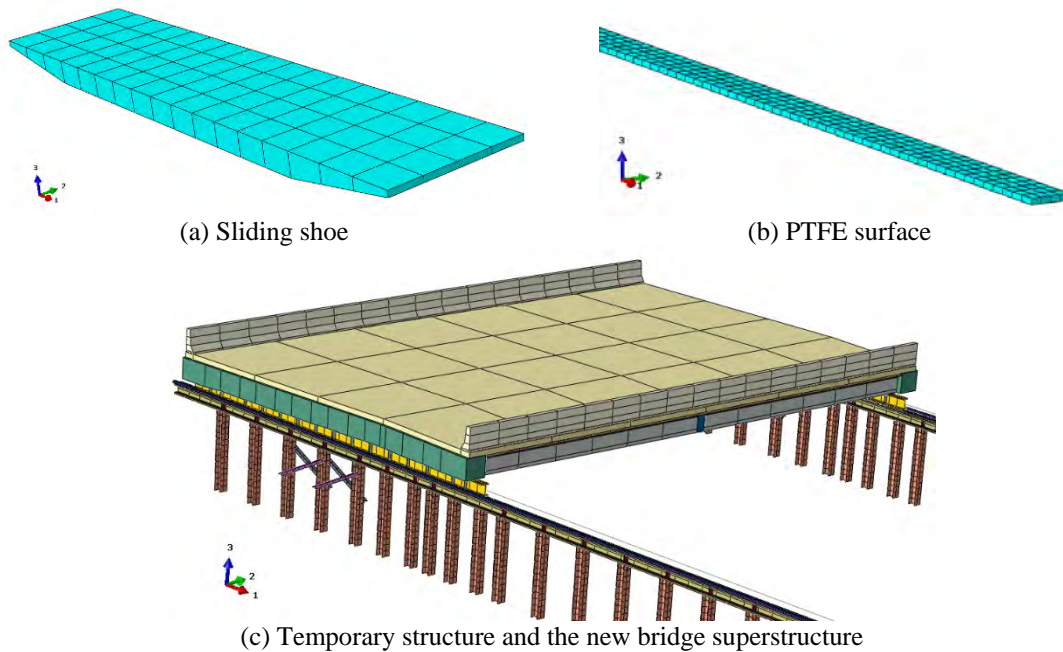


Figure 6-114. FE representation of the sliding shoe, PTFE surface, and the temporary structure and the new bridge superstructure

6.5.1.6 Boundary Conditions

Extended pile and column ends at the ground level are constrained for translations and rotations simulating a fixed support. While one end of the pulling rod is connected to the sliding girder, the other end is constrained for all the degrees of freedoms, except for the translation in direction 1 (slide direction) as shown in Figure 6-115. The boundary condition at the end of the pulling rod allows maintaining the sliding direction during load control or displacement control analysis.

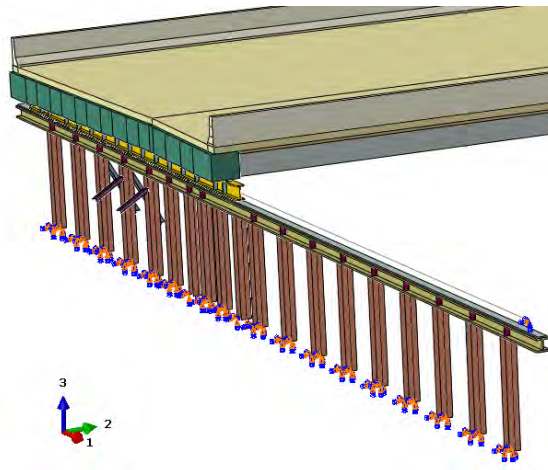


Figure 6-115. Boundary conditions

6.5.1.7 Loads and Prescribed Displacements

Self-weight of all the components is applied using the *DLOAD command in Abaqus. Since Abaqus Explicit is used to perform the sliding simulations, application of the gravity load at once generates a large dynamic response, which can eventually affect the rest of the analysis results. In order to suppress the dynamics that are not naturally occurring in the system, self-weight is applied as a gradually increasing load using the AMPLITUDE option in Abaqus. For consistent units, the gravitational acceleration is defined as 386 in/s^2 .

For displacement control models, a displacement is defined at the free end of the pulling rod. The magnitude of the prescribed displacement is equal to the total slide distance. The acceleration, velocity, and displacement against time under displacement control are presented in Section 6.5.2.2.

For force control models, pulling force is defined at the free end of the pulling rod. The applied force on each pulling rod is 85 kips. This force is defined as slightly more than the friction force at the PTFE-steel interface. The friction force is calculated based on the nominal stress at each sliding shoe and the static friction coefficient of 10% as 144 kips. The pulling force is gradually increased to 85 kips and maintained. Applied force, velocity, and displacement against time in a force control system are presented in Section 6.5.3 and 6.5.3.2., respectively.

For simulating a discrete slide event (a close representation of a typical slide) the force control method is utilized. In this case, the applied force is gradually increased until the sliding structure reaches a predefined velocity. At that time, the force is removed, and the superstructure is allowed to slide until motion stopped due to frictional resistance.

6.5.2 Displacement Control Continuous Slide

The total slide distance is 62.5 ft. The structure is pulled gradually, starting from a resting position, until the sliding velocity reaches 10 in/sec. After that, a constant velocity of 10 in/sec is maintained. Superstructure movement in the slide direction with respect to time is shown in Figure 6-116. Under the displacement control method, as prescribed, uniform displacements are recorded over each railing girder, irrespective of the friction variation at the PTFE-steel interface.

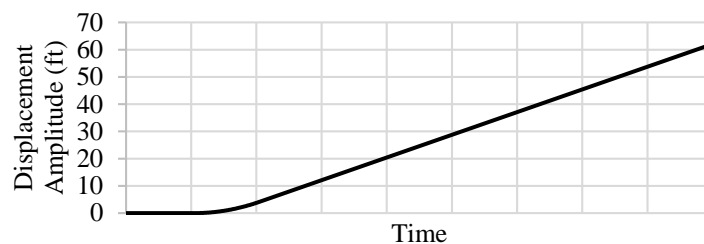


Figure 6-116. Superstructure movement in the direction of slide

6.5.2.1 Sliding Friction Forces

Friction forces developed under the displacement control sliding method are presented in Figure 6-117. As shown in Figure 6-117, forces developed when sliding begins. As soon as the sliding initiates, there is a sudden increase in the friction force. As the velocity increases,

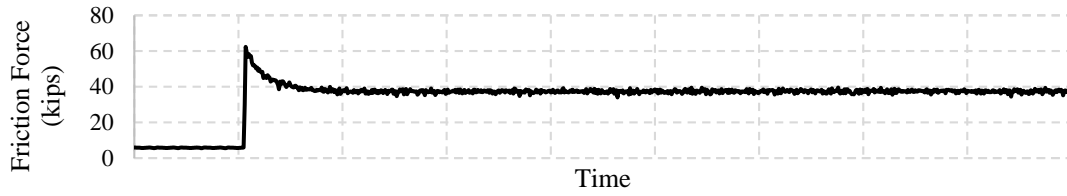
the friction force decreases due to a reduction in the coefficient of friction as per defined decay rate. Once the sliding velocity becomes constant, the friction force becomes constant.

With the static friction coefficient of 10% and a vertical force of 720 kips acting on each rail, the total friction force expected on each rail is 72 kips (i.e., 0.1×720 kips). However, at the onset of sliding, the maximum total friction force observed on each temporary structure in the direction of sliding is 65 kips, which is little more than 90% of the expected value. The difference is due to numerical error with force being calculated at each time increment. The time increment used in the calculations is less than 10^{-5} seconds.

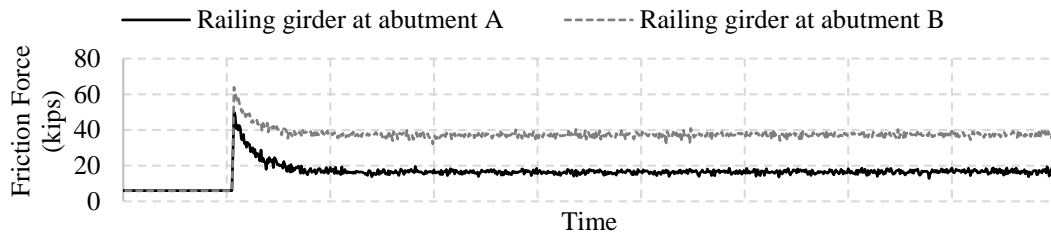
As shown in Figure 6-117a, when the system is sliding at a constant velocity, the friction forces developed at each rail are 36 kips (i.e., 0.05×720 kips). This is because the kinetic friction remains a constant value over a time during steady state sliding.

In order to account for the friction variation between sliding surfaces, the railing girder at abutments A and B are assigned 2% and 5% kinematic friction coefficients, respectively. Both temporary structures are assigned the same static friction coefficient of 10%; hence, it is expected to have the same friction force acting on both temporary structures. The total friction force acting on each temporary structure is shown in Figure 6-117b. As shown in the figure, the forces acting on each structure at the onset of sliding are slightly different. As the velocity increases and reaches steady state sliding velocity of 10 in/sec, the forces are decreased to 15 kips and 36 kips for temporary structures at abutments A and B, respectively. Even with unequal friction, under displacement control, the sliding progresses in alignment without any drift to the transverse direction.

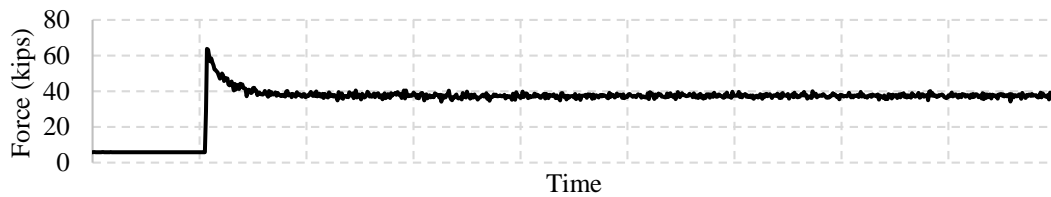
The impact of unequal railing girder alignment on the sliding forces and movement is investigated. During this analysis, equal friction properties are maintained on both railing girders. In this case, the railing girder at abutment B is raised 0.31 ft above the railing girder at abutment A. This creates a bridge superstructure grade of about 0.4%. Even with such a small grade, the superstructure drifted about 0.75 in. towards abutment A (Figure 6-118). This drift is smaller than the tolerance specified for the side rollers and the sliding girder. Since the equal friction is maintained on both railing girders, friction forces acting on each temporary structure remained same (Figure 6-117c).



(a) Equal railing girder alignment and friction



(b) Equal railing girder alignment, but unequal friction



(c) Unequal railing girder alignment, but equal friction

Figure 6-117. Friction force developed under displacement control sliding method

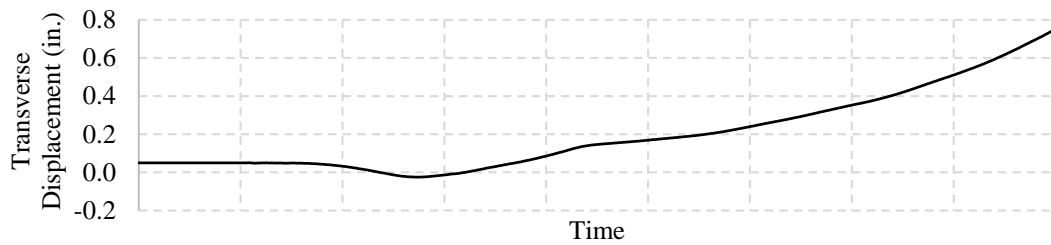


Figure 6-118. Transverse drift during slide under displacement control conditions with unequal railing girder alignment

6.5.2.2 Acceleration, Velocity, and Displacement Histories

Under a prescribed displacement, an initial acceleration is developed in the system. With the initial acceleration and the prescribed displacement, the velocity increases (Figure 6-119).

The relation between the displacement, acceleration, and the velocity is described in Section 2.5.2.1.

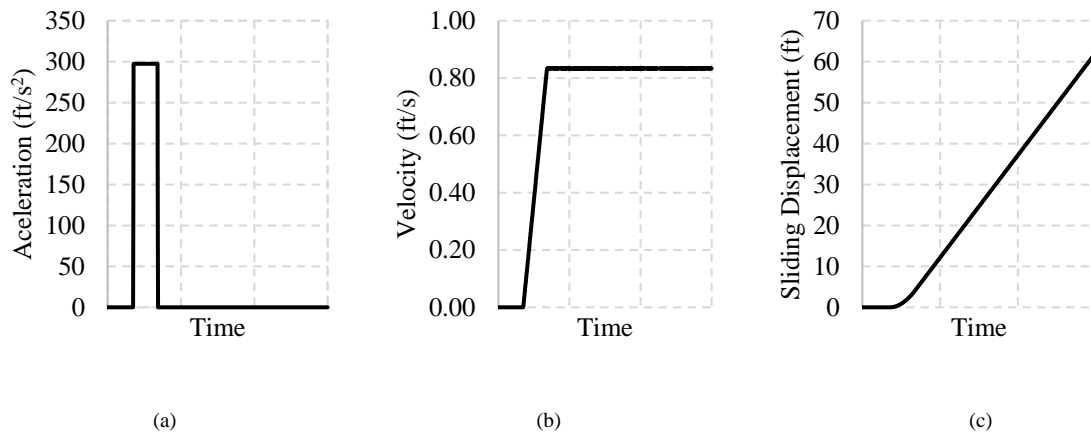


Figure 6-119. Variation of acceleration, velocity, and displacement with respect to time under displacement control sliding

6.5.2.3 Forces on the Temporary Structure

Forces generated at the sliding surfaces are the horizontal forces transmitted to the temporary structure. The normal forces at the sliding surface and the temporary structure self-weight represent the vertical reactions at the temporary structure supports. In design, the vertical loads are calculated from the dead loads. The horizontal load is calculated from static friction and the normal force acting on the sliding surface. Sliding can also generate dynamic loads that are larger than the typically calculated static design forces. SIBC being new, there is a lack of data for the designers to account for the dynamic effects.

The analysis results are useful to understand the structural response during a bridge slide and the nature of forces that develop. Figure 6-119 shows the initial acceleration, sliding velocity, and the displacement with respect to time. Figure 6-120 shows the temporary substructure reactions with respect to time under (a) equal railing girder alignment with equal friction, (b) equal railing girder alignment with unequal friction, and (c) unequal railing girder alignment with equal friction. The horizontal reaction expected at the temporary structure under static friction is 72 kips. Due to the acceleration introduced into the system at the onset of sliding as well as the unequal friction and unequal railing girder alignment, forces as large as 110 kips developed. As per the displacement control analysis parameters used in this analysis, an impact factor of 1.53 (i.e., 110 kips/72 kips) is calculated. The

application of slower displacement rates (i.e., velocities) at the beginning of the slide will reduce the impact factor.

Two most recent slides documented an average velocity of 0.033 in/sec and 0.045 in/sec. This velocity is calculated considering the total move distance of the bridge during sliding. Several discrete slides move the bridges. Hence, the actual sliding velocity is larger than the average. Due to lack of reliable data, the velocity used for continuous slide analysis is 10 in/sec, and this generated an impact factor of 1.53 for the specific bridge configuration used in the simulation. The analysis capabilities demonstrated here, along with monitoring future bridge moves, will be useful for developing a design impact factor for SIBC.

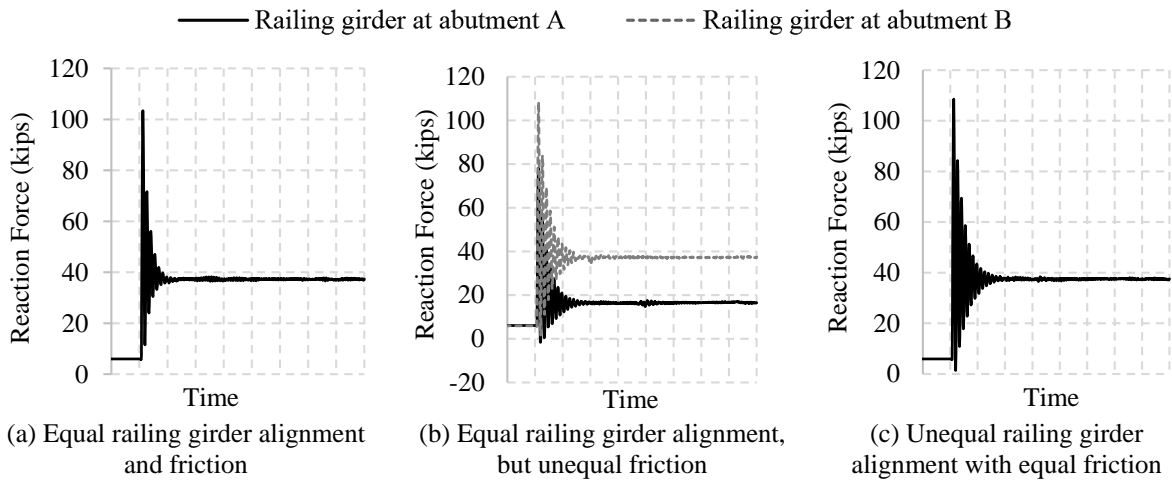


Figure 6-120. Temporary structure reactions in the sliding direction

The vertical reactions at the temporary structure supports are shown in Figure 6-121. Sliding structure dynamics have created the fluctuations in the vertical reactions. However, the amplifications are less than 2%.

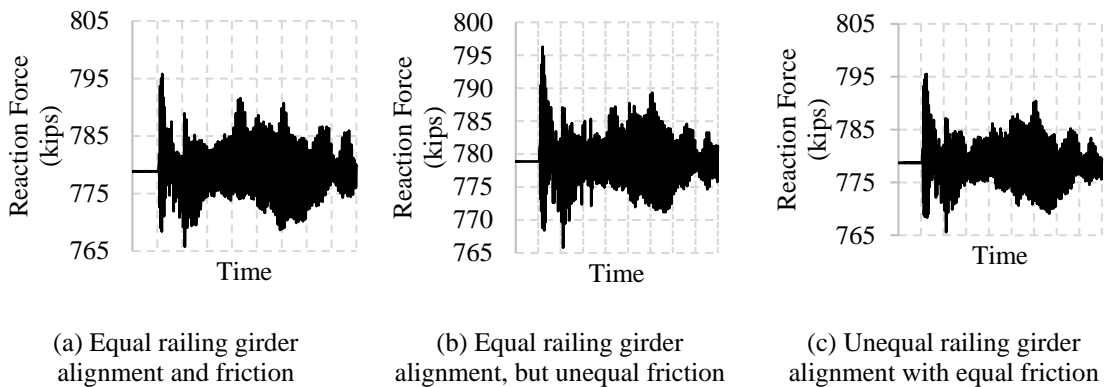
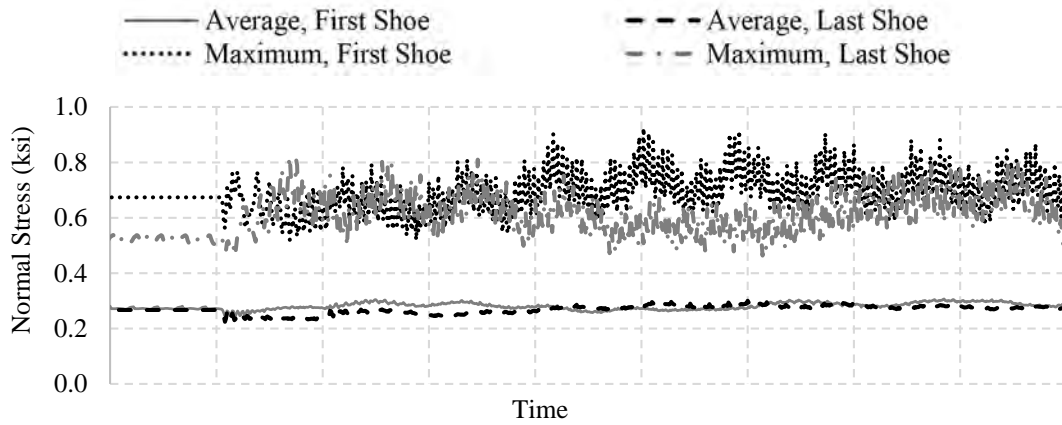


Figure 6-121. Vertical reactions at the temporary structure support

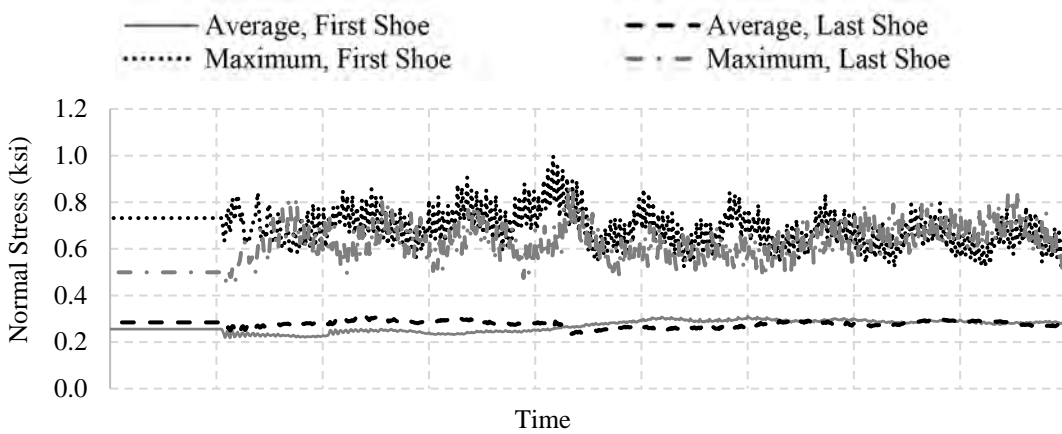
6.5.2.4 Normal Stress at PTFE – Steel Interface

Typically, the normal stress at the sliding surface (i.e., PTFE-steel interface) is calculated assuming that the number of sliding shoes equally shares the total gravity load. However, the bridge superstructure configuration and the railing girder tolerances will lead to non-uniform stress distribution between the sliding shoes. Further, during bridge slide, non-uniform stiffness of the railing girder changes the normal stress acting on a sliding shoe, based on its position along the sliding girder. As described earlier, a sliding shoe will attract larger stress when positioned on or near the support. This change in normal stress changes the friction forces developed at each shoe. Subsequently a change in friction force between all sliding surfaces during a bridge slide is unavoidable.

In order to understand the normal stress distribution at PTFE-steel interface, the maximum normal stress on the first and the last sliding shoes on one of the railing girders is presented in Figure 6-122. According to Figure 6-122a, the average stress on both shoes varies between 0.22 and 0.30 ksi. Even with equal friction specified for both railing girders, the maximum normal stress varies between 0.45 and 0.92 ksi. As shown in Figure 6-122b, the railing girder elevation difference creates a small displacement in lateral direction, and the average normal stress varies between 0.21 and 0.31 ksi; the maximum normal stress varies between 0.45 and 1.0 ksi.



(a) Equal railing girder alignment and friction



(b) Unequal railing girder alignment with equal friction

Figure 6-122. Normal stress at sliding shoes

6.5.3 Force Control Continuous Slide

Under force control sliding analysis, the structure is expected to slide when the applied force exceeds the resisting force of 72 kips. In the analysis described herein, the pulling force is gradually applied to each sliding rail with a ramp function as shown in Figure 6-123. The pulling force is gradually increased to 85 kips and maintained at that level until the bridge moves 62.5 ft.

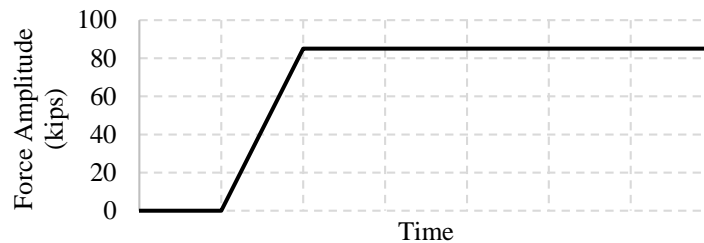


Figure 6-123. Pulling force applied in the direction of slide

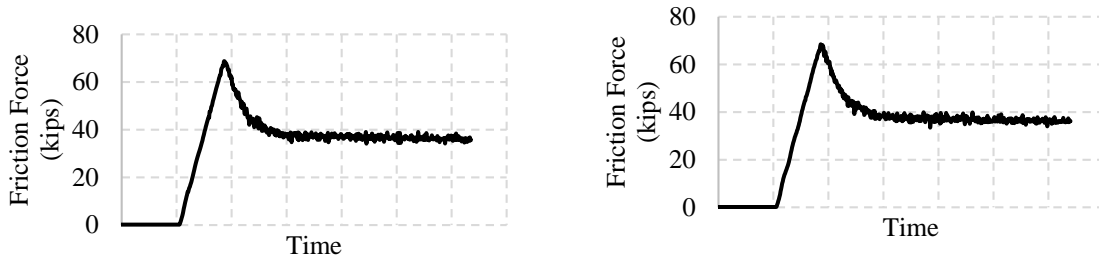
6.5.3.1 Sliding Friction Forces

Friction forces developed during force control sliding are presented in Figure 6-124. As shown in Figure 6-124, friction force is linearly proportional to the applied force until the applied force equals the static friction force. Once the sliding initiates and the velocity increases, the friction force decreases by the reduction in the coefficient of friction as per defined decay rate and remains constant during the remaining time of the move.

The static friction coefficient at each sliding surface is specified as 10%. The vertical force acting on each temporary structure is 720 kips. Hence, the expected total friction force on each temporary structure at the onset of sliding, and in the direction of sliding, is 72 kips (i.e., 0.1×720). The maximum friction force displayed is 69 kips. The discrepancy is from numerical error as discussed in Section 6.5.2.1. Once the sliding velocity reaches 10 in/s, a kinetic friction coefficient of 5% is in effect until the slide is completed. The constant friction force acting on each rail during that time is 36 kips (i.e., 0.05×720) (Figure 6-124).

The impact of unequal railing girder alignment on the sliding forces and movement is analyzed. During this analysis, equal friction properties are maintained on both railing girders. The railing girder at abutment B is raised 0.31 ft above the railing girder at abutment

A. No significant transverse movement is observed under force control. Friction forces acting on each temporary structure remained the same (Figure 6-124b).



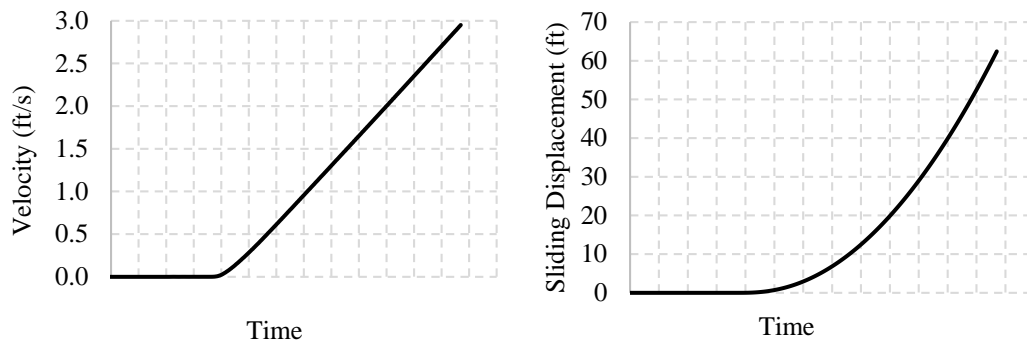
(a) Equal railing girder alignment and friction

(b) Unequal railing girder alignment, but equal friction

Figure 6-124. Friction force developed under the force control sliding method

6.5.3.2 Velocity and Displacement Histories

When the force that is gradually increased exceeded the resistance, the bridge superstructure started moving. At this initial stage, the superstructure also developed acceleration. Acceleration is reduced when the difference between the applied force and the friction force becomes constant. Velocity increases linearly until the end of the move (Figure 6-125a). As a result of linearly increasing velocity, displacement rate also increases (Figure 6-125b). Additional discussion of the force control slide-in procedure is given in Section 2.5.2.2.



(a) Velocity vs. time

(b) Displacement vs. time

Figure 6-125. Variation of velocity and displacement with respect to time under force control sliding

6.5.3.3 Forces on the Temporary Structure

Forces transmitted to the temporary structure during slide and their influence on the support reactions are discussed in Section 6.5.2.3. Figure 6-126 shows the variation of velocity against time under displacement and force control sliding. In displacement control sliding

simulation, the rate of displacement (i.e., velocity) is increased from zero to 0.833 ft/s (i.e., 10 in/s) within a short duration, and it is maintained at a constant rate beyond that (Figure 6-126a). The change in the displacement rate generated acceleration subjecting the structure to amplified loads as presented in Section 6.5.2.3. However, in the force control sliding simulation, the bridge superstructure's initial motion is slow, and the rate of change of velocity is quadratic until achieving a linear profile (Figure 6-126b). Because of the small acceleration at the beginning of the motion, dynamic effects are not significant. Figure 6-127 shows the variation of the temporary structure horizontal reactions with respect to time under (a) equal railing girder alignment with equal friction, and (b) unequal railing girder alignment with equal friction.

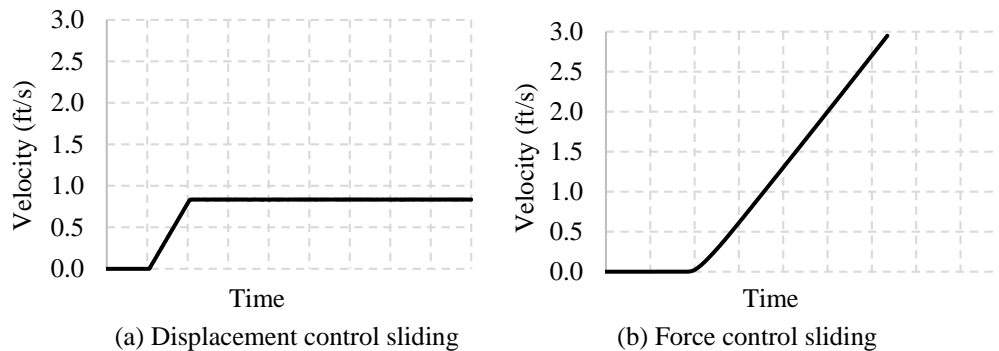


Figure 6-126. Variation of velocity with respect to time under displacement control and force control sliding

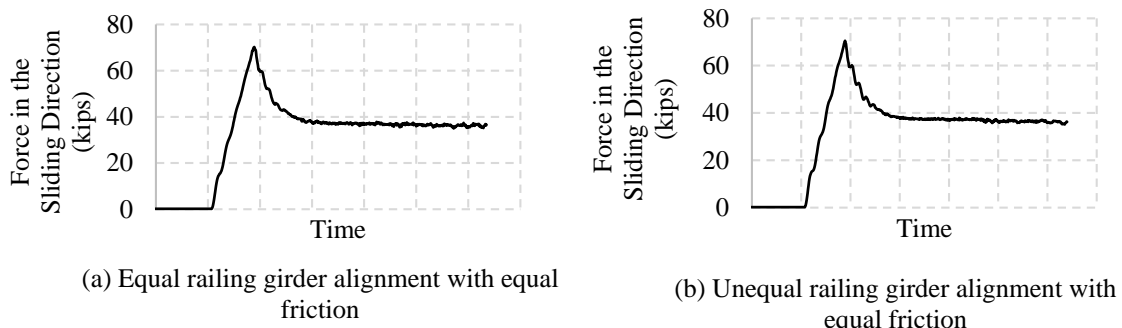
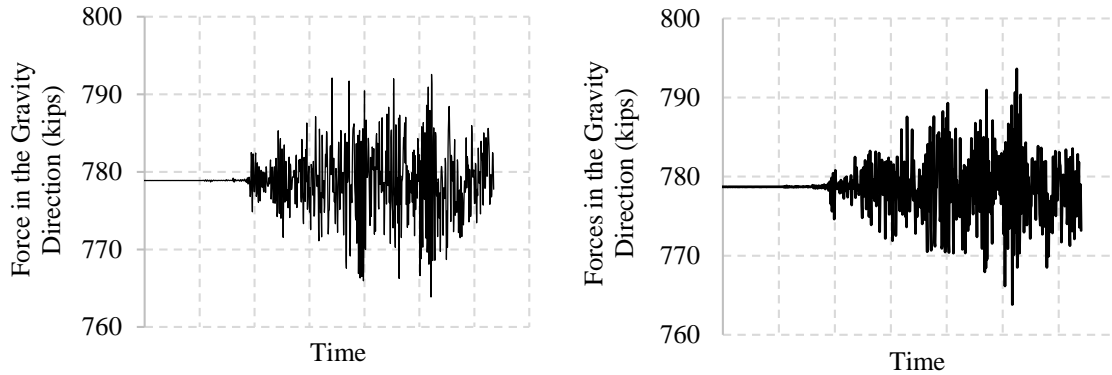


Figure 6-127. Temporary structure's horizontal reaction in the sliding direction

The vertical reactions at the temporary structure supports are shown in Figure 6-128. A sliding structure's dynamic effects create the fluctuations in the vertical reactions. However, the amplifications are below 1%.



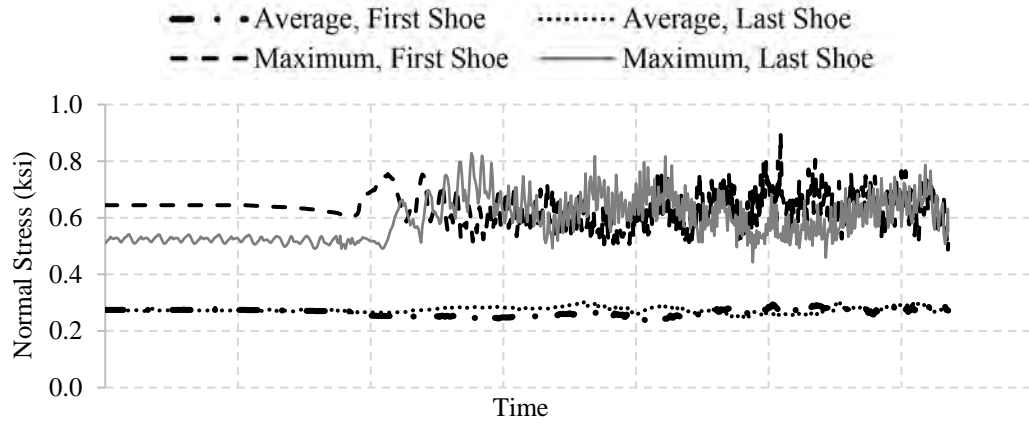
(a) Equal railing girder alignment with equal friction

(b) Unequal railing girder alignment with equal friction

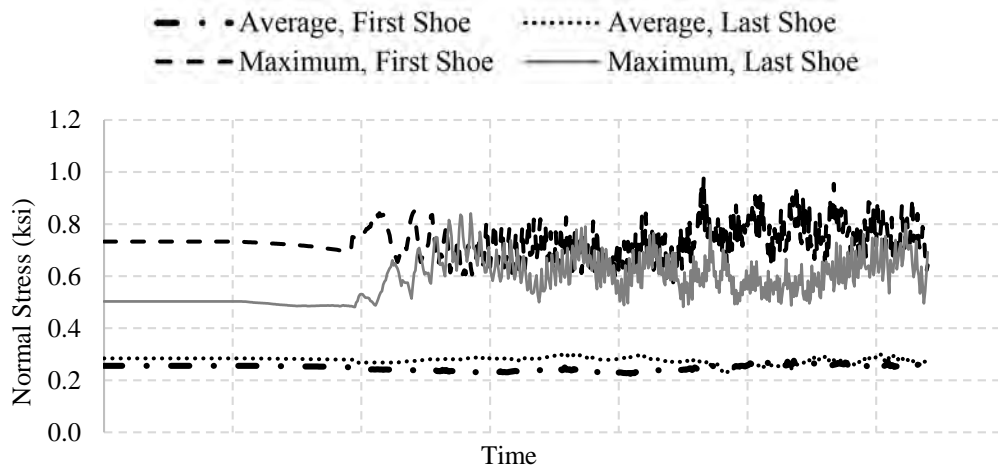
Figure 6-128. Vertical reactions at the temporary structure supports

6.5.3.4 Normal Stress at PTFE – Steel Interface

Normal stress distribution at the PTFE-steel interface is not uniform. The reasons are discussed in Section 6.5.2.4. The normal stress calculated under force control is shown in Figure 6-129. According to Figure 6-129a, the average stress on both shoes varies between 0.24 to 0.30 ksi, and the maximum stress varies between 0.44 ksi to 0.90 ksi. Unequal railing girder alignment influence is minimal. The average stress varies between 0.22 to 0.30 ksi while the maximum stress varies between 0.48 to 0.98 ksi (Figure 6-129b).



(a) Equal railing girder alignment and friction



(b) Unequal railing girder alignment with equal friction

Figure 6-129. Normal stress at sliding shoes

6.5.4 Force Control Discrete Sliding

6.5.4.1 Sliding Process and Parameters

Pulling or pushing of a bridge superstructure is not a continuous operation. The superstructure is pulled or pushed to a certain distance, depending on the stroke capacity of the jacks. The impact of this pulling or pushing process on the sliding process, as well as the temporary structure, is of interest.

The static friction force at each rail is 72 kips. Under force control sliding analysis, the structure is expected to slide at the instance pulling force overcomes the resisting force of 72 kips. As shown in Figure 6-130, the pulling force is gradually increased to 85 kips and maintained at that value until the velocity reaches 10 in/s. At that time, the force is removed, and bridge continues to slide for a while. The following four cases are simulated representing discrete sliding:

Case I:

- Both railing girders are at the same elevation.
- Equal friction occurs on both girders (10% static and 5% kinetic).

Case II:

- Unequal railing girder alignment (railing girder at abutment B is raised 0.31 ft above the railing girder at abutment A).
- Equal friction occurs on both girders (10% static and 5% kinetic).

Case III:

- Both railing girders are at the same elevation.
- Unequal kinetic friction occurs on railing girders (10% static on both, and 2% and 5% kinetic friction on railing girder at abutment A and B respectively).

Case IV:

- Unequal railing girder alignment (railing girder at abutment B is raised 0.31 ft above the railing girder at abutment A).
- Unequal kinetic friction occurs on railing girders (10% static on both, and 2% and 5% kinetic friction on railing girder at abutments A and B respectively).

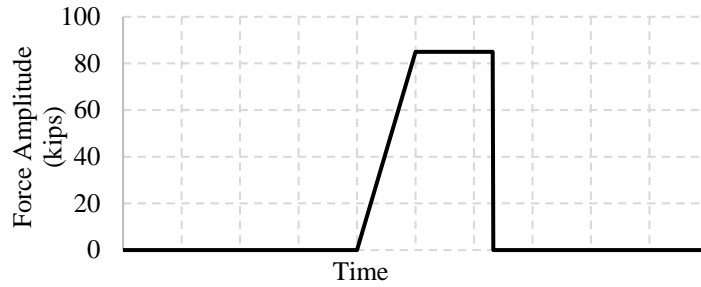


Figure 6-130. Pulling force applied in the sliding direction

6.5.4.2 Sliding Friction Forces

Sliding friction forces are presented in Figure 6-131. Initially, the friction forces developed follow the same pattern that is determined under continuous sliding under force control. After the pulling force is removed, the friction force started to increase until the superstructure stopped. This behavior is expected from the friction model used in the analysis. At the stoppage of motion, dynamic forces developed in the structure.

The maximum static friction force developed at the railing girder is reduced to 38 kips after sliding for a limited time (i.e., 0.05×720) (Figure 6-131). Once the pulling force was removed, the friction force jumped from 38 kips to 69 kips. The dynamic action at the time of stoppage developed cyclic loads between 24 and 32 kips, irrespective of the friction or alignment difference used in the analysis.

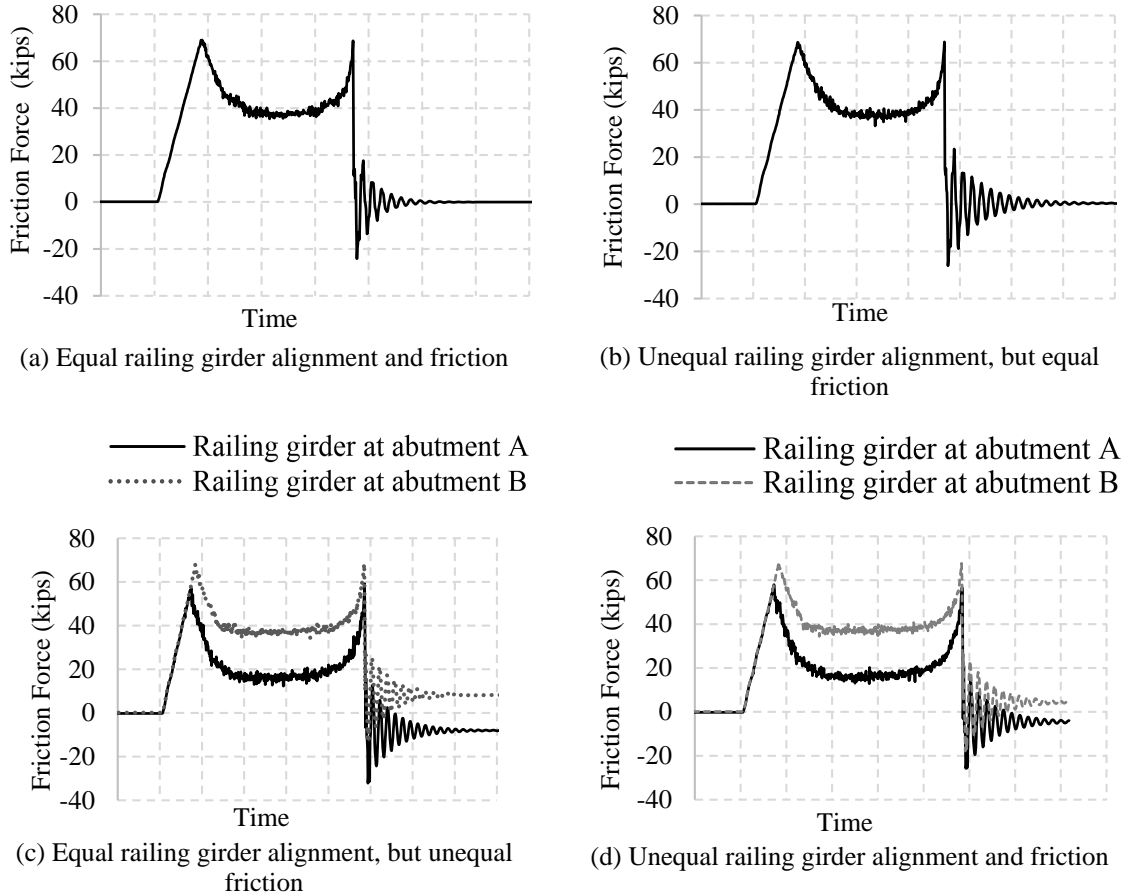


Figure 6-131. Friction force developed under discrete sliding

In addition to the friction forces that developed at the sliding surface, transverse drifting of the bridge superstructure is evaluated. An unequal railing girder alignment of 0.31 ft did not generate a noticeable drift. One reason for this can be the limited sliding distance, where the bridge superstructure is moved only about 9 ft during this discrete event.

Unequal friction of the railing girders caused a transverse drift of the bridge. Transverse drift of the bridge is restraints at one inch as shown in Figure 6-132. Analysis results show the influence of unequal friction and, under force control, the need for transverse restraints even when the railing girders are at equal alignment.

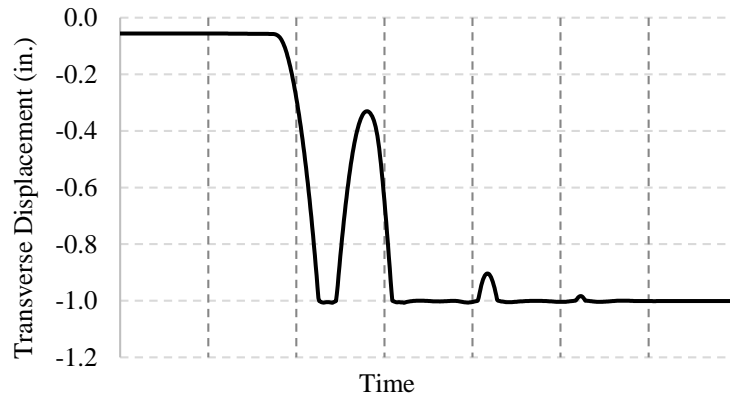
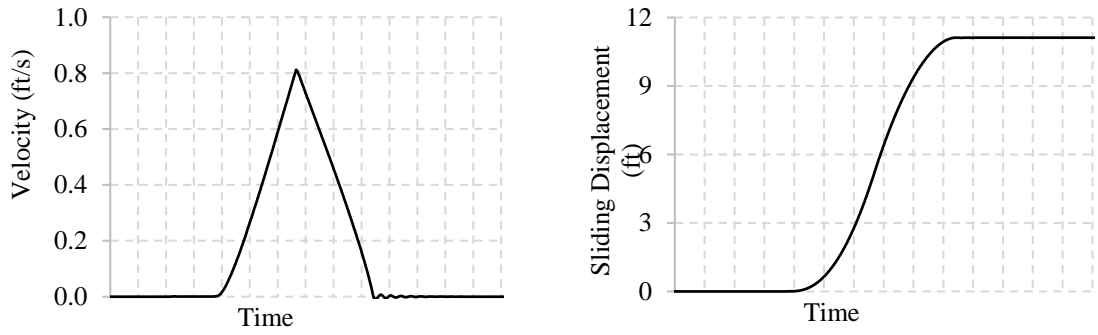


Figure 6-132. Transverse drift during sliding under force control with unequal friction

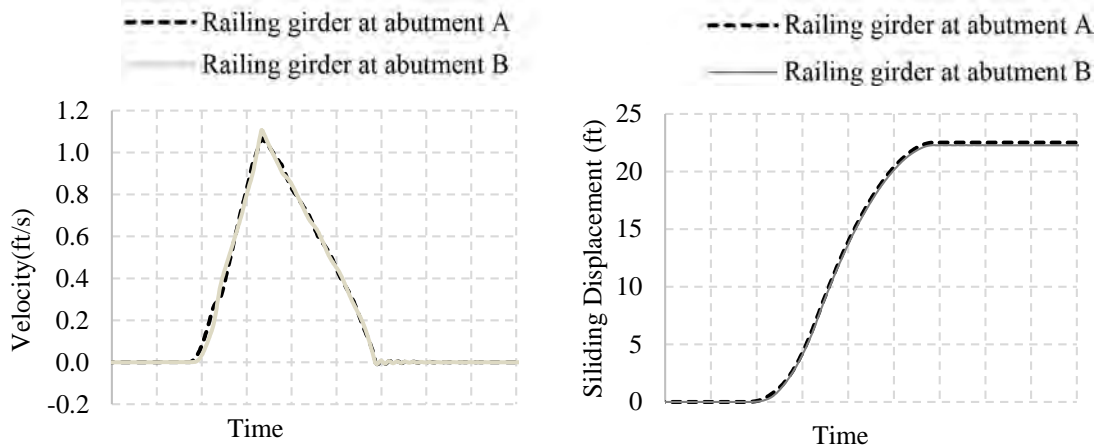
6.5.4.3 Velocity and Displacement Histories

Out of the four simulation cases listed earlier, only Case I and Case III are included for further analysis. The difference between Case I and III is the friction coefficients of railing girders. Case I incorporates equal friction, and Case III includes unequal friction on girders.

In Case I, once the sliding velocity reached 10 in/sec, the force is removed, and the superstructure is allowed to slide under the resisting forces until stopped. The superstructure moved about 6 ft after the force was removed. The superstructure velocity in Case III reached 13 in/sec before removing the force. The increase in velocity is due to the lower kinetic friction at the railing girder at abutment A. Once the force was removed, the superstructure moved about 15 ft. Figure 6-133 shows velocity and displacement histories for these two cases. Table 6-16 summarizes the model parameters and observations.



(a) Equal railing girder alignment and friction



(b) Equal railing girder alignment, but unequal friction

Figure 6-133. Discrete sliding velocity and displacement with respect to time under force control

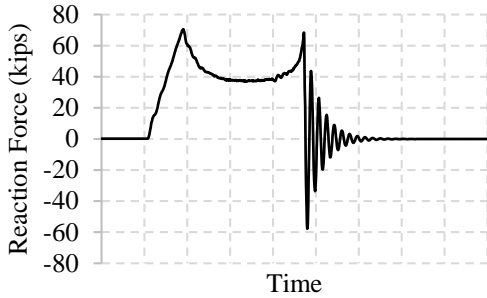
Table 6-16. Model Parameters and Observations

Description	Parameters and Observations	
	Case I	Case III
Railing girder	At same elevation	At same elevation
Static friction	10%	10%
Kinetic friction	5%	2% at railing girder at abutment A 5% at railing girder at abutment B
Maximum sliding velocity (in/sec)	10	13
Distance moved after removing the force (ft)	6	15
Superstructure transverse drift	No	Yes

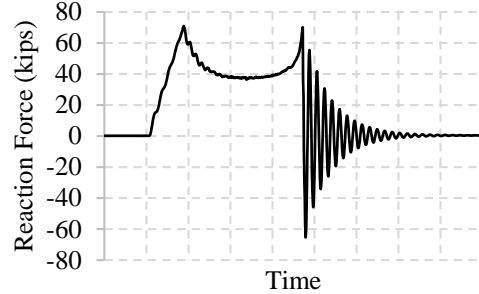
6.5.4.4 Forces on the Temporary Structure

Figure 6-134 shows the horizontal reactions with respect to time under (a) equal railing girder alignment with equal friction, (b) unequal railing girder alignment with equal friction, (c) equal railing girder alignment with unequal friction, and (d) unequal railing girder alignment with unequal friction. As shown in Figure 6-134, once the superstructure stopped,

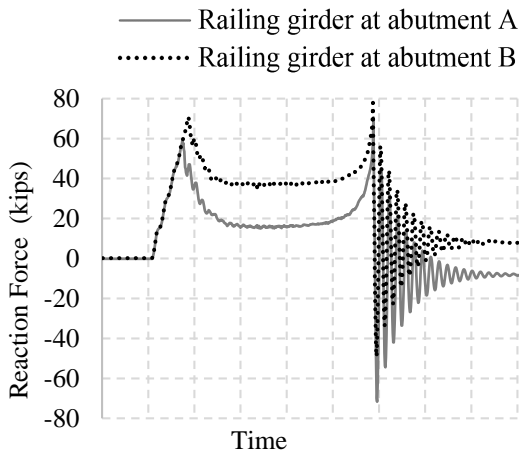
dynamic forces were generated with the maximum amplitude of about 72 kips. The dynamic force amplitude at the railing girder ranged between 24 kips and 32 kips. Forces developed at the temporary structure supports were amplified due to dynamic effects.



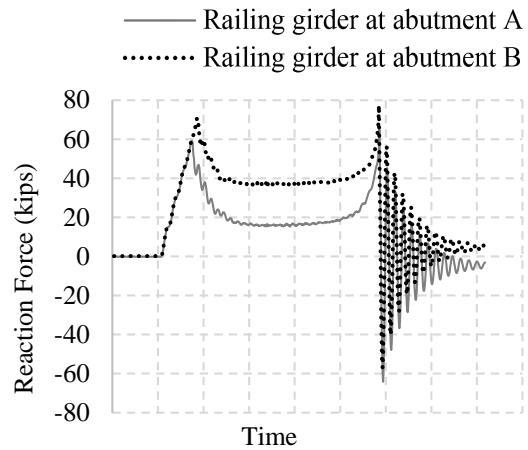
(a) Equal railing girder alignment and friction



(b) Unequal railing girder alignment, but equal friction



(c) Equal railing girder alignment, but unequal friction



(d) Unequal railing girder alignment and friction

Figure 6-134. Temporary structure reactions in the sliding direction

The vertical reactions at the temporary structure supports are shown in Figure 6-135. Sliding structure dynamics also generate fluctuations in the vertical reactions. However, the maximum dynamic amplification in the vertical reaction is about 2.5%.

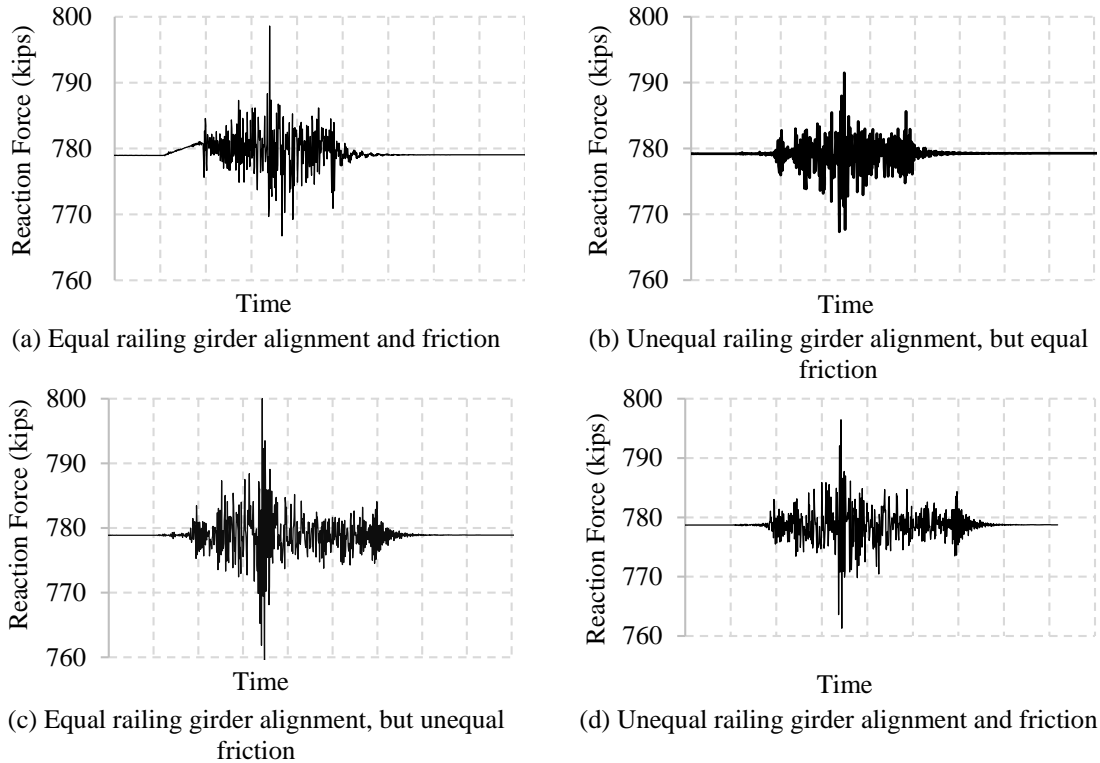
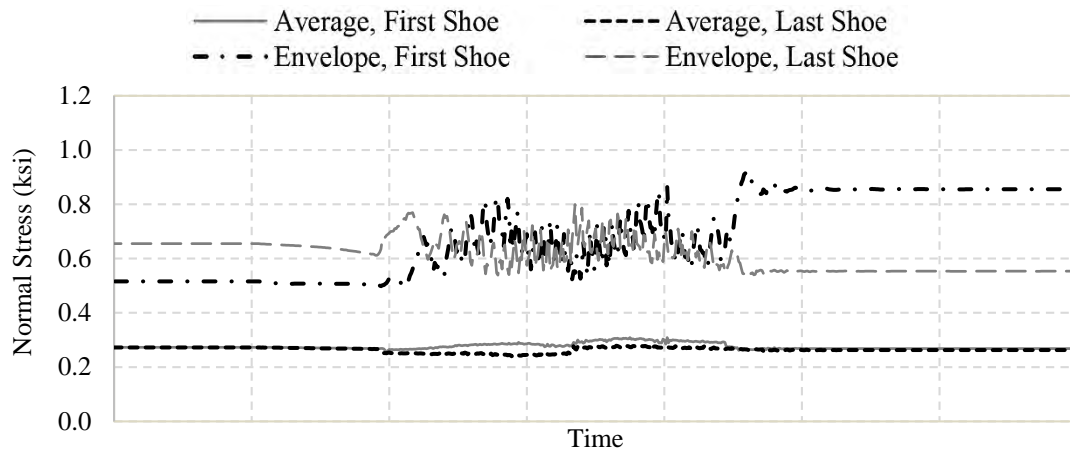


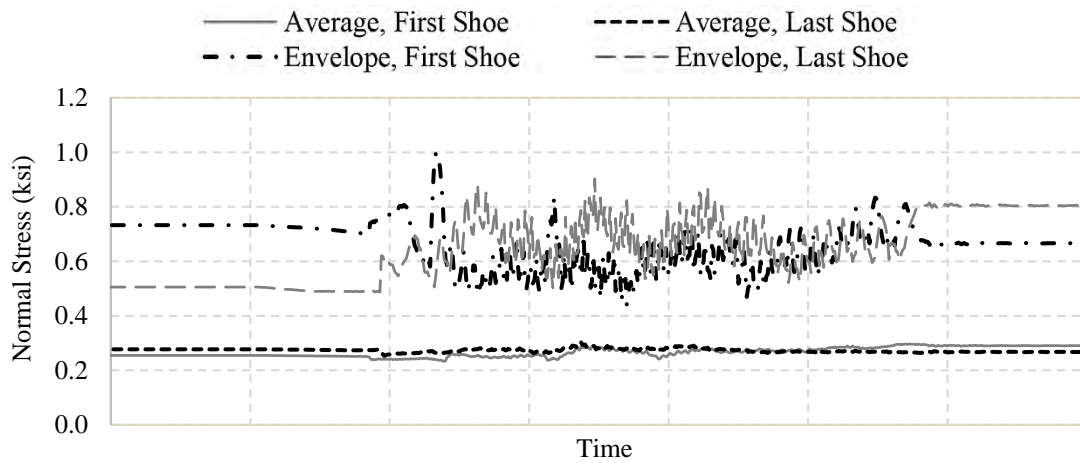
Figure 6-135. Vertical reactions at the temporary structure supports

6.5.4.5 Normal Stress at PTFE-Steel Interface

Normal stress distribution at the PTFE-steel interface is not uniform, and the reasons are discussed earlier as non-uniform vertical flexibility and surface tolerances of the railing girders. The normal stress calculated under the force control discrete move simulation is shown in Figure 6-136. According to Figure 6-136a, the average stress on both shoes varies between 0.24 and 0.30 ksi. When the kinematic friction is different, the average stress varies between 0.23 and 0.30 ksi, and the maximum stress varies between 0.44 and 1.00 ksi (Figure 6-136b).



(a) Equal railing girder alignment and friction



(b) Equal railing girder alignment, but unequal friction

Figure 6-136. Normal stress at sliding shoes

6.5.4.6 Transverse Support Reactions

The sliding girder drifted in the transverse direction due to unequal friction (Figure 6-137). Constraints (or transverse supports) are provided to limit this movement. Reaction forces developed at these supports due to the horizontal restraints are presented in this section. Analysis cases III and IV are considered. Analysis case III is equal alignment between the railing girders with unequal friction. Analysis case IV is unequal friction and unequal alignment between the railing girders. The unequal friction is 2% and 5% kinetic friction at the railing girder at abutments A and B, respectively. In addition, the railing girder at abutment B is raised 0.31 ft above the railing girder at abutment A.

The 3% unequal friction is large enough to cause transverse drift of the sliding superstructure. This is aggravated by the unequal alignment. The drift would have been greater than 1 in. tolerance. The constraints provided in the model contained the bridge while allowing the longitudinal move. The forces developed as a result of the transverse restraints are shown in Figure 6-138.

During the move, the sliding girder made repeated contact with the lateral supports until a continuous contact was maintained. Contact with the lateral supports generated impact forces of between 75 kips and 110 kips at the both temporary abutments A and B, irrespective of the railing girder alignment (Figure 6-138). A larger force is developed at the temporary structure at abutment B because of the higher kinetic friction. In Case III and Case IV, with continuous contact with the lateral support, restraining forces are reduced to 3-kip and 8-kip forces, respectively. In Case IV, unequal railing girder alignment marginally increased the forces developed at transverse supports.

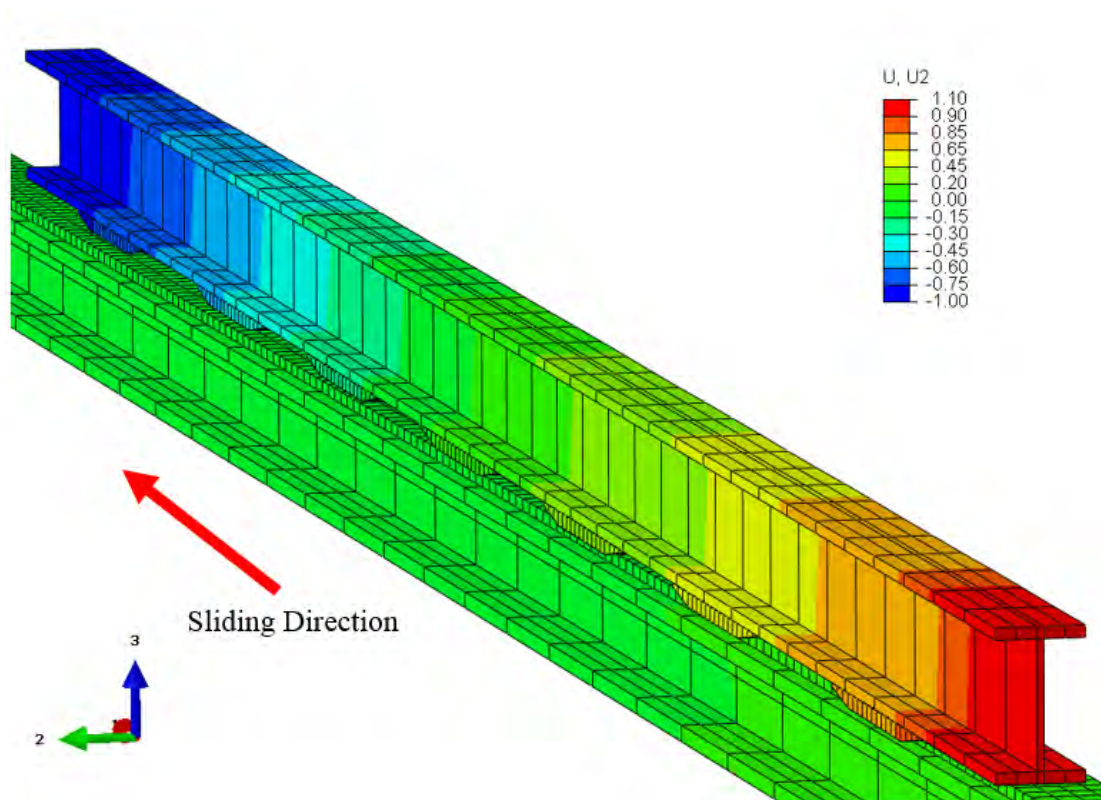
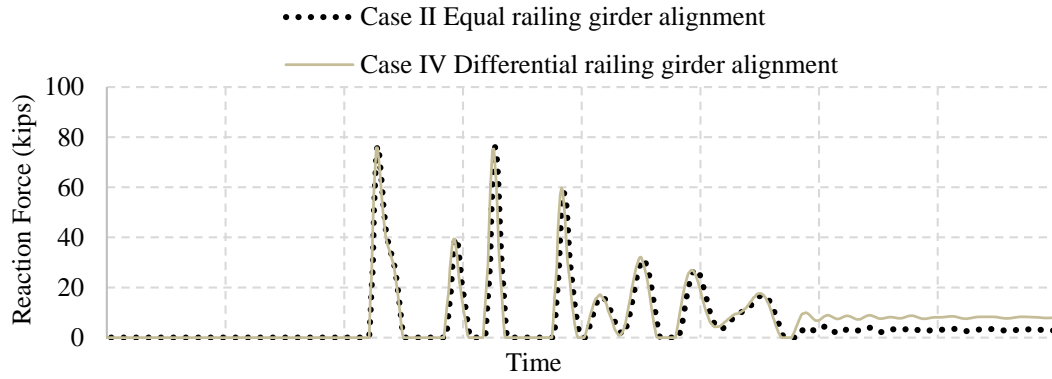
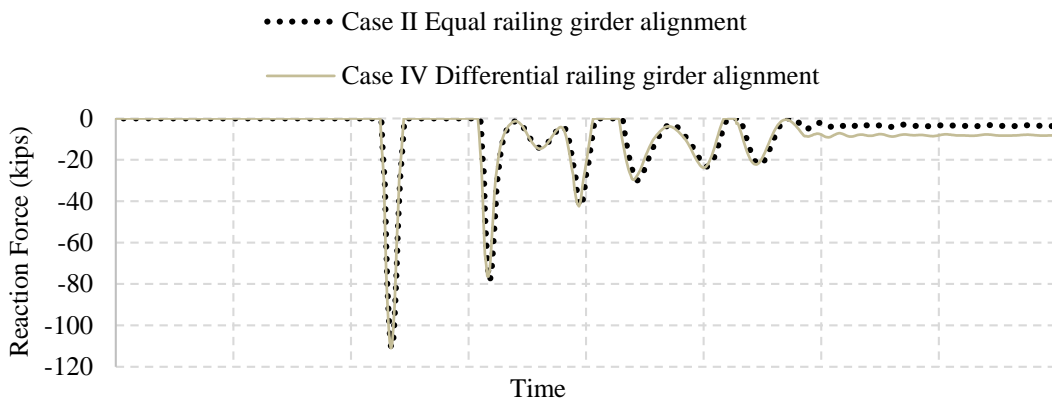


Figure 6-137. Transverse drift of sliding girder (5 times amplified)



(a) Temporary structure at abutment A



(b) Temporary structure at abutment B

Figure 6-138. Transverse support reaction forces

6.5.5 Permanent Bearing Installation Process

6.5.5.1 Overview

Following the move of the US-131 over 3 Mile Road bridge superstructure to its final alignment, bearings were installed. The bridge superstructure was lifted with jacks placed on the backwall; the temporary supports (wooden blocks) on the sliding girder are removed, and the bridge superstructure was lowered onto the permanent bearings. To lift the bridge, the original plan was to use seven jacks with the equal hydraulic pressure. The seven jacks were supplemented by two additional jacks, placed underneath each fascia beam. The permanent bearing replacement process is described in Section 6.3.1.9.

The objective of this simulation is to evaluate the stresses developed in the deck and backwall, and assess their potential impact on structural integrity. The original jacking plan with seven jacks is considered in this analysis. Figure 6-139 shows the hydraulic jack locations. Since the jacks were supplied with equal pressure, this represents the force control process discussed in Section 2.5.2.2.

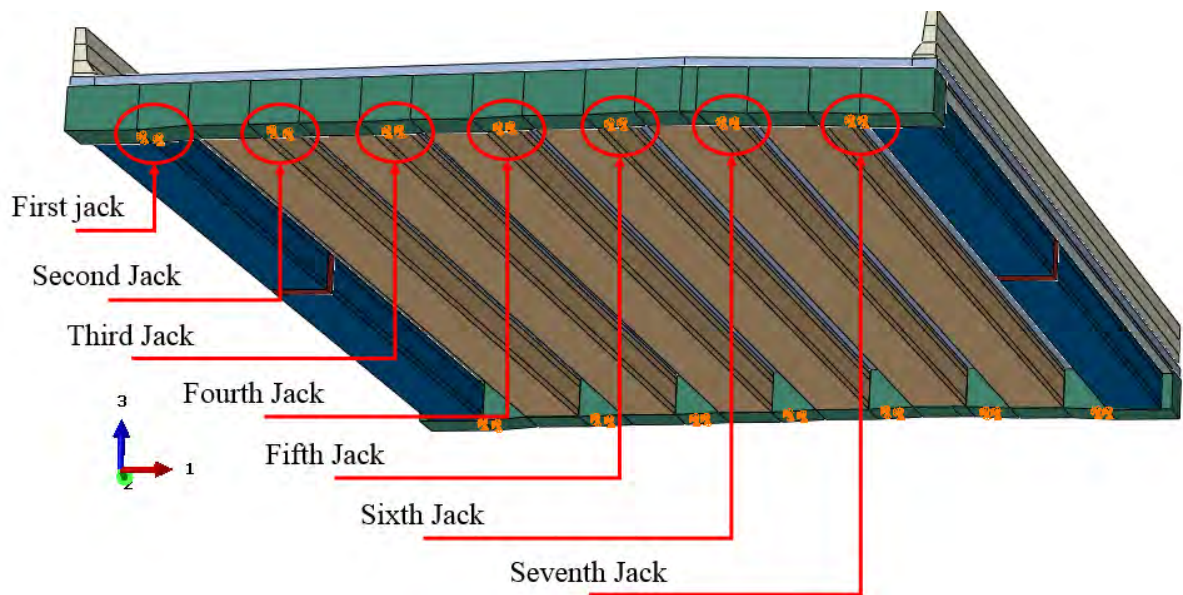


Figure 6-139. Hydraulic jack locations

6.5.5.2 Finite Element Model

The objective of the analysis is to evaluate deck and backwall stresses. The bridge superstructure is discretized by a refined FE mesh. The bridge deck and backwall mesh and element aspect ratios are defined to yield accurate stresses. Figure 6-140 shows the FE mesh configuration.

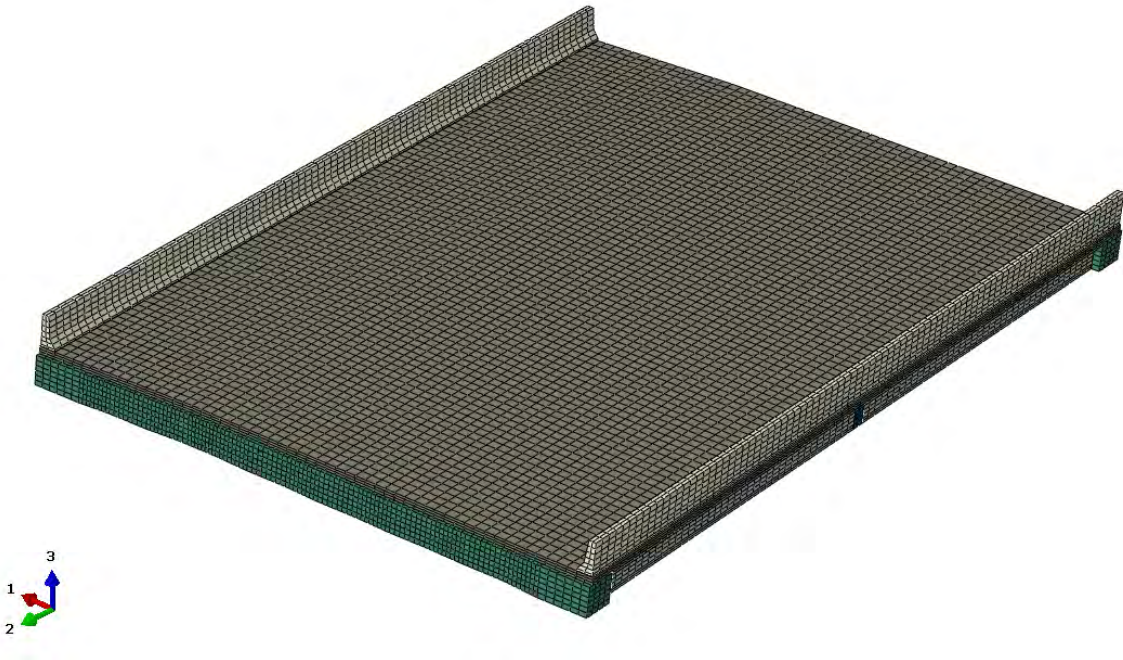


Figure 6-140. FE mesh configuration

6.5.5.3 Analysis Results

Boundary conditions imposed at the supported end of the bridge emulated wooden block supports. Hydraulic jacks support the other end. Initially, the gravity load is applied, and the reactions at the hydraulic jack locations are calculated. These reactions represent the load carried by the respective jacks placed underneath the backwall (Figure 6-141).

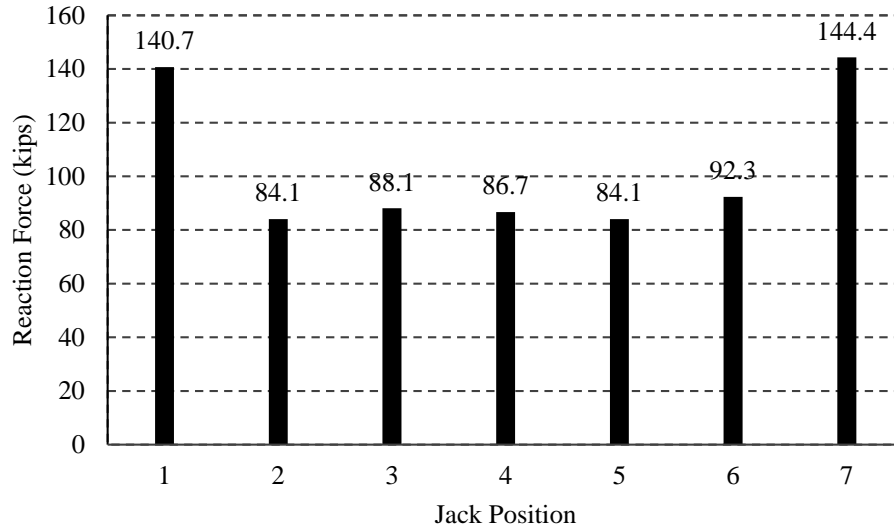


Figure 6-141. The expected force carried by each hydraulic jack

Under the force control lifting the structure using multiple jacks, each jack generates equal force and may not displace equally. Hence, force control develops differential deformations resulting in stresses in the bridge deck and the backwall. Analysis is performed by applying equal force at each hydraulic jack location (Figure 6-142). The force is gradually increased while displaying the deck stresses and the deformations. Under non-uniform dead load on each jack location, the non-uniform deformation of the backwall is shown in Figure 6-143.

During the analysis, the differential deflection (Δ) and the tensile stresses developed in the deck were calculated. Differential deflection is the difference between the maximum backwall deflections measured with respect to a reference drawn between the ends of the backwall as shown in Figure 6-143. Deck tensile stress variation over the backwall against the calculated differential deflection is shown in Figure 6-144.

The design compressive strength of deck concrete is 4 ksi. Specified ACI and AASHTO tensile strength limits are given in Table 6-17. Based on the tensile strength limits, the limits for differential deflection are established to avoid deck cracking. As per the strength and differential deflection limits shown in Table 6-18, the differential deflection should be kept below 0.23 in. to minimize the deck cracking potential. The analysis results show that when the backwall is lifted 0.25 in. to remove the wooden blocks, a maximum tensile stress of 480

psi develops in the deck. The results show that even without the extra two jacks the bridge superstructure can be lifted without reaching tensile strength of deck concrete.



Figure 6-142. Application of forces at the hydraulic jack positions

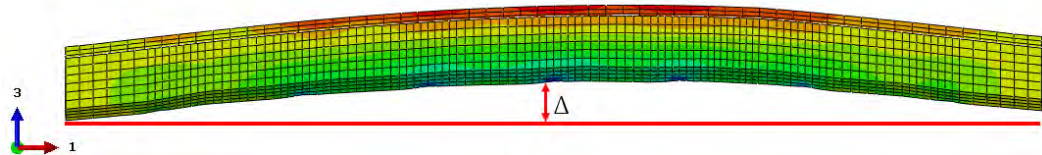


Figure 6-143. Deformed shape of the backwall

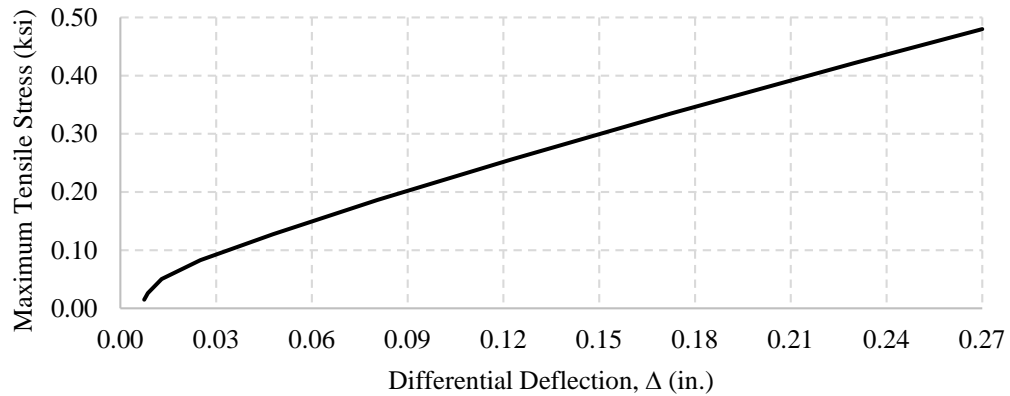


Figure 6-144. Maximum tensile stresses developed in the deck over the backwall vs. differential deflection (Δ)

Table 6-17. Tensile Strength of Concrete

ACI 318 Article R10.2.5	10 to 15% of compressive strength
AASHTO LRFD Article 5.4.2.6	$0.24\sqrt{f'_c}$

Table 6-18. Tensile Strength and Critical Differential Displacement

Compressive strength (ksi)	Tensile Strength (ksi)		Critical differential deflection, Δ (in.)	
	ACI 318 R10.2.5	AASHTO 5.4.2.6	Minimum	Maximum
4.0	0.4-0.6	0.48	0.23	0.36

6.5.6 Summary

The US-131 over 3 Mile Road Bridge slide-in and vertical jacking processes for permanent bearing installation are simulated. The objective is to evaluate the impact of unequal alignment of the abutments, unequal friction between sliding surfaces, continuous and discrete sliding, and sliding under displacement and force control and the associated stresses or stress resultants developed in the temporary structures.

Analysis is performed under displacement and force control procedures. Analysis is also performed in continuous and discrete move modes. In the continuous analysis, the superstructure was moved to the final position without a pause. In the discrete case, the superstructure moved with several pauses, more closely representing the typical slide operation. The purpose of the discrete move is to evaluate the dynamic forces that developed with each start and stop. For each analysis, railing girders at abutments A and B are positioned at the same alignment or unequal alignment with abutment B's railing girder raised 0.31 ft above the railing girder at abutment A. In addition, the analysis is performed with equal friction and unequal friction on the sliding surfaces of the railing girders. The breakaway friction of 10% and a kinetic friction of 5% are defined. For unequal friction, the static friction is kept at 10%, but the kinetic friction of 2% and 5% are defined for the railing girder sliding surfaces at abutments A and B, respectively.

The following conclusions are derived based on the finite element simulation results presented in this chapter:

1. The dynamic forces developed in the displacement control sliding simulation are not observed with the force control sliding. This is due to the small acceleration developed at the onset of sliding. A properly designed hydraulic system with a computerized control can be utilized to limit the initial acceleration that develops under the displacement control method. Implementation of the displacement control sliding method allows sliding the superstructure without transverse drift, irrespective of the difference in friction of the sliding surfaces.
2. Unequal friction develops under the sliding surfaces due to non-uniform stress at the PTFE-steel interface, sliding surface tolerances, substructure flexibility and many

other factors. Non-uniform interface stress is primarily due to unequal loads on the sliding shoes caused by changing railing girder flexural stiffness with discrete support locations, superstructure drifting, and other superstructure deformations. As a result of unequal friction, the superstructure drifts in the direction transverse to the direction of sliding. Hence, providing lateral restraints is important to keep the bridge aligned with the slide direction irrespective of the railing girder alignment difference.

3. During discrete sliding, larger horizontal reactions are calculated at the temporary structure supports, in the direction of slide. This is due to the dynamic effects and requires additional work and monitoring to accurately quantify these forces and to develop design recommendations.
4. To remove the temporary supports (wooden blocks) placed on the sliding girder and place the bridge on permanent bearings required lifting the superstructure. Simulation of this jacking operation showed that limiting the differential deflection to about 0.23 in. is needed to minimize the deck cracking potential of this structure.
5. Having access to field data is highly desirable to validate the analysis results. The analysis capabilities demonstrated here, with field monitoring from future projects, can be implemented to standardize SIBC activities.
6. Use of the displacement control method with force monitoring for moving the bridge is recommended for SIBC to resolve the majority of the complexities documented in the implemented projects.

7 SUMMARY, CONCLUSIONS, AND RECOMMENDATIONS

7.1 SUMMARY AND CONCLUSIONS

Accelerated bridge construction (ABC) projects completed and currently being implemented include prefabricated bridge elements and systems (PBES), slide-in bridge construction (SIBC), and self-propelled modular transporter (SPMT) moves. The goal of this project is to advance the implementations by developing scoping guidelines for all ABC alternatives, standardizing the bridge slides operations, and developing guidelines for foundation construction while the existing bridge is in service. The specific tasks were (a) reviewing the ABC activities nationally and monitoring ongoing ABC projects in Michigan, (b) defining scoping parameters for the implementation of SIBC and SPMT moves, (c) reviewing and evaluating substructure construction and upgrades, along with constructability of deep foundations while the existing bridge is in service, (d) developing specific cost methodologies for SIBC, SPMT moves, and foundation construction, and (e) developing recommendations to improve SIBC implementations.

The first task was the review and synthesis of the state-of-the-art and practice of ABC. A total of 123 completed ABC projects were reviewed, including 76 PBES, 30 SIBC, and 11 SPMT moves. The documentation of ABC projects is the primary source of information. The synthesized knowledge base also compiled from the literature review established the foundation of the findings and recommendations presented in this report.

A multi-criteria decision-making process and the associated software platform were developed during an earlier project. The platform, named the Michigan Accelerated Bridge Construction Decision (Mi-ABCD) tool, formalizes the choice between Accelerated Bridge Construction (ABC) alternatives and Conventional Construction (CC) for a specific site. The framework of Mi-ABCD is expanded to incorporate SIBC and SPMT move activity parameters. The parameters specific to SIBC and SPMT move are incorporated under the (1) Site and structure considerations (S&ST), (2) Cost, (3) Work zone mobility (WZM), (4) Technical feasibility and risk (TF&R), (5) Environmental considerations (EC), and (6) Seasonal constraints and the project schedule's (SC&PS) major parameters. An update to Mi-ABCD will be simpler with the structure of the framework remaining the same. The next

version will include the capability to evaluate the construction delivery alternatives between SPMT moves, SIBC, CC, and PBES for a specific site.

One of the tasks of this study was to identify methodologies for foundation construction while the existing bridge is in service. A comprehensive literature review was conducted to document (a) typical foundation types and advantages and limitations with respect to their implementations in ABC, (b) foundations implemented in completed ABC projects, (c) published and documented foundation policies of highway agencies, and (d) a summary of foundations implemented in other non-bridge projects including implementation details and difficulties. In this task, a foundation type classification was developed based on the degree of disturbance to the surrounding soil during foundation installation. Additionally, a scoping flowchart was developed and presented for foundation reuse, retrofit, or replacement decisions. Also included were conceptual examples of foundation reuse, retrofit, and replacement.

The scoping process that involves evaluating bridge construction alternatives for a specific site needs to account for the costs associated with ABC. Thus, a cost-benefit analysis was warranted. The mobility impact restrictions specific to ABC generate benefits to the agency and users. However, ABC implementations, especially SIBC and SPMT move, require methodologies and staging work, prior to on-site construction, which create additional costs. The initial cost activities specific to SIBC include temporary structures, equipment and accessories, and slide operations. The SPMT move-specific initial costs include specialty equipment/contractor, mobilization cost, along with travel path and staging area preparation cost. The costs data presented in Chapter 5 are extracted from a detailed analysis of completed ABC projects. The benefits of ABC are often only represented as user cost. In this task, a list of quantifiable benefits in addition to user cost is defined. The benefit parameters are (i) economic impact to nearby businesses and surrounding communities, (ii) seasonal limitations, (iii) work zone risk to traffic, and (iv) site condition complexities. These parameters are quantitative and qualitative. The quantitative parameters include costs such as maintenance of traffic (MOT), user, and life-cycle. These costs contribute to ABC's benefits because of short work-zone construction duration and anticipated long-term durability performance. The cost benefit methodology proposed is the conversion of

quantitative parameters to qualitative. With this process, all benefit parameters are evaluated using an Analytical Hierarchy Process in the Mi-ABCD where the quantitative values are converted to preference ratings. Chapter 5 presented ABC costs, benefit parameters, and models.

SIBC is different from conventional bridge construction because of the activity required to move the bridge to its final position following construction. The critical components of SIBC are the temporary substructure, sliding system, transition substructure, and actuation system. In the two recent SIBC projects in Michigan, different sliding and actuation systems are incorporated. Also, there are differences in temporary substructures and transition structures. In both cases, however, observations indicated that primary difficulties during the moves appear from the sliding and actuation system.

For example, the M-50 over I-96 bridge pier is supported on a shallow foundation. A preliminary analysis indicated that, as the bridge is being moved onto the pier, there might be measurable vertical deformations. The pier was instrumented with laser targets, and a non-contact laser tacker measured the movement during the slide. The conclusions from monitoring data analysis and the associated FE analysis are as follows:

- During the move, forces and deformations on the pier were expected in the vertical and sliding direction from friction and gravity due to the weight of the superstructure. The monitoring data indicated large transverse deformations, from an unexpected force in the lateral direction (normal to sliding direction). The transverse force calculated was between 158 kips and 357 kips whereas the slide direction forces were between 294 kips and 313 kips. These forces were generated from the differential friction between the skid-track. Since the push force of jacks that are equal does not balance with the resistance force due to friction, a force couple was created rotating the superstructure. The skid track resisted this rotation. Once the superstructure was released from the skid-track, the force transferred to the groove in the pier.
- The reported capacity of the jack specified for the move at pier was 187 kips. With the malfunction of the pier jack, the superstructure was pushed from the abutments only. Therefore, the distance between two push points was approximately the length of the bridge. As the distance between jacks increased, the transverse force created by the

couple due to differential friction also increased. Even with an experienced move contractor, a comprehensive analysis needs to be requested before allowing procedural changes to the move operation. Additionally, the temporary substructure was directly in contact with the pier cap. This connection allowed force transfer in the move direction from the temporary substructure to the pier. The temporary and permanent substructures needed to include a key allowing only vertical force transfer to the permanent substructure.

- The maximum tensile stress calculated by FE analysis at the pier cap was 0.80 ksi. The maximum tensile stress calculated in the wall and foundation was 0.44 ksi. The largest stresses were generated at the column wall interface. The level of stress, although above the cracking strength, was not a concern. This is because the superstructure weight would apply compressive stresses at those locations and reduce the tensile stresses. No visible cracks were expected at the wall and foundation. This analysis was based on limited displacement measurements. The forces were calculated from the structural properties of the pier and foundation. In order to evaluate the move forces to the superstructure and substructure, a robust monitoring program is required.

An FE analysis of the US-131 over 3 Mile Road Bridge slide-in and vertical jacking processes for permanent bearing installation was performed. The objective was to evaluate the impact of unequal abutment alignment, unequal friction between sliding surfaces, push and stop (discrete) sliding process, and displacement and force control of the hydraulic system. In addition, the simulations were performed to demonstrate the capability that can be useful in the future for implementation on complex projects. The simulations explained the reasons of lateral drift of the superstructure during the move. Dynamic effects and substructure loads were also an outcome of the simulations. The following conclusions were derived from the simulations performed on the specific bridge and temporary structure configuration:

- A hydraulic system with computerized operation needs to be utilized to limit the initial acceleration; thus, to limit the dynamic forces developed at the onset of sliding.
- Implementing displacement control of the sliding will prevent the transverse drift, irrespective of the difference in friction between the sliding surfaces.

- During discrete sliding, larger horizontal reactions, in the direction of slide, were calculated at the temporary structure supports. This was due to the dynamic effects and requires additional monitoring and analysis to accurately quantify these forces while developing temporary structure design recommendations.
- Simulation of the jacking operation for removing temporary supports (wooden blocks) and placing the structure on permanent bearings showed that differential deflection should be limited to 0.23 in. to minimize the deck cracking potential.

7.2 RECOMMENDATIONS

The recommendations developed in this study are specific to (1) scoping parameters for the implementation of SIBC and SPMT moves, (2) foundation and substructure construction while the existing bridge is in service, (3) cost-benefit analysis, and (4) SIBC implementations. As a result, the following actions are advised:

1. Update the current version of Mi-ABCD platform (the decision-making model) to incorporate a full group of ABC alternatives.
2. Incorporate a cost-benefit analysis as part of the decision-making by incorporating the methodology developed in this project. The cost-benefit analysis can be a part of or an option in Mi-ABCD.
3. Implement the scoping process to evaluate the potential for foundation reuse or need for replacement.
4. Consider the following with regards to foundation reuse:
 - Adopt guidelines similar to Illinois DOT and associated analysis procedures for foundation reuse until additional research is performed to develop guidelines and procedures for reusing foundations specific to Michigan bridges.
 - Evaluate the existing foundation under lateral loads generated during bridge slides.
 - Develop a program to document unknown foundations to promote their reuse potential.
5. Shallow foundations, micropiles, or drilled shafts with supported excavations are suitable for replacing foundations within the vicinity of existing foundations.
6. The following recommendations are developed from the field monitoring, field measurements, and subsequent analysis of bridge slide operations:

- Provide details to maintain sliding superstructure alignment by controlling drift to the transverse direction. Unequal friction between the sliding surfaces develops due to numerous causes. Some causes are non-uniform pressure at the PTFE-steel interface, sliding surface and alignment tolerances, and variable substructure flexibility along the slide path. Unequal friction creates a force differential between jack locations. Unequal push force rotates the superstructure so that the slide alignment cannot be maintained.
- External use of lubrication to reduce the sliding friction is not recommended. Evaluate the use oil impregnated linear bearings to achieve a reliable sliding surface.
- Specify the quantitative analysis of sliding methodology. The slide analysis should include the deformability of all components. The bearing pad uplift and associated riding over the stopper bars is one of those complications that could have been avoided.
- Specify the use of a servo controlled hydraulic system with integrated force and displacement sensors that can be operated continuously while providing a feedback display of position. Such a push system will control the alignment of the bridge during the slide.
- The temporary design specifications need to be updated for SIBC implementations. Unaccounted factors include horizontal forces arising from slide operation, flexibility of horizontal members, and force transfer between the temporary and permanent substructures. For example, a key mechanism is required for eliminating the axial force while allowing the vertical load transfer to the permanent substructure.

8 REFERENCES

- AASHTO (2008). *Guide Specification for Bridge Temporary Works*, 1st Ed., 1995 with 2008 Interim Revisions, American Association of State Highway and Transportation Officials (AASHTO), Washington, D.C.
- AASHTO (2014). *LRFD Bridge Design Specifications*, Customary U.S. Units, 7th Ed., American Association of State Highway and Transportation Officials, Washington, DC.
- Abaqus (2015). *Abaqus Analysis User's Manual*, Version 6.14, SIMULIA, Dassault Systèmes, Waltham, MA.
- ABC Center (2014). "Archive of Past Accelerated Bridge Construction Events." *Accelerated Bridge Construction (ABC) Center, Florida International University*, <<http://www.abc.fiu.edu/archive-of-past-events/>> (April 17, 2014)
- Aggour, M.S., and Radding, W.R. (2001). *Standard Penetration Test (SPT) Correction*, Report: SP007B48, State Highway Administration, Maryland Department of Transportation, College Park, MD.
- AISC (2011). *Steel Construction Manual*, 14th Ed., American Institute of Steel Construction, Chicago, IL.
- Aktan, H. and Attanayake, U. (2013). *Improving Bridges with Prefabricated Precast Concrete Systems*, Report: MDOT RC 1602, Michigan Department of Transportation, Lansing, MI.
- Aktan, H.M., Attanayake, U., and Mohammed, A.W. (2014). *Accelerated Bridge Construction and Structural Move – Workshop*, Report No. RC-1610, Research Administration Michigan Department of Transportation, Lansing, MI.
- Algin, H. M. (2009). "Elastic Settlement under Eccentrically Loaded Rectangular Surface Footings on Sand Deposits." *J. Geotech. Geoenviron. Eng., ASCE*, 135(10), 1499–1508.
- Ardani, A, Mallela, J., and Hoffman, G. (2009). *Utah Demonstration Project: Rapid Removal and Replacement of the 4500 South Bridge over I-215 in Salt Lake City*, Final Report, the Federal Highway Administration, Washington, D.C.
- Armour, T., Groneck, P., Keeley, J., and Sharma, S. (2000). *Micropile Design and Construction Guidelines: Implementation Manual*. FHWA-SA-97-070, Office of Technology Application, Office of Federal Lands Highway Division, Federal Highway Administration, U.S. Department of Transportation, 400 Seventh Street, S.W., Washington D.C., 20590.
- Attanayake, U. B., Servi, A. and Aktan, H. M. (2012). "Noncontact bridge deformation monitoring using laser tracking technology," *Sixth International Conference on Bridge Maintenance, Safety and Management, IABMAS 2012*, Villa Erba, Cernobbio, Como, Italy, July 8-12.

AWS (2006). *Welding Codes (D1.1/D1.1M and D1.5/D1.5M)*, American Welding Society (AWS), Miami, FL.

Blau, P. J., (2009). *Friction Science and Technology from Concepty to Applications*, 2nd Ed., CRC Press, Boca Raton.

Bondonet G., and Filitrault A.(1997). "Frictional Response of PTFE Sliding Bearings at High Frequencies" *Journal Of Bridge Engineering*, 2:139-148.

Bonstedt, H. (2010). "A presentation on Life-cycle cost analysis for bridges – In search of better investment and engineering decisions." *Proc., Prestressed Concrete Association of Pennsylvania*, PA.

Bowles, J.E. (1997). *Foundation Analysis and Design*, Ed. 5th, the McGraw-Hill Companies, Inc., New York, NY.

Brady, N. C. and Weil, R. R. (2007). *The nature and properties of soils*, 14th edition, ISBN-13: 978-0132279383, Prentice Hall, Upper Saddle River, NJ.

Brown, D. A., Dapp, S. D., Thompson, W. R., and Lazarte, C. A. (2007). *Design and construction of continuous flight auger (CFA) piles*. Geotechnical Engineering Circular No. 8, FHWA-HIF-07-03, Office of Technology Application, Office of Engineering/Bridge Division, Federal Highway Administration, U.S. Department of Transportation, 400 Seventh Street, S.W., Washington D.C., 20590.

Brown, D. A., Turner, J. P., and Castelli, R. J. (2010). *Drilled Shafts: Construction Procedures and LRFD Design Methods*. FHWA NHI-10-016, National Highway Institute, U.S. Department of Transportation, Federal Highway Administration, Washington, D.C. 20590.

Buehler, D. (2004). "Transportation- and Construction-Induced Vibration Guide Manual," the California Department of Transportation, Noise, Vibration, and Hazardous Waste Management Office, Sacramento, CA 94274.

Chan, A., Keoleian, G., and Gabler, E. (2008). "Evaluation of life-cycle cost analysis practices used by the Michigan Department of Transportation." *J. of Trans. Engr., ASCE*, 134(6), 236–245.

Chapman, T., Anderson, S., and Windle, J. (2007). *Reuse of Foundations*, CIRIA C653, CIRIA, Classic House, 174-180 Old Street, London, EC1V 9BP.

Coduto, D. P. (2001). *Foundation Design, Principles and Practices*, Ed. 2nd, Prentice Hall, Upper Saddle River, New Jersey 07458, USA.

Collin, J. G. and Jalinoos, F. (2014). “Foundation Characterization Program (FCP): TechBrief #1— Workshop Report on the Reuse of Bridge Foundations,” FHWA-HRT-14-072, Research, Development, and Technology, Turner-Fairbank Highway Research Center, 6300 Georgetown Pike, McLean, VA 22101-2296.

Constantinou, M. (1994). “Properties of Sliding Bearings: Theory and Experiments.” *CISM International Centre for Mechanical Sciences*, 97-109.

CSU. (2015). Charles Sturt University, New South Wales, Australia.
http://hsc.csu.edu.au/engineering_studies/application/civil/1-1/answers.html (Last accessed: June 12, 2015)

Dalmatov, B.I., Ershov, V.A. and Kovalevsky, E.D. (1968), “Some Cases of Foundation Settlement in Driving Sheet piling and Piles,” Proceedings International Symposium on Wave Properties of Earth Materials, University of New Mexico, Albuquerque, New Mexico, pp.607-613, 1968.

DiMillio, A. F. (1982). *Performance of Highway Bridge Abutments Supported by Spread Footings on Compacted Fill*. FHWA/RD-81/184, Federal Highway Administration, Washington, D.C.

DSI. (2015). *DYWIDAG-Systems International (DSI)*, <<http://www.dsiamerica.com/>> (March 1, 2015)

Duncan, J.M., and Buchignani, A.L. (1976). *An Engineering Manual for Settlement Studies*, Geotechnical Engineering Report, University of California Berkeley, CA.

Dupond® (1996). *Teflon® PTFE Properties Handbook*, Wilmington, DE.

Ehlen, M.A., and Marshall, H.E. (1996). *The Economics of New-Technology Materials: A Case Study of FRP Bridge Decking*, Report NISTIR 5864, National Institute of Standards and Technology (NIST), U.S. Department of Commerce Technology Administration, Gaithersburg, MD.

Especiais, G.F. (2014). “Continuous Flight Auger (CFA) Piles.” *Geofund Fundacoes Especiais*, <<http://www.geofund.com.br/en/?p=229>> (April 21, 2014)

FDOT (2005). *District Five Operations Supplemental Agreement Worksheet for I-94 Saxon Blvd*, Project No. 0042215I & 0042227I, Florida Department of Transportation (FDOT), DeLand, FL.

FHWA. (2004). *Life-Cycle Cost Analysis – RealCost User Manual*, Office of Asset Management, Federal Highway Administration (FHWA), Washington, DC.

FHWA. (2007). *Manual of Use of Self-Propelled Modular Transporters to Remove or Replace Bridges*, No. FHWA-HIF-07-022, Federal Highway Administration (FHWA), Washington, D.C.

FHWA (2011). *Accelerated Bridge Construction-Experience in Design, Fabrication and Erection of Prefabricated Bridge Elements and Systems*. No. FHWA-HIF-12-013, Federal Highway Administration (FHWA), McLean, VA.

FHWA (2013a). “Accelerated Bridge Construction.” *Federal Highway Administration (FHWA)*, < <http://www.fhwa.dot.gov/bridge/abc/>> (April 17, 2014)

FHWA (2013b). “Accelerating Innovation.” *Federal Highway Administration (FHWA)*, <http://www.fhwa.dot.gov/everydaycounts/>> (April 17, 2015)

FHWA. (2013c). *Slide-In Bridge Construction Implementation Guide: Planning and Executing Projects with the Lateral Slide Method*, Final Report: F-ST99 (232), Office of Asset Management, Federal Highway Administration (FHWA), Washington, D.C.

FHWA (2014). “Slide-In Bridge Construction.” *Federal Highway Administration (FHWA)*, < <http://www.fhwa.dot.gov/construction/sibc/big.cfm>> (April 17, 2014)

FHWA. (2015). “Accelerated Bridge Construction (ABC) Project Exchange.” *Bridge Collaboration Portal, Federal Highway Administration (FHWA)*, <<https://www.transportationresearch.gov>> (Jan. 15, 2015)

Holtz, R.D., and Kovacs, W.D. (1981). *An Introduction to Geotechnical Engineering*, ISBN: 9780134843940, Prentice Hall, Upper Saddle River, NJ.

Hurd, M. K. (1995). *Formwork for Concrete*. 6th Ed., American Concrete Institute, Detroit, MI.

Hwang J.S., Chang K.C., & Lee G.C. (1990). "Quasi-Static and Dynamic Sliding Characteristics of Teflon-Stainless Steel Interfaces." *Journal Of Structural Engineering*, 2747-2762.

IDOT (2011). *Bridge Condition Report: Procedures & Practices*. Illinois Dept. of Transportation, Bureau of Bridges and Structures, Springfield, Illinois.

Iowa DOT. (2003). *Instructional Memorandums to County Engineers-Appendix F (Soils Information)*, No.: I.M. 3.131, Office of Local Systems, Iowa Department of Transportation (DOT), Ames, IA.

IowaDOT. (2012). *Accelerated Bridge Construction Policy*, Draft Report, Office of Bridges and Structures, Iowa Department of Transportation (DOT), Ames, IA.

IowaDOT (2013). “Massena Lateral Bridge Slide” *Iowa Department of Transportation*.<<http://www.iowadot.gov/MassenaBridge/index.html>> (November 2, 2014)

Iowa DOT. (2014). *LRFD Bridge Design Manual – Section 6*, Office of Bridges and Structures, Iowa Department of Transportation (DOT), Ames, IA.

JLARC. (2010). *Washington State Department of Transportation's Scoping and Cost Estimating for Highway Construction Projects*, Report No. 10-3, State of Washington Joint Legislative Audit and Review Committee (JLARC), Olympia, WA.

Kendall, A., Keoleian, G.A., and Helfand, G.E. (2008). "Integrated life-cycle assessment and life-cycle cost analysis model for concrete bridge deck applications." *J. of Infrastructure Systems, ASCE*, 14(3), 214–222.

Kenig, M. E. (2011). *AGC Project Delivery Systems for Construction*, ISBN 978-1-936006-28-1, The Associated General Contractors of America (AGC) Inc., Arlington, VA.

Lee, E.B., Kim, C., and Harvey, J.T. (2011). "Pavement type selection for highway rehabilitation based on a life-cycle cost analysis: Validation of California Interstate 710 Project (phase 1)." *Proc., 90th Annual Meeting of Transportation Research Board*, Washington, D.C., 11-1127.

MassDOT. (2009). *Accelerated Bridge Program-Decision Flow Chart*, Massachusetts Department of Transportation (MassDOT), Boston, MA.

MDOT (2013a). *Project Scoping Manual*, Michigan Department of Transportation (MDOT), Lansing, MI.

MDOT (2013b). *Prefabricated Superstructure, Laterally Slide*, Special Provision: S06-41024, Michigan Department of Transportation (MDOT), Lansing, MI.
< <http://mdotcf.state.mi.us/public/specprov/index.cfm?sy=439690#4cd95d99-9ed5-4634-bc2d-3ff2e624fb55>>

MDOT. (2014a). *Michigan Bridge Design Manual*, 5th Ed., Michigan Department of Transportation (MDOT), Lansing, MI.
<<http://mdotwas1.mdot.state.mi.us/public/design/englishbridgemanual/>>

MDOT. (2014b). *MDOT Accelerated Bridge Construction Projects Lessons Learned*, Michigan Department of Transportation (MDOT),
<<https://docs.google.com/document/d/1uEQJ7ri0iXFILAlSJIBToFer4q-7XE2KAaMsdjDoar0/edit?pli=1>> (Sept. 15, 2014)

MDOT. (2014c). *M-50 Bridge Jacking Plans-Mammoet Company*, Michigan Department of Transportation (MDOT), Lowell, MI.

MDSHA. (2002). *Construction Manual*, Office of Construction, Maryland State Highway Administration (MDSHA), Maryland Department of Transportation, Hanover, MD.

MDSHA. (2014). *Bridge Standards Plotsets – 02 Bridge Foundation*, Maryland State Highway Administration (MDSHA), Maryland Department of Transportation, Baltimore, MD.

MDT. (2002). *Structures Manual*, the Montana Department of Transportation, Helena MT 59620, USA.

NCDOT. (2013). *Request for Proposals (RFP) Volume II, Book 2, Technical Provisions*, No. TIP I-3311C, I-5405, I-4750AA, State of North Carolina Department of Transportation (NCDOT), Raleigh, NC.

NCDOT. (2014a). *Book 2, Technical Provisions*, No. TIP I-3311C, I-5405, I-4750AA, State of North Carolina Department of Transportation (NCDOT), Raleigh, NC.

NCDOT. (2014b). *LRFD Driven Pile Foundation Design Policy*, No. 6th Update, Geotechnical Engineering Unit, North Carolina Department of Transportation (NCDOT), Raleigh, NC.

NCHRP (1991). *Manuals for the Design of Bridge Foundations*, Report: NCHRP 343, National Cooperative Highway Research Program (NCHRP), Transportation Research Board, Washington, D.C.

NIST. (2003). *BridgeLCC - Life-Cycle Costing Software*, Version 2.0, National Institute of Standards and Technology (NIST), Gaithersburg, MD.

Oden, J.T., and Martins, J.A.C. (1985). “Models and Computational Methods for Dynamic Friction Phenomena.” *J. of Computer Methods in Applied Mechanics and Engineering*, Elsevier, 52(1-3), 527–634.

Olson, L. D. and Aouad, M. F. (1998). “NCHRP 21-5 Research Results on Determination of Unknown Bridge Foundation Depths,” Proceedings of the Mini-Symposium on Bridge Scour, the International Water Resources Engineering Conference, Memphis, Tennessee, August 3 – 7.

Oregon DOT. (2005). *ODOT Bridge Foundation design Practices and Procedures*, Bridge Engineering Section, Oregon Department of Transportation (DOT), Salem, OR.

Oregon DOT. (2010). *Introduction to Bridge Foundations – Section 8*, Oregon Department of Transportation (DOT), Salem, OR.

Oregon DOT. (2014). *Bridge Inspector Training Manual – Driven Piles*, Oregon Department of Transportation (DOT), Salem, OR.

Ostrom, T. (2013). “Why does CT use so many CIDH piles?” *Proc., March 2013 Bridge Forum*, Bridge Contractor/Caltrans Liaison Committee, Los Angeles, CA, <http://www.dot.ca.gov/hq/esc/construction/br_contractor_outreach/> (July 08, 2014)

Ouyang, J. F., Liu, W. L., Sun, D. X., and Yan, Y. G. (2005). *Laser Tracker Calibration Using Coordinate Measuring Machine*, 20th ASPE Annual Meeting, Norfolk, VA, October 9-14.

Picornell, M. and Monte, E. (1985). “Pile Driving Induced Settlements of a Pier Foundation”, Proceedings of a Symposium sponsored by the Geotechnical Engineering Division in conjunction with the ASCE Convention in Detroit, Michigan, October 1985, pp. 174-186.

- Rabeller, R. C., Bedenis, T. H., and Thelen, M. J. (2000). "High Capacity Drilled Cast-in-Place Piles." *Proceedings of Sessions of Geo-Denver 2000: New Technological and Design Developments in Deep Foundations*, ASCE, Denver, Co., 125-139.
- Rangaraju, P.R., Amirghanian, S., and Guven, Z. (2008). *Life cycle cost analysis for pavement type selection*, Report FHWA-SC-08-01, South Carolina Department of Transportation & Federal Highway Administration, Clemson, SC.
- Ratay, R. T. (1996). *Handbook of Temporary Structures in Construction*. 2nd Ed., University of Washington: McGraw Hill, New York.
- Rister, B.W., and Graves, C. (2002). *The cost of construction delays and traffic control for life-cycle cost analysis of pavements*, Report KTC-02-07/SPR 197-99 & SPR218-00-1F, University of Kentucky and Kentucky Transportation Center, Lexington, KY.
- Sabatini, P. J., Tanyu, B., Armour, T., Groneck, P., and Keeley, J. (2005). *Micropile Design and Construction*. FHWA NHI-05-039, National Highway Institute, U.S. Department of Transportation, Federal Highway Administration, Washington, D.C. 20590.
- Samtani, N. C., Nowatzki, E. A., Mertz, D. R. (2010). *Selection of Spread Footings on Soils to Support Highway Bridge Structures*. FHWA-RC/TD-10-001, Federal Highway Administration Resource Center, 4749 Lincoln Mall Drive, Suite 600 Matteson, IL, 60443.
- Schaefer, V. R. and Jalinoos, F. (2013). "Characterization of Bridge Foundations Workshop Report," FHWA-HRT-13-101, Office of Infrastructure Research and Development Federal Highway Administration 6300 Georgetown Pike McLean, VA 22101-2296.
- SCST (2013). *Preliminary Structure Foundation Report – Z Drain Bridge English Road*, Southern California Soil & Testing (SCST) Inc., San Diego, CA.
- Shahawy, M. A. (2003). *Prefabricated Bridge Elements and Systems to Limit Traffic Disruption during Construction*, NCHRP Synthesis 324, Transportation Research Board, Washington, D.C.
- SHRP. (2012). *Continuous Flight Auger Piles: Technology Fact Sheet*. GeoTechTools. <<http://www.GeoTechTools.org>> (November, 2013).
- SHRP 2 R04 (2013). *Innovative Bridge Designs for Rapid Renewal: ABC Toolkit*, SHRP 2 Report No. S2-R04-RR-2, Transportation Research Board of the National Academies, Washington, D.C.
- SHRP 2 R04 (2015), *ABC Standard Concepts: The Lateral Slide Addendum Report*, Transportation Research Board of the National Academies, Washington, D.C.
- Shutt, C.A. (2013a). "Sliding and Rolling Bridge Solutions – Part 1." *Accelerated Bridge Construction, ASPIRE*, Winter, 21-23.

- Shutt, C.A. (2013b). “Sliding and Rolling Bridge Solutions – Part 2.” *Accelerated Bridge Construction, ASPIRE*, Spring, 19-20.
- Shutt, C.A. (2013c). “SPMT Solutions -WisDOT.” *Accelerated Bridge Construction, ASPIRE*, Fall, 39-41.
- Strauss, J., Nicholls, R., Chapman, T., and Anderson, S. (2007). “Drivers Affecting Frequency of Foundation Reuse and Relevance to U.S. Cities,” Proceedings of the ASCE Geo-Denver 2007 Conference, Contemporary Issues In Deep Foundations: pp. 1-10.
- Strömblad, N. (2014). *Modeling of Soil and Structure Interaction Subsea*, Master’s thesis, Department of Applied Mechanics, Division of Material and Computational Mechanics, Chalmers University of Technology, Sweden.
- Sturgill, R.E., Taylor, T.R.B., Ghorashinezhad, S., Zhang, J. (2015). *Methods to Expedite and Streamline Utility Relocations for Road Projects*, Report: KTC-14-15/SPR460-13-1F, Kentucky Transportation Center, University of Kentucky, Lexington, KY.
- Subramanian, N. (2010). *Design of Steel Structures*, Ed. pbk, ISBN-13: 9780198068815, Oxford University Press, Don Mills, ON, Canada, 1396–1398.
- Surdahl, R., Miller, D., and Glenn, V. (2010). “The Positive Legacy of a Bridge Collapse.” *Public Roads*, 73(5).
- UDOT (2008) “Accelerated bridge construction (ABC) and the Utah experience.” *Proc., AASHTO Subcommittee on Construction Annual Meeting*, San Antonio, TX.
- UDOT (2009). *Accelerated Bridge Construction - SPMT Process Manual and Design Guide*, Utah Department of Transportation (UDOT), Salt Lake City, UT.
- UDOT (2013). *Slide-In Bridge Construction Implementation Guide*, Final Report No. F-ST99(232), Utah Department of Transportation (UDOT), Salt Lake City, UT.
- UDOT. (2014). *Geotechnical Manual of Instruction*, Utah Department of Transportation (UDOT), Salt Lake City, UT,
<<http://www.udot.utah.gov/main/uconowner.gf?n=11917505197795830>> (July 14, 2014)
- USDA (2013). “Web Soil Survey.” *Natural Resources Conservation Service, United States Department of Agriculture (USDA)*,
<<http://websoilsurvey.sc.egov.usda.gov/App/HomePage.htm>>
- VDOT. (2012). “VDOT Project Development Process – Scoping Phase.” *Virginia Department of Transportation (VDOT)*,
<http://www.virginiadot.org/business/resources/Scoping_Phase_Narrative.pdf>
- Walls, J. and Smith, M.R. (1998). *Life-Cycle Cost Analysis in Pavement Design – Interim Technical Bulletin*, Report FHWA-SA-98-079, Federal Highway Administration, Washington, D.C.

Williamson, S. H. (2014). “Compute the Relative Value of a U.S. Dollar Amount, 1774 to present–CPI converter.” *MeasuringWorth*, <<http://www.measuringworth.com/uscompare/>> (April 25, 2015)

WisDOT. (2013). *WisDOT Bridge Manual – Accelerated Bridge Construction Chapter-7*, Wisconsin Department of Transportation (WisDOT), Madison, WI.

WSDOT. (2008). *Cost Estimating Manual for WSDOT Projects*. Washington State Department of Transportation (WSDOT), Olympia, WA.

Zekkos, A. A., Woods, R. D., and Grizi, A. (2013). “Effect of Pile-Driving Induced Vibrations on Nearby Structures and Other Assets.” Report No. OR10-046, the Michigan Department of Transportation, Lansing, MI, USA.